Terms and Conditions of Use of Digitised Theses from Trinity College Library Dublin

Copyright statement

All material supplied by Trinity College Library is protected by copyright (under the Copyright and Related Rights Act, 2000 as amended) and other relevant Intellectual Property Rights. By accessing and using a Digitised Thesis from Trinity College Library you acknowledge that all Intellectual Property Rights in any Works supplied are the sole and exclusive property of the copyright and/or other IPR holder. Specific copyright holders may not be explicitly identified. Use of materials from other sources within a thesis should not be construed as a claim over them.

A non-exclusive, non-transferable licence is hereby granted to those using or reproducing, in whole or in part, the material for valid purposes, providing the copyright owners are acknowledged using the normal conventions. Where specific permission to use material is required, this is identified and such permission must be sought from the copyright holder or agency cited.

Liability statement

By using a Digitised Thesis, I accept that Trinity College Dublin bears no legal responsibility for the accuracy, legality or comprehensiveness of materials contained within the thesis, and that Trinity College Dublin accepts no liability for indirect, consequential, or incidental, damages or losses arising from use of the thesis for whatever reason. Information located in a thesis may be subject to specific use constraints, details of which may not be explicitly described. It is the responsibility of potential and actual users to be aware of such constraints and to abide by them. By making use of material from a digitised thesis, you accept these copyright and disclaimer provisions. Where it is brought to the attention of Trinity College Library that there may be a breach of copyright or other restraint, it is the policy to withdraw or take down access to a thesis while the issue is being resolved.

Access Agreement

By using a Digitised Thesis from Trinity College Library you are bound by the following Terms & Conditions. Please read them carefully.

I have read and I understand the following statement: All material supplied via a Digitised Thesis from Trinity College Library is protected by copyright and other intellectual property rights, and duplication or sale of all or part of any of a thesis is not permitted, except that material may be duplicated by you for your research use or for educational purposes in electronic or print form providing the copyright owners are acknowledged using the normal conventions. You must obtain permission for any other use. Electronic or print copies may not be offered, whether for sale or otherwise to anyone. This copy has been supplied on the understanding that it is copyright material and that no quotation from the thesis may be published without proper acknowledgement.

Young Brown Dwarfs And Their Environments

Testing Star And Planet Formation

by

Paul Dawson B.A. (Mod)

A thesis submitted to the
University of Dublin
for the degree of
Doctor of Philosophy

February 2014

School of Physics
University of Dublin
Trinity College

School of Cosmic Physics
Dublin Institute for
Advanced Studies

I hereby declare that this thesis has not been submitted as an exercise for a degree at this or any other University and that, except where otherwise stated, it is entirely my own work.

I agree that the Library may lend or copy this thesis upon request.

Signed,

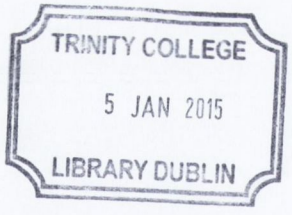

Paul Dawson

Paul Dawson

May 23, 2014.

Abstract

This thesis presents a new contribution to our understanding of the formation of brown dwarfs. From a description of their discovery, to an analysis of their disks and photospheres, it sheds new light on the conditions under which stars, brown dwarfs, and planets, form and evolve. It explores new challenges to further studies of young brown dwarfs, and offers a means of advance.

A significant number (65) of new young brown dwarfs are successfully identified from wide-field photometric surveys. A search for brown dwarfs in the Upper Scorpius Association was undertaken using data from the UKIRT Infrared Deep Sky Survey (UKIDSS) Galactic Cluster Survey. Candidate young brown dwarfs were first chosen by their position in colour magnitude diagrams with further selection based on proper motions to ensure Upper Scorpius membership. Proper motions were derived by comparing UKIDSS and 2 Micron All Sky Survey (2MASS) data.

A follow-up spectroscopic examination of 24 of the 65 new objects discovered confirms that all 24 are young very low mass objects. Their spectral types range from M5 to L1. This high yield confirms that brown dwarfs in Upper Scorpius can be reliably identified from photometry and proper motions alone, with negligible contamination ($< 4\%$) from field objects.

The formation of every 10 stars of $1\,M_{\odot}$ or less in Upper Scorpius is shown to be accompanied approximately by the formation of 3-4 brown dwarfs. This lends weight to the idea that the formation of brown dwarfs is a common process which is either an extension of, or is caused by, the process of star formation. The ratio of stars to brown dwarfs ($3.5^{+2.0}_{-1.3}$) in the south of Upper Scorpius was determined. This parameter was found to be consistent with other areas in Upper Scorpius. It was also found to be similar to other results from young clusters with OB associations, but lower than those without. This suggests that the brown dwarf formation rate may be a function of environment.

An examination of disks around brown dwarfs suggests that they are as suitable as sites of planet formation as those around low-mass stars. A census of the disk population in Upper Scorpius was conducted on a sample of 116 brown dwarfs originally identified via UKIDSS, including the 65 newly discovered ones. Photometry for these objects was obtained from the WISE

database. The resulting colour-magnitude and colour-colour plots clearly show two separate populations of objects, interpreted as brown dwarfs with disks (Class II) and without disks (Class III). This led to the identification of 27 Class II brown dwarfs, 14 of which were not previously known. The disk fraction (27 out of 116 or 23%) among brown dwarfs was found to be similar to results for K/M stars in Upper Scorpius, suggesting that the lifetimes of disks are independent of the mass of the central object for both low-mass stars and brown dwarfs.

5 out of 27 disks (19%) lack excess at 3.4 and 4.6 μm and are potential transition disks (i.e. are in transition from Class II to Class III). The transition disk fraction is comparable to that of low-mass stars. An estimate of the timescale for a typical transition from Class II to Class III of less than 0.4 Myr for brown dwarfs is derived. These results suggest that the evolution of brown dwarf disks mirrors the behaviour of disks around low-mass stars, with disk lifetimes on the order of 5-10 Myr and a disk clearing timescale significantly shorter than 1 Myr. This is further evidence that the precursive conditions for planet formation around K/M stars also prevail around brown dwarfs.

A new catalogue of near-infrared spectral templates of brown dwarfs is provided, and its necessity is demonstrated. Some very low mass Class II objects are shown to exhibit radically different near-infrared (0.6 - 2.5 μm) spectra from Class III objects, having strong excess emission, which increases at longer wavelengths, as well as partially filled in features at wavelengths shorter than 1.25 μm. These characteristics can obscure the contribution of the photosphere within such spectra. Therefore, I caution that spectral types of objects with disks, derived from portions of near-infrared spectra, may be limited in their reliability. As well as being present in all the Class II objects, the same characteristics were observed in a significant fraction ($\sim$ 40%) of the Class III objects, indicating that some of them are still surrounded by traces of dust and gas.

The spectra of the remaining Class III objects were found to be clean and clear of discernible contributions from anything other than their photospheres. A catalogue of their near-infrared spectra has been made available. In order to improve the accuracy and reliability of the spectral typing of both Class II and Class III young brown dwarfs in the future, I recommend the use of the objects in this catalogue as spectroscopic templates.

Acknowledgements

Many thanks are due to everyone who helped and contributed to the production of this thesis. Astrophysics research is a team sport, and I could not have completed this work without your help.

I thank my supervisors, and co-authors of my research papers, Dr. Aleks Scholz and Prof. Tom Ray, for all your instruction, coaching and guidance. I also appreciate the courteous, patient and good-humoured way in which you imparted it.

To my other co-authors, Prof. Antonella Natta, Donna Rodgers-Lee, Dr. Vincent Geers, Dr. Dawn Peterson, Dr. Mike Ressler, Dr. Deborah Padgett, Dr. Ken Marsh, Dr. Kenny Wood, I wish to express my gratitude for all your expert advice, assistance and training, which was vital to the success of my research.

I am also very grateful to my fellow DIAS students Rachael Ainsworth, Donna Rodgers-Lee, Carlo Romoli, Dr. Gráinne Costigan, Dr. Lisa Fallon, Dr. Seán Delaney, Dr. Nakisa Noorae and Dr. Denys Malyshev for all your help with technical questions and, more importantly, for being such friendly and pleasant colleagues.

The contributions of other academic staff at DIAS to my understanding of star formation, and astrophysics in general, are greatly appreciated. I thank Prof. Luke Drury, Prof. Malcolm Walmsley, Dr. Turlough Downes, Dr. Ruyman Azzollini, Dr. Andrew Taylor, Dr. Deirdre Coffey, Dr. Gareth Murphy, Dr. Emma Whelan and Dr. Julien Morin for all the informative discussions, explanations and elucidations of the outer reaches of astrophysics research.

For taking care of so much administrative work and so many organisational details, special credit is due to Eileen Flood who did it so efficiently and effectively. Thanks go to Philippe Grange and Dr. Dmitri Grigoriev for keeping the computers running smoothly. And to Anne, Phyllis, Patricia, Hilary and Keith, thank you for also helping to make working in DIAS such an enjoyable experience.

All the research work outlined in this thesis was supported by Science Foundation Ireland within the Research Frontiers Programme under grant no. 10/RFP/AST2780.

I am very grateful for all the support and encouragement given by my friends and family while I worked on this thesis. In particular, I wish to thank my mother, Kathleen and my sister Elizabeth. Your help and support was vital on my journey through the world and universe of astrophysics. I also wish to remember, with gratitude, my late father Larry, who was such an important inspiration in my decision to return to the study of physics.

List Of Publications And Presentations

Publications:

Dawson P., Scholz A., Ray T.P., Peterson D.E., Rodgers-Lee D., Geers V., *Near-Infrared Spectroscopy of Young Brown Dwarfs in Upper Scorpius*, 2014 MNRAS, in press arXiv:1405.3842.

Mužić K., Scholz A., Geers V.C., Jayawardhana R., Tamura M., Dawson P., Ray T.P., *The SONYC survey: Towards a complete census of brown dwarfs in star forming regions*, 2013, MmSAI, 84, 931M.

Dawson P., Scholz A., Ray T.P., Marsh K.A., Wood K., Natta A., Padgett D., Ressler M.E., *New brown dwarf disks in Upper Scorpius observed with WISE*, 2013, MNRAS, 429, 903D.

Dawson P., Scholz A., Ray T.P., *New brown dwarfs in the south part of the Upper Scorpius Association*, 2011, MNRAS, 418, 1231.

Conference Presentations:

Geers V., Scholz A., Mužić K., Dawson P., Jayawardhana R., Tamura M., (Poster) *SONYC: Substellar Objects in Nearby Young Clusters*, Protostars and Planets VI, Heidelberg, July 15-20, 2013.

Dawson P., *Clean And Clear - A New Sample Of Brown Dwarfs In Upper Scorpius*, Brown Dwarfs and Low Mass Stars, NAM 2013 St Andrews, July 1-5, 2013.

Dawson P., *Brown Dwarfs in Upper Scorpius: new results from 3 surveys*, Formation and Early Evolution of Very Low Mass Stars and Brown Dwarfs, ESO Garching, October 11-14, 2011.

Dawson P., *Brown Dwarfs in Upper Scorpius: new results from 3 surveys*, DIAS Astronomy & Astrophysics Seminars, DIAS Dublin, October 7,

2011.

Dawson P., *New Brown Dwarfs in the south of Upper Scorpius*, ASGI Autumn Meeting, Armagh Planetarium, September 5, 2011.

Cabut A., Dawson P., Herrero-Illana R., Meingast S., Navarro-Gonzalez J., Nizenkov P., Saavedra G., Schmid D., Schreyer K., Skjaeveland A., Strandet M., Sundl M., Szalai N., Vellutini E., Warth G., and Wende H. *PIRANHA: Project for InfraRed Astrometry aNd High Accuracy*, Star Formation Across The Universe, ESA Summer School Alpbach,July 28, 2011.

Scholz A., Mužić K., Geers V., Jayawardhana R., Tamura M., Dawson P., Ray T. P., *The Brown Dwarf Population in Nearby Star-Forming Regions*, Stellar Clusters & Associations: A RIA Workshop on Gaia, Granada, May 23-27, 2011, 2011sca..conf..250S

Dawson P., (Poster) *New Brown Dwarfs in South of the Upper Scorpius Association*, ASGI Spring Meeting, NUI Maynooth, April 1, 2011.

Contents

Chapter 1

Introduction

1.1 Brown Dwarfs

The luminosity of a star is a result of the release of energy from nuclear fusion processes occurring in its core. The rate at which energy is radiated from the star is exactly compensated by the energy release from the internal nuclear reactions. Hence, once an object has sufficient mass to allow nuclear ignition, or hydrogen burning, to occur, it settles into a state of thermal equilibrium which lasts as long as it has sufficient nuclear fuel. For a low mass star (i.e. similar to, or less than the mass of the Sun) this state lasts for ten or more billion years.

The minimum mass of a star is about $0.08\,M_{\odot}$. Below that mass and above $0.013\,M_{\odot}$ the maximum interior temperature of the object (about 10^6K) only permits the ignition of deuterium burning. The relatively small amount of nuclear energy released cannot compensate for the radiative energy loss from the object and so it cools and fades rapidly in a few tens of millions of years. This inability to reach long term thermal equilibrium is the defining characteristic of a brown dwarf.

Brown dwarfs have been the focus of much investigation, both theoretical and observational, for several decades now. Several hundreds of brown dwarfs, including many young brown dwarfs, are now known, (see Briceño et al. (2007); Luhman (2012) and references therein), making it possible to explore the nature of these substellar objects. From the initial postulation of their existence (Kumar, 1963), to their eventual discovery (Nakajima et al., 1995), and up to the present day, the study of brown dwarfs has sought

to answer many fundamental astrophysical questions. While some of these questions have been answered, (e.g. brown dwarfs do not account for unseen Dark Matter in the galaxy), many others remain. One of the greatest dilemmas concerns the formation of brown dwarfs. Do many brown dwarfs form? What is their formation mechanism? Can planets form around brown dwarfs as they do around stars?

This thesis explores these questions using observations of young brown dwarfs in the Upper Scorpius star forming region. It probes the relationship between star forming environment and the mass of the objects formed. It tests the mass dependence of critical parameters in stellar evolution e.g. planet formation. It identifies phenomena that can improve the characterisation of brown dwarfs in the future.

1.2 A Historical Context - The Questions Emerge

By the early years of the 20th century, stars had been grouped into different spectral types. Most of the different lines observed in stellar spectra had been reproduced in laboratories, so their chemical origin was understood, and the relationship between the different spectral types was becoming clearer. Attempts were now made to see if the spectral type groupings could also be linked to physical parameters (e.g. mass, or luminosity) intrinsic to the stars.

The Hertzsprung-Russell Diagram

The most important work of this nature was begun independently by both Hertzsprung (1905) and Russell (1913), who began to group stars according to their brightness, colour and spectral type. Several important relationships became apparent as a result, and the Hertzsprung-Russell diagram went on to become perhaps the single most important graphical tool used in astrophysics since. The first graph published by Hertzsprung (1911) showed the apparent magnitude versus colour for stars in the Hyades and Pleiades cluster, whereas Russell (1914) used data from stars for which parallaxes were available and graphed their absolute magnitude against their spectral types. A simplifed Hertzsprung-Russell diagram, illustrating the most im-

portant features, and the position of brown dwarfs, is shown in Fig. 1.1. Spectral types vary from early to late along the horizontal axis, while absolute magnitudes vary from faint to bright along the vertical axis. The vast bulk of stars appear on what we now know as the Main Sequence. A lesser number of stars appear to the upper right of the Main Sequence. Russell (1914) had already noted that: "the main cause of the differences of the spectral classes is difference of temperature of the stellar atmospheres". So the horizontal axis in the diagram was also a scale of temperature. Both Hertzsprung (1905) and Russell (1914) had also shown that the horizontal axis was also a scale in colour varying from white to red. This was consistent with the still relatively new idea of blackbody radiation, reinforcing the idea that stars were blackbody radiators and that their colour was due to their surface temperature.

Hertzsprung (1905) had already concluded that the reason stars in the range of K and M exhibited a range of luminosities was because they had a range of surface areas, the brighter stars being giant objects while the Main Sequence objects were perhaps at the minimum size for an object of that spectral type. However, both authors had realised that the difference in size did not imply a difference in mass and were of the view that it corresponded to a difference in density, with giants being swollen stars. Hence the conclusion of Russell (1914) that there were "two great classes of stars"..."one of great brightness...and varying little in brightness from one class of spectrum to another" (the giants), "the other of smaller brightness, which falls off very rapidly with increasing redness" (the Main Sequence). In one graph, the Hertzsprung-Russell diagram had encapsulated many fundamental parameters of the stars. Writing about his memories of Hertzsprung many years later, Strand (1977) recalled that Hertzsprung, with characteristic modesty, remarked of the graph which now bore his name: "Why not call it the colour-magnitude diagram? Then we know what it is all about."

The information contained in the Hertzsprung-Russell diagram related many of the properties of stars based on observations of their surfaces. It did not directly yield information on the internal processes that cause them to shine, nor did it reveal how they evolve with time. Russell (1914) himself was of the opinion that stars shone as a result of Kelvin-Helmholtz contraction only and that they began life as low density M giants in the top right of the diagram. They then contracted and heated up until they reached a max-

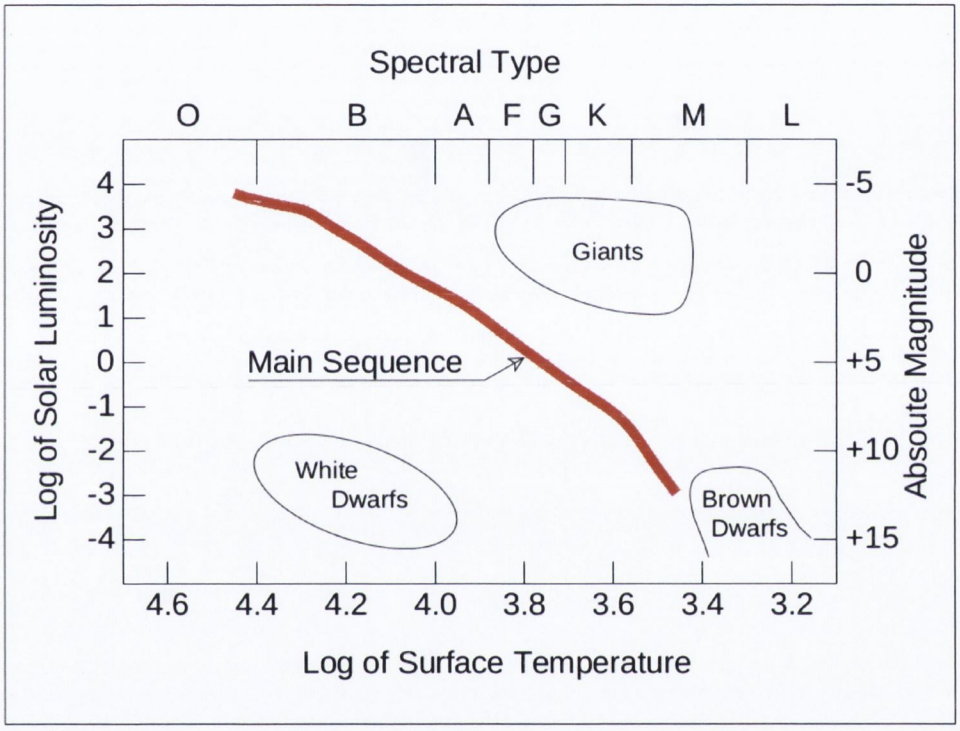

Figure 1.1 The Hertzsprung-Russell diagram, indicating the most salient features. Most stars occupy a position on the Main Sequence, with hot, bright O stars at the top left and cool, faint M stars down at the bottom right. The much less populous giant stars are distributed around the region indicated in the top right, while the rarer white dwarfs cluster away from the Main Sequence in the region shown at bottom left. Evolved brown dwarfs are located in the coolest and faintest corner of the diagram.

imum temperature and became type B stars on the Main Sequence. From there they cooled slowly, while still contracting at a slower rate than before, and descended down through the spectral types on the Main Sequence until they had become M dwarfs. This concept still finds an echo in the categorisation of spectral types as "early" or "late". He interpreted the fact that few giants are seen by comparison to Main Sequence stars by concluding that the initial period of stellar contraction and temperature increase was rapid. The later evolutionary stage on the Main Sequence, as it cooled from its maximum temperature, was much slower, hence the high numbers of type K and M stars on it. The reason that the Main Sequence finished among stars of late M type was simply because later stars were too faint to be seen.

Russell's ideas about stellar luminosity and evolution were soon overtaken by new developments. However, he had demonstrated the importance of a condition, which all those new developments would have to fulfill. Any new theory of stellar luminosity and evolution would still have to be able to explain the position of a star on the diagram.

"What is the Stars?"

By 1924, audiences at Juno and The Paycock heard Captain Boyle tell Joxer Daly how he often asked himself the question: "what is the stars?". He wasn't the only one. Eddington (1919) had pointed out that the discrepancy between geological time, and the much shorter time that the sun could shine via conversion of gravitational potential into heat, was a major obstacle for stellar physics. He postulated that nuclear reactions could provide the energy in a star like the sun that would let it maintain its luminosity on a scale of billions of years. It took another two decades before satisfactory theoretical nuclear mechanisms for stellar energy production were elucidated (von Weizsacker, 1938; Bethe, 1939).

The concept of a star as a long lived nuclear fusion engine now explained the Main Sequence feature on the Hertzsprung-Russell diagram. Most stars were concentrated there because the production of energy from nuclear reactions was the longest phase of their evolution. The sequence was a narrow feature because the stars were in stable equilibrium and their luminosity did not vary. The rate at which the nuclear reactions produced energy was just enough to balance the gravitational self-contraction of the star. This established that there was a link between the mass of any star and its po-

sition on the Main Sequence. The O and B stars at the top of the Main Sequence, being the hottest and most luminous, had to be the most massive. Conversely, the M stars at the bottom were faintest, because their nuclear reactions proceeded at a slower rate, hence they had to be the least massive.

This raised the question of the minimum rate at which nuclear reactions could proceed in a star. The mass of the star supplied the gravitational potential which was converted to the kinetic energy of the nuclear reactants inside it. There was now known to be a threshold amount of kinetic energy that had to be available to those reactants to allow bulk fusion reactions to proceed. Ergo, there was a critical minimum mass that a star had to have. In terms of the Hertzsprung-Russell diagram, this meant that there was a real physical limit to the Main Sequence. The Main Sequence did not end just because some stars were too faint to observe. It ended at the minimum mass required to burn hydrogen in equilibrium.

This now raised some new questions. What would happen in an object with less mass? Could such an object form?

Below The Hydrogen Burning Minimum Mass

Kumar (1963) probed that first question by investigating the internal structure of stars of very low mass using theoretical models. The models evaluated the central temperature and density of collapsing stars in the range of 0.04 - 0.09 $M_{\odot}$. The results presented showed that as the central density increased in these very low mass objects, the temperature rose to a maximum before levelling off and beginning to fall. This maximum temperature was not high enough for hydrogen burning to begin in objects of less than about 0.07 - 0.09 $M_{\odot}$. These substellar objects, which Kumar (1963) referred to as black dwarfs, would never go through a Main Sequence phase. Unlike stars in the Main Sequence that are supported against gravitational collapse by thermal pressure, these black dwarfs would be supported by electron degeneracy pressure. This theoretical exploration had yielded the first quantitative predictions for such substellar objects.

The black dwarfs of Kumar (1963) were later dubbed brown dwarfs by Tarter (1975), and this phrase has become the de facto name of such substellar objects in the years since. Kumar (1963) had predicted the lower limit of the Main Sequence, by modelling the interior of a brown dwarf. The model gave no information on the appearance of its atmosphere. Nor did it

deal with the question of whether or not such an object could form in the first place.

A Matter Of Time

Kumar (1963) had drawn on the work of Hayashi (1961), who had also been modelling the interiors and atmospheres of low mass stars, but who had not yet modelled objects of brown dwarf mass. Hayashi now turned his attention to very low mass objects (Hayashi & Nakano, 1963), and confirmed the results of Kumar (1963), finding that $0.08\,M_{\odot}$ was the critical mass for hydrogen burning. Hayashi & Nakano (1963) also modelled the atmospheres of low mass objects and was able to place them on theoretical Hertzsprung-Russell diagrams. By showing where an object of a given mass appeared when its interior was at different densities and temperatures, Hayashi & Nakano (1963) was also tracking its evolution in time. This work showed that prior to the start of hydrogen burning, low mass stars descended on a nearly vertical track on the diagram.

Brown dwarfs followed a similar path, to the right of the stars on the diagram. Having no equivalent of the Main Sequence to arrive on, they continued to get fainter, their tracks eventually becoming less vertical, but continuing to descend. Hayashi & Nakano (1963) had demonstrated a key feature of brown dwarfs that would be of great importance to future observers. Brown dwarfs are at their brightest when they are young.

A Star is Born

As 1937 cinema audiences flocked to see A Star Is Born, physics was also getting to grips with how stars are born in the cosmos. Two questions needed to be addressed. What were stars made from? How did they evolve towards the Main Sequence? The general hypothesis was still the same as it had been since the beginning of the century. As a star was held together by gravity it was reasonable to presume that stars began to coalesce from diffuse clouds of gas and dust as a result of some gravitational instability within the cloud. Jeans (1929) had established the theoretical criteria under which a gravitational instability in a homogeneous gaseous medium would begin a process of runaway gravitational collapse. If any disturbance compressed some of the gas in the medium a corresponding rarefaction would

form elsewhere and the gas pressure would tend to even out, oscillating between states of compression and rarefaction in the two locations until the energy that caused the disturbance was dissipated by viscosity. However, the increased gravitational self attraction of the mass of gas compressed into a smaller volume would tend to compress and contract it into yet a smaller volume. The system would return to equilibrium as long as the restoring forces could out compete the gravitational forces. If the gravitational energy available within the compressed volume was greater than the energy of the oscillating wave propagating through the medium the condensed mass would not return to equilibrium and would continue to collapse. For such a localised gravitational instability to form, a critical mass, now known as the Jeans mass, had to be compressed within an equally critical volume. These factors were related to the sound speed within the medium, hence they depended on the temperature and density of the cloud.

The Jeans mass (M_{Jeans}) can be expressed relative to the temperature (T) and density (ρ) of a cloud via

$$M_{Jeans} = \left(\frac{5kT}{\mu m_H G}\right)^{\frac{3}{2}} \left(\frac{3}{4\pi\rho}\right)^{\frac{1}{2}} \tag{1.1}$$

where k is Boltzmann's constant, μ is the mean molecular weight of the particles in the cloud, m_H is the mass of a proton and G is the gravitational constant. If the critical volume into which the Jeans mass must be compressed is assumed to be spherical then it will have a characteristic radius. This Jeans radius (R_{Jeans}) can then be given by

$$R_{Jeans} = \left(\frac{15k}{4\pi\mu m_H G}\right)^{\frac{1}{2}} \left(\frac{T}{\rho}\right)^{\frac{1}{2}} \tag{1.2}$$

The conditions necessary for a star to be born, from a diffuse cloud of gas, had now been quantified theoretically.

At this stage there were no clouds identified where star formation was taking place. In Jeans (1929) opinion, the only suitable conditions for star formation were to be found in the arms of spiral galaxies, contending that elliptical galaxies and the centres of spiral galaxies could not be made of stars. A Star Is Born was remade in 1954 and again in 1976. Star formation theory has been updated considerably more often, but the Jeans mass remains a valid and critical factor. For any star or brown dwarf to form, its

natal cloud must be unstable to gravitational collapse. This can only occur if the mass of the material contained in the cloud exceeds the critical Jeans mass value.

Joy Unconfined

Some new questions had arisen as a result of these early forays into star formation theory. Was star formation in the universe a completed process, or were stars still being formed? What was the Jeans mass of a typical star forming cloud? How many stars formed from one cloud? What was the possible range of masses of such stars? Unless a star forming cloud was identified, these questions might prove impossible to answer.

Joy (1945) described observations of some irregular variable stars whose prototype was T-Tauri. He noted that they were all located in or near dark clouds. Ambartsumian (1947) realised the significance of these objects in terms of star formation, and suggested that they were pre Main Sequence stars. Around the same time Bok & Reilly (1947) identified many small dark globules in nebulae in Saggitarius, Ophiuchus and Scutum, suggesting that they might well be on the cusp of collapsing to form stars. Now it appeared that the type of clouds that form stars might well have been identified and could finally be quantitatively investigated.

Once Hayashi (1961) had shown that pre Main Sequence stars evolve down vertical tracks in the Hertzsprung-Russell diagram, he also noted that the T-Tauri stars were located along those tracks. This reinforced the idea that the T-Tauri objects were stars in the process of formation, going through an as yet little understood phase, before they began to burn hydrogen in equilibrium. It also supported the idea that the dark nebulae in the vicinity of these objects might be typical of the clouds from which they had formed.

If they were, then the conditions within such molecular clouds could now be investigated. Their densities and temperatures could be quantified and Jeans criteria could be applied to see what sort of stars and brown dwarfs might be expected to form.

1.3 Current Ideas Of Star Formation

Theories of star formation have been continuously refined since Hayashi's first models appeared. Further developments by Iben (1965) probed the evolution of the high mass stars. Hayashi (1970) probed the earlier stages of formation between the initial rapid collapse of a cloud and subsequent formation of a slowly contracting pre Main Sequence star.

Observations of star forming processes have also progressed, and have constrained theories, as well as making new findings that theory has yet to satisfactorily explain. Molecular clouds have been analysed and their temperatures and densities measured. Present day observations are beginning to show structures in the clouds that will have a direct bearing on their star forming properties. Pre Main Sequence stars, and young brown dwarfs, have been observed during their contraction phase. The T-Tauri stars first identified by Joy (1945) have been the subject of extensive investigation (Bertout, 1989). Their place in the evolution of a star is now understood, but much remains to be learnt about the mechanisms of this short lived phase.

A comprehensive overall understanding of the formation of Main Sequence stars from the cold, rarefied material of molecular clouds has now emerged.

Molecular Clouds

Both stars and brown dwarfs form within gravitationally bound molecular clouds comprised of very low density gas molecules, mostly hydrogen, but with some CO, NH_3 and more complex molecular species e.g. ethanol. The clouds also contain a trace, typically 1% by mass, of dust (Ray, 2007). Nearby molecular clouds ($< 500\,\mathrm{pc}$ away) were first identified because the dust within them is sufficient to obscure the view of background stars (Herschel, 1785; Barnard, 1907). This extinction of background starlight by such clouds has since been used to assess their extent and to probe their structure (Cambrésy, 1999; Lada et al., 1999; Lombardi & Alves, 2001; Dobashi, 2005). While the dust content of the clouds can make them dark in the optical and infrared, they are made bright in radio wavelengths by their CO content. CO molecules have proved to be invaluable probes of the gas content of the clouds, yielding information on gas temperature, composition and density.

The characteristic properties of molecular clouds have been established by many observations over the past few decades (for a review of the findings of these studies see Shu et al. (1987); Williams et al. (2000); Ray (2007); Bergin & Tafalla (2007) and references therein). Molecular clouds are categorised as either small or giant. These categories are not merely an arbitrary division. They are based on the observation that the vast bulk of clouds have characteristic sizes and masses that fall within the limits of each category, and only a very few have interim sizes and masses. While they are distinguished in terms of their size and mass, they also exhibit large differences in other properties. A typical giant molecular cloud (e.g. Orion) has a size of up to 100 pc across and contains between 10^5 to 10^6 $M_\odot$. Small molecular clouds (e.g Taurus-Auriga) only extend up to about 30 pc, and have a mass range from 10^3 to 10^4 $M_\odot$. The small and giant clouds also have distinct and different distributions. Giant molecular clouds are only known to occur in the spiral arms of the Galaxy, whereas small molecular clouds have been observed in both the spiral arms and the regions between the arms. The temperature of the gas molecules in small clouds is in the region of 10 to 30 K, whereas giant clouds are observed to have temperatures in the region of 50 to 100 K. The temperature of the dust, in each category of cloud, will be in the same range as the gas, but may be slightly different. Gas and dust in the cloud has a number density of the order of 100 cm^{-3} (Shu et al., 1987; Bergin & Tafalla, 2007).

Although gravitationally bound to itself, a molecular cloud may be supported against collapse by its temperature and/or magnetic fields. In order to compress its gas and dust to the density of a star, parts of the cloud must become unstable to gravitational collapse.

Gravitational Collapse And Contraction

Our knowledge of the properties of molecular clouds have been derived from observations. By contrast, our understanding of the initial stages of gravitational collapse have been led by theory. The first theories developed by Larson (1969) and Hayashi (1970) outlined the main features of the collapse and contraction process. Subsequent modifications, e.g. those of D'Antona & Mazzitelli (1985); Chabrier & Baraffe (2000); Siess et al. (2000), have refined and expanded the theories, but the overall picture they provided, described below, remains essentially unaltered.

In order to become unstable to gravitational collapse, regions of higher density must develop within a cloud. Such regions may be the result of external influences, e.g. a shock wave from a supernova, or dynamic interaction between substructures within the cloud (Ballesteros-Paredes et al., 2007; Preibisch & Zinnecker, 1999). Once a high density region contains a core of material more massive than the Jeans mass, and in the abscence of magnetic fields, the self gravity of the core is sufficiently strong to overcome the pressure forces within it. The entire core is pulled in on itself, and the process of star formation begins.

Material throughout the entire core initially begins to free-fall inwards. The density at the centre rises, while the density near the edge of the core decreases. This introduces a pressure gradient which slows the collapse in the outer regions of the core to less than the free-fall rate. Hence, the collapse of the core effectively proceeds from the inside out, as only the material nearest the centre collapses inwards at the free-fall rate. As the density increases, this compresses and heats the gas and dust at the centre. At the same time, energy is transferred from gas to dust via collisions, and radiative cooling of the dust inhibits the rise of temperature in the centre of the core. As long as the temperature in the centre remains low enough, there is insufficent thermal pressure to resist the compression of more gas and dust into it. This situation changes once the density of dust at the centre increases to the point where its bulk opacity becomes sufficient to prevent radiative cooling. Once this occurs the temperature rises to about 200 K, at which point the thermal pressure within the centre is enough to support it against further gravitational collapse. This now defines a surface around a central object which is in a state of near hydrostatic equilibrium. Material still falls onto the central object, but it is now halted at the surface and the resulting shock heats it, before it passes through at a much reduced velocity.

The rapid collapse at the centre of the core may have been halted, but the central object is still accumulating mass. This increases its self gravity, so the central object continues to contract. The increased compression within the central object also continues to raise its temperature.

In high mass stars, so much material has already been compressed into the central object at this point that its temperature gets high enough to initiate hydrogen burning. In terms of the Hertzsprung-Russell diagram, as

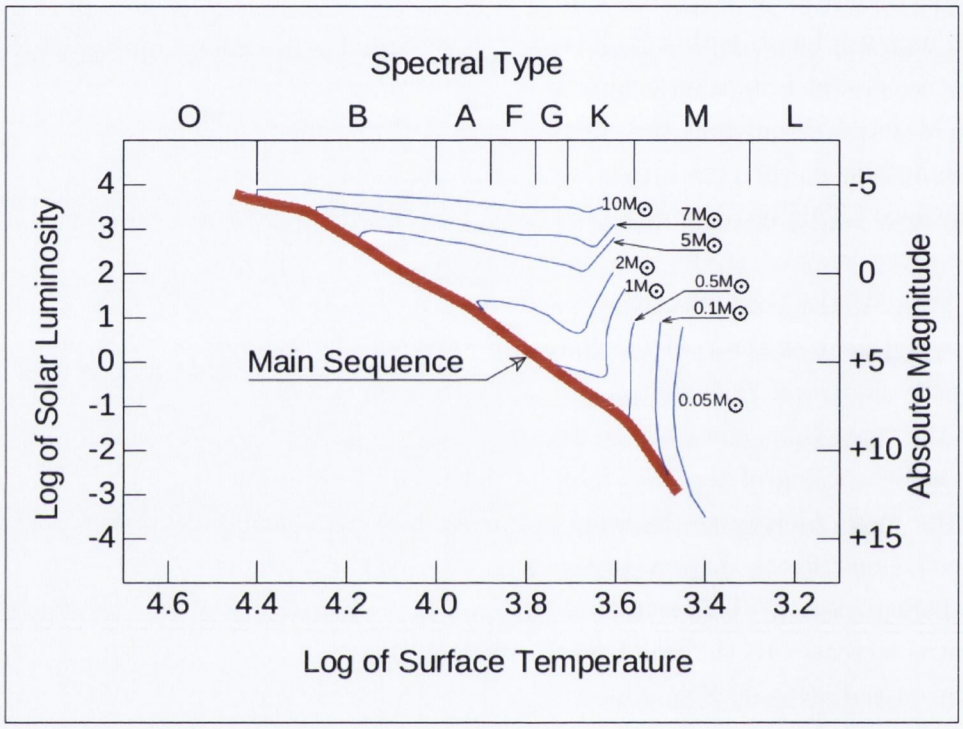

Figure 1.2 Evolutionary tracks in the Hertzsprung-Russell diagram for protostars of 10, 7, 5, 2, 1, 0.5 and 0.1 $M_\odot$ and a brown dwarf of 0.05 $M_\odot$. The tracks shown are adapted from the works of Iben (1965); Hayashi (1970); D'Antona & Mazzitelli (1985); Chabrier & Baraffe (2000); Siess et al. (2000). They start from the points after initial collapse of the molecular cloud where a central object in near hydrostatic equilibrium has formed in each core. The brown dwarf track can be seen to miss the end of the Main Sequence.

illustrated in Fig 1.2, where the tracks shown are adapted from the works of Iben (1965); Hayashi (1970); D'Antona & Mazzitelli (1985); Chabrier & Baraffe (2000); Siess et al. (2000), such stars begin to proceed on a nearly horizontal track towards the Main Sequence very soon after their central object develops, i.e. before they have accreted most of the material from the core envelope. In lower mass stars, this process does not begin until most of the material has accreted onto the central object. Convection from centre to surface slows the rise of the central temperature. They continue to shrink in volume while maintaining their surface temperature. Their surface area is therefore decreasing while their surface temperature does not change. Hence their luminosity decreases, while their colour remains the same. So on the Hertzsprung-Russell diagram, as in Fig 1.2, these objects proceed on a mostly vertical track from the start of their pre Main Sequence phase down towards the Main Sequence. Some of them will begin to burn hydrogen at their centre before arriving at the Main Sequence and so they trace a short horizontal track just prior to arrival. The lower the mass of the object, the shorter the horizontal track. The lowest mass stars arrive at the Main Sequence having followed the nearly vertical track only. The track of a brown dwarf will follow a path parallel to that of the lowest mass star, but, as shown in Fig. 1.2, does not arrive at the Main Sequence.

Rotation And Disks

The presence of rotation in a molecular cloud introduces a complication into the process of gravitational contraction and collapse. The gravitational field of a collapsing molecular cloud exerts a force which is directed radially inwards towards its centre. Any rotation present in the cloud exerts a centrifugal force which is directed radially outwards from the centre, varying from zero at the the poles of rotation to a maximum at the equator. Hence, in a reasonably uniform, gravitationally collapsing, rotating molecular cloud the resultant net inward force is greater at the poles than at the equator. As a result, during the collapse of a molecular core a rotating disk of material forms around the young stellar object at its centre.

The disk mediates the accretion process. Once it has formed, infalling material in the envelope of the core accretes firstly onto the disk, and from there onto the surface of the newly forming star (Dullemond et al., 2006). As noted by Natta et al. (2006) such accretion disks have become part of the

accepted paradigm of star formation although much is still unknown about their physical properties.

Outflows

Subsequent studies of the T-Tauri stars, first described by Joy (1945), have shown that there are outflows of material emanating from them (for a review of such studies, see Ray (2007) and references therein). Their existence was not predicted by any star formation theory, but observations have established that they are a feature of the early stages of star formation (Bally et al., 2007). Such outflows further add to the complexity of the star formation process.

The predominant factor in star formation is the gravitational contraction of material into the centre of a molecular core. Outflows, and accretion disks, in young stellar objects show that this process does not result in a straightforward compression of material into a sphere. Instead, infalling material from the envelope of a core is accreted onto a complex rotating system. Much of it settles into an orbit around the centre, forming a disk. From there it accretes onto the surface of the young star. A portion is removed from the system by an outflow, and never reaches the surface of the star.

Stages of Protostellar Evolution.

Models indicate that a star with a surface temperature of several 1,000 K and a radius of less than 0.01 au will have formed from a molecular core with a temperature of around 30 K and an extent of several 1,000 au (André et al., 1993). As this cold, extended object evolves into a hot, compact object, via the processes described above, it passes through several distinct stages. Each stage is characterised by the relative importance of the various factors, e.g. growth of a disk, strength of an outflow, at that point in the process.

Class Differences

Observations of the differences in spectral energy distributions (SEDs) of pre Main Sequence stars, from optical to mm wavelengths, led to them being classified into groups. The original classifications were Class I, Class II and Class III (Lada, 1987). These classes are now understood as representing

different phases of evolution. Subsequent discovery of objects with another class of spectral energy distribution, representing the earliest phase, resulted in the definition of Class 0 objects (André et al., 1993). The different phases of star formation that these classes represent are illustrated schematically in Fig. 1.3. A schematic sketch of the different classifications of spectral energy distributions associated with each phase is shown in Fig. 1.4. A Class 0 object has a distribution which closely resembles a blackbody peaking in the sub-mm range. A much broader distribution, extending to the shorter wavelegth side of the Class 0 peak, is the hallmark of a Class I object. The characteristic Class II distribution is narrower, and can be characterised as a composite of a blackbody spectrum, peaking in the near-infrared, with excess emission in the mid-infrared wavelengths superimposed. A Class III distribution closely resembles a blackbody, but with a much higher temperature than a Class 0 distribution. In the case of a low-mass star or brown dwarf, a Class III object distribution peaks in the near-infrared.

In the Class 0 phase, as a molecular core collapses, from the inside out, an envelope of infalling material is left surrounding an accreting system at the centre. The envelope contains more material than the newly developed accreting system. The dust in the envelope is sufficiently dense to obscure the view of the centre at optical, infrared and sub-mm wavelengths. As a result, the only contribution to the Class 0 spectral energy distribution across these wavelengths is from the outer layers of the cold and dusty envelope. Hence the characteristic spectral energy distribution resembling a blackbody with a temperature of between 15 and 30 K, as depicted in Fig. 1.4. The system embedded in the centre of a Class 0 object already has all the features of a young stellar object. A protostar is surrounded by an accretion disk. Material from the envelope accretes onto the disk and from the disk onto the protostar. Outflows have developed over the poles of the protostar, removing both material and angular momentum from the system. As the envelope obscures any optical or infrared view of these features, their presence has to be confirmed via radio observations, typically at cm wavelengths (e.g. see AMI Consortium: Ainsworth et al. (2012) and references therein). This phase is very short lived (of the order of a few 10^5 years) and Class 0 objects are correspondingly rare.

The subsequent Class I phase occurs when more of the mass is concentrated in the central object and accretion disk than in the envelope. The

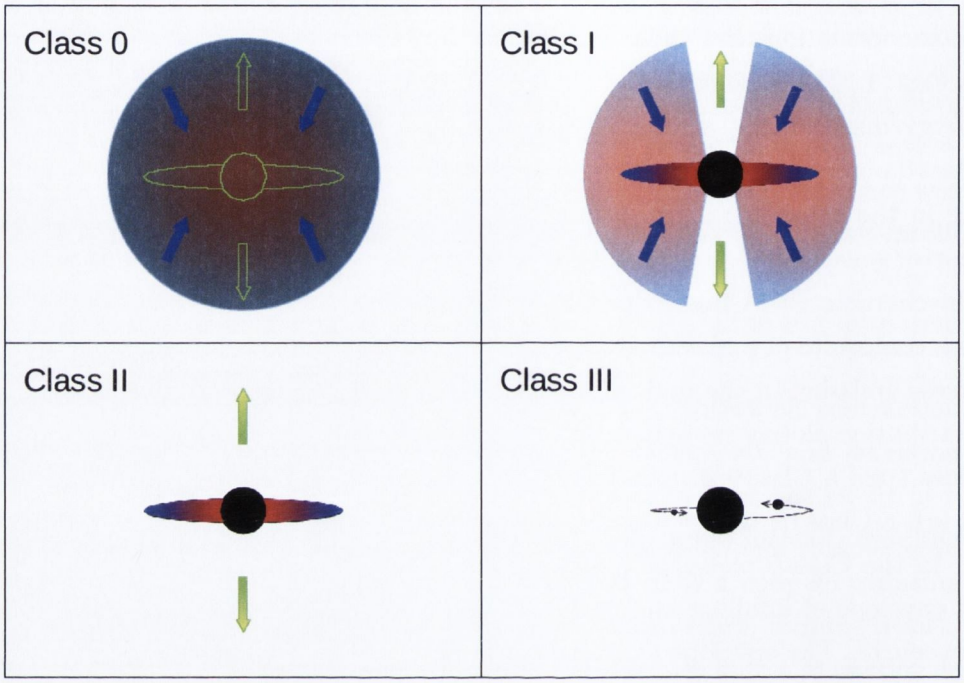

Figure 1.3 Schematic illustration of the different phases of star formation and the classification of young stellar objects. In the Class 0 phase, collapse of a molecular core has occurred, from the inside out. An envelope of infalling material surrounds a system at the centre which is accreting from it. Most of the material in the system is still in the envelope at this stage, obscuring the view of the centre. By the Class I phase, most of the mass is concentrated in a central object and accretion disk. Material from the envelope accretes onto the disk and from the disk onto the central object, while an outflow removes some material from the system. The much diminished envelope no longer obscures the system at the centre to the same extent as before. When the Class II phase has been reached, the star at the centre has already accreted most of the mass that it will ever accumulate. The envelope has now been either accreted onto the disk and star, or dispersed by the outflow. At this point the star will be visible, and together with its associated outflow, may be classed as a T-Tauri star. The final Class III phase is reached when the inner disk has cleared. Planets may have already formed at this point, and what may remain of the disk will be very tenuous by comparison with the previous stages.

envelope has been diminished by the process of accretion onto the central system, as well as by the outflow. It still retains enough material to obscure the view of the central system, but to a lesser extent than during the Class 0 phase. The Class I spectral signature is a combination of contributions from the diminished envelope and the partly revealed star and accretion disk at the centre.

When the Class II phase has been reached, the star or brown dwarf at the centre has already accreted most of the mass that it will ever accumulate. The material that was in the envelope has now been either accreted, or dispersed by the outflow. The young star or brown dwarf is now visible, as is the hot inner part of the accretion disk. It is during the Class II phase when the view of the central system is no longer obscured that the T-Tauri stage of formation is observed. The spectral energy distribution is now dominated by the black body spectrum of the central object. The hot inner part of the accretion disk contributes an excess of emission in the red and infrared part of the spectrum. It may also have a small amount of excess emission in the ultraviolet and blue, caused perhaps by accreting material impacting the surface of the central object. Overall, the effect is that the spectral energy distribution looks like a blackbody spectrum with excess emission on the long wavelength side of the peak.

Class III objects represent the last stage in this evolutionary sequence. Such objects do not have a hot dusty inner disk, but may well yet have a disk of cold material further out from the star. In star forming terminology, a Class II object is regarded as possessing a disk, while a Class III object is generally referred to as being without a disk, even though this only pertains to the hotter inner part of any such disk. The spectral energy distribution of a Class III object closely resembles a blackbody and it is effectively the spectrum of the hot central object, be it star or brown dwarf, only. Contributions from any other source e.g. planets or cold outer disk, are negligible, if they are present at all. As the lowest mass stars and young brown dwarfs have surface temperatures in the range of 2,000 to 3,000 K, this blackbody spectrum peaks in the near-infrared.

Deuterium Burning

The summary of star formation outlined above makes no mention of deuterium burning. This is because as far as star formation is concerned it

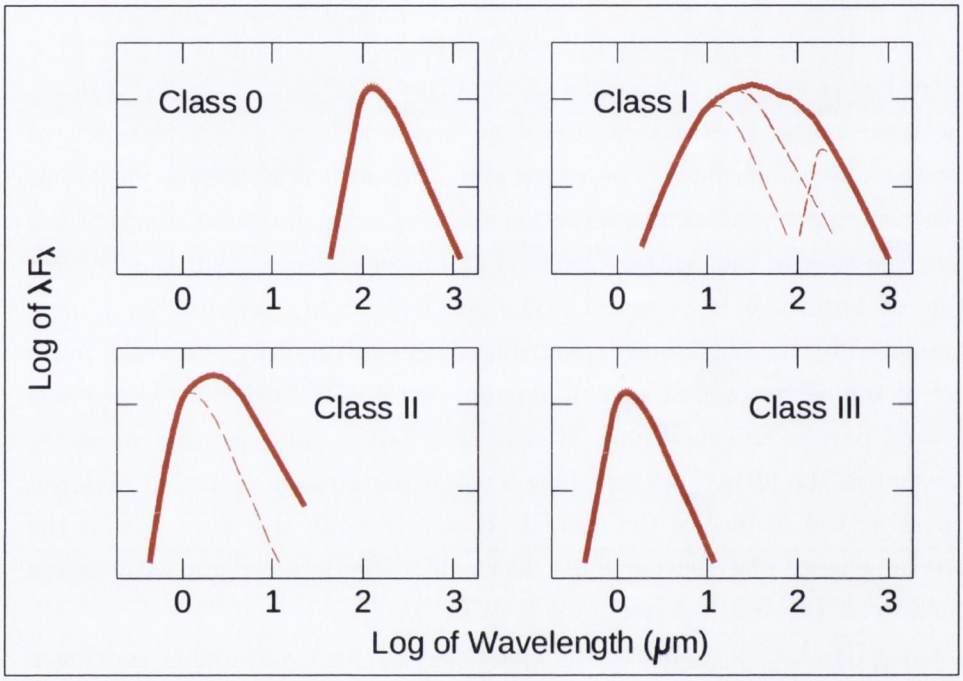

Figure 1.4 Schematic sketch of the different classifications of spectral energy distributions of young low-mass stars and brown dwarfs. The Class 0 spectrum closely resembles a low temperature blackbody distribution. The Class I spectrum exhibits a much broader distribution, extending to shorter wavelengths. It is a combination of contributions from the spectra of the partly revealed central object, the accretion disk and the remaining portion of the envelope (represented by the dashed lines going from left to right). The Class II spectrum can be regarded as a composite of a blackbody spectrum peaking in the near-infrared (shown by the dashed line), plus an excess of emission in the mid-infrared wavelengths. The Class III spectrum closely resembles a blackbody distribution, peaking in the near-infrared.

is of little importance. During the pre Main Sequence contraction phase, and if there is sufficient mass present, the central temperature does get high enough to initiate deuterium burning. The fraction of deuterium in the central object is very small, and so the deuterium burning is completed very quickly. In the greater scheme of star formation, it barely affects the evolution of the star, and does not significantly impede the process of gravitational contraction towards the Main Sequence (Chabrier & Baraffe, 1997, 2000). In a brown dwarf, the deuterium burning is also not sufficient to support it against further collapse, but it can significantly affect its luminosity for several hundred million years (Burrows et al., 2001). Yet again this raises the question of a minimum mass, only this time its the minimum mass for deuterium burning that is under consideration.

Current models, such as those developed by Burrows et al. (1997, 2001), have placed this minimum mass at around $0.013\,M_{\odot}$. An object less massive than this simply cools after formation and does not go through any significant nuclear fusion phase. The evolution of the luminosity of a series of model objects ranging from low mass stars into the brown dwarf mass regime and down below the mass limit for deuterium burning is illustrated in Fig. 1.5. The objects that are not massive enough to burn deuterium are in the mass range of the gas giant planets that have been observed orbiting stars.

1.4 Theories of Brown Dwarf Formation

The first confirmed observation of a brown dwarf occurred in 1995 (Nakajima et al., 1995) and was soon followed by many others (see Oppenheimer et al. (2000) for a review of these early discoveries). Since then, several hundreds have been identified, including populations of brown dwarfs in star forming regions and young open clusters (see Briceño et al. (2007); Luhman (2012) and references therein). The issue of whether or not brown dwarfs can form has been settled. The question of how they form is still very much open.

Those questions are held open by the results of observations of giant molecular clouds. These clouds, now established as the site of formation for large populations of stars, have been found to have average Jeans masses that are too high to allow brown dwarfs to form in the same way as stars. Summing up the conundrum, Mohanty et al. (2009) stated "The central

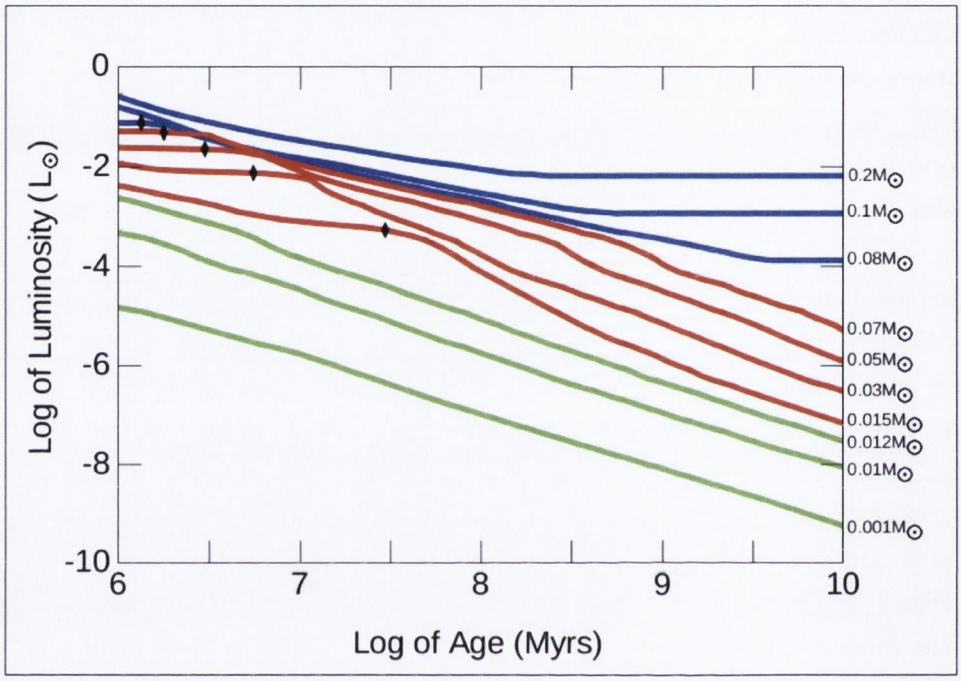

Figure 1.5 Evolution of the luminosity of low mass stars (blue), brown dwarfs (red) and planets (green) between 1 Myr and 10Gyr after formation, adapted from the work of Burrows et al. (2001). The luminosity of each star stabilises and remains constant once it has evolved onto the Main Sequence, the lowest mass star taking longest to reach this point. The planets have no significant contributions to their luminosity from nuclear reactions at any stage, and their tracks decrease steadily. The brown dwarfs show a distinct plateau in their luminosity for up to several tens of Myr, during the time they burn deuterium. The same effect can be seen in the youngest part of the evolutionary track of the lowest mass star ($0.08\,M_{\odot}$). Once the deuterium has been burned the brown dwarfs continue to cool, eventually parallelling the paths of the planets. The diamonds mark the point when 50% of the deuterium has been burned in that object.

dilemma of brown dwarf origins is easily framed: The very low Jeans mass required to form brown dwarfs implies gas densities far in excess of the mean in molecular clouds". This dilemma is a serious obstacle to our understanding of how populations of brown dwarfs can form. Do molecular clouds have denser and colder regions than observations indicate? Do other factors reduce the Jeans mass? Or do brown dwarfs form in a different manner to the stars?

Several theories have been developed that detail different ways in which brown dwarfs may form. Each one seeks to find ways around the problems outlined above. The theories are not necessarily mutually exclusive. Brown dwarfs may form by several means, and some processes may be more significant than others. The main theories proposed are outlined below.

Ejection from a stellar mass core via dynamic interactions

In this scenario, stellar mass cores can form, but isolated brown dwarf cores cannot. However, dynamic interactions with other objects, in multiple systems, in the star forming cluster can cause the ejection of a central object from its stellar mass core. The central object is then removed from the reservoir of gas and dust from which it was accreting and can no longer acquire enough material to reach the mass of a Main Sequence star. When this theory was first developed, the results of modelling it indicated that objects formed in this way would typically have a higher dispersion velocity than other members of the cluster (Reipurth & Clarke, 2001). If a population of very low mass members of a cluster with greater proper motions than the other members were observed, it would be an indication that they had been formed by ejection from a stellar mass core. More recent results (Bate et al., 2003; Bate, 2009) have revised this, and find that objects formed in this way would not have significantly higher dispersion velocities than other cluster members.

Photoevaporation of the outer parts of stellar mass cores by nearby OB stars

As with the ejection concept, this theory envisages a situation where stellar mass cores can form but substellar mass cores cannot. In this case, the accretion process is terminated because photoionising radiation from nearby OB

stars disperses the material in the outer regions (the envelope and disk) of the core, so that it can no longer accrete onto the system at the centre of the core (Hester et al., 2001; Whitworth & Zinnecker, 2004). The central object left behind may then be substellar in mass. Using Hubble Space Telescope observations of photoevaporation in M16, Hester et al. (2001) concluded this was the dominant process for determining the masses of many young stellar objects. Whitworth & Zinnecker (2004) explored this idea further and concluded that it should be a common mechanism for the formation of brown dwarfs. They also noted that brown dwarfs formed by this process should tend to occupy the central regions of large clusters, where the largest concentrations of OB stars have occurred. If photoevaporation is a common mechanism in forming brown dwarfs, then OB associations, such as Upper Scorpius, should contain relatively many brown dwarfs, while there should be a paucity of them in non-OB associations such as Taurus-Auriga.

Fragmentation of massive circumstellar disks

According to this idea, substellar cores can form within the cold outer parts of massive, self-gravitating circumstellar disks. In this location the Jeans mass is much lower than it is in the cloud from which the star has formed. The outer parts of the disk may also be liable to fragment. Once this occurs, it further limits the growth of the cores, as they now have a reduced amount of material available for accretion (Stamatellos et al., 2007, 2011). The fragmentation may occur because the outer parts of the disk are gravitationally unstable. Fragmentation may also be caused by interaction with another star/disk system, or between the objects within the disk itself (Goodwin & Whitworth, 2007), in a process similar to that outlined by Reipurth & Clarke (2001). So any brown dwarf formed may remain bound to the star that provided the natal disk or it may end up free-floating. The simulations of Bate et al. (2002, 2003) showed brown dwarfs forming, mainly from the fragmentation of disks, but their simulation also showed a substantial number of brown dwarfs forming in filaments of gas that had developed in the molecular cloud as it collapsed. These simulations also indicated that brown dwarfs should be more numerous than stars. The effect of radiative feedback on the massive circumstellar disk was, however, ignored in these early simulations. When this factor was accounted for, in the revised simulations of Bate (2009), the number of brown dwarfs produced by this theoretical

formation mechanism was reduced by at least tenfold.

Gravitational fragmentation and compression of the gas caused by star formation in a molecular cloud

In this theory, as developed by Bonnell et al. (2008), based on the results of Bate et al. (2002, 2003), a molecular cloud begins to collapse and forms a cluster of stellar cores within it. At this stage substellar cores cannot form. The gravitational potential of this newly formed cluster then causes filaments to form in the gas and dust that subsequently falls towards its centre. Within these filaments, the gas is compressed and reaches high enough densities that substellar cores can form. Tidal shearing of the infalling filament also disfavours the formation of higher mass cores within it. This new set of low mass and substellar cores continues to fall towards the centre of the original stellar cluster. The high velocity of these new low mass objects relative to the original cluster inhibits their ability to accrete any further material from the reservoir of gas and dust still in the cluster centre. As a result, any cores formed in the filament cannot accumulate as much material as the other objects in the cluster. Thus, in this theory, fast moving filamentary fragments not only provide the conditions in which substellar cores can form, they also inhibit the subsequent growth of these cores, further favouring the production of brown dwarfs. Bonnell et al. (2008) also concluded that such brown dwarfs should preferentially form in regions of high stellar density within any star forming cluster.

These first two theories listed above rely on the interruption of the accretion of material onto the central object of a stellar mass core that would otherwise have become a Main Sequence star. The second two ideas are somewhat different as they rely on the formation of stars to produce localised conditions within which a substellar mass core can form. The one concept they all have in common is that brown dwarfs can only form in the presence of stars. The formation of an isolated substellar mass core is not possible within the framework considered by these four theories.

Turbulent compression and fragmentation

This theory takes a different approach. It holds that the compression and fragmentation of gas in a molecular cloud, due to supersonic turbulence,

produces the conditions in which collapsing cores will cover a wide range of masses *including substellar masses* (Padoan & Nordlund, 2002, 2004; Hennebelle & Chabrier, 2008; Elmegreen, 2011). Turbulent compression proposes the existence of a set of conditions in molecular clouds, such that stars and brown dwarfs are a continuum of objects that can form via the one mechanism. Ergo, the distinguishing feature of this theory with respect to the others is that it modifies the entire star forming paradigm. This theory allows substellar mass cores to form alongside stellar mass cores. It also permits the formation of isolated brown dwarf cores. Some indication that this occurs came with the first spectroscopic confirmation that FU Tau A and B are brown dwarfs that appear to have formed in isolation Luhman (2009). The recent discovery, by André et al. (2012), of an isolated self gravitating core with a mass within the brown dwarf range, is the strongest evidence to date that brown dwarfs can form by this mechanism.

Testing The Theories

The competing theories can be tested by observations of brown dwarfs and low mass stars to see if they have any of the characteristics predicted by the theories (Whitworth et al., 2007). A key relationship for probing many theories is the amount of objects of differing masses in any one association. Observations are only now reaching a stage where tentative conclusions can be reached, but further investigation remains necessary.

1.5 Disks And Planet Formation

Circumstellar disks are the site of planet formation, often being referred to as protoplanetary disks (Blum & Wurm, 2008). On the basis of observations of the planets in our own solar system, theories of planet formation have been developed (Edgeworth, 1949; Safronov, 1969; Weidenschilling, 1977). These theories assume the presence of a circumstellar disk around the newly forming Sun, which contained the material from which the planets formed.

Core Accretion

The terrestrial planets may have formed via core accretion (Pollack et al., 1996). Dust grains in the original disk initially aggregate by adhesion. Once

they have formed objects larger than several hundred metres across, their gravitational strength becomes a significant factor in the accretion of more material. These larger objects continue to grow as they deplete the material in the disk, eventually reaching the sizes of the known terrestrial planets. The exact mechanism is not completely understood (Blum & Wurm, 2008; Dullemond, 2013). In particular, theory does not yet fully account for the growth of objects through every stage from dust particles to planets. Several different theoretical barriers to such growth have been identified, but as pointed out by Dullemond (2013), the presence of planets, asteroids and comets in our solar system shows that, in practice, those barriers are overcome.

The gas giants may also have begun to form in this way (see Chabrier et al. (2007); Lissauer & Stevenson (2007) and references therein). Forming further out than the terrestrial planets, their cores became more massive than the inner terrestrial planets. This occurred, in part, because there were larger reservoirs of dust solids than in the inner regions of the disk. Beyond the distance from the Sun at which ices could condense - the frost line - there were also icy solids present that could stick to any newly forming core. Lissauer & Stevenson (2007) also notes that massive cores should only form in a region where the Kepler shear environment is low, i.e. several au from the Sun, while Thommes et al. (2003) has shown that conditions beyond 20 au should also not be favourable to the formation of massive cores. These rock/ice cores became massive enough to gravitationally accrete some of the gas in the disk. In the case of Jupiter and Saturn, the gas eventually became their biggest component, outstripping the mass of the rocky core. As noted by both Chabrier et al. (2007) and Lissauer & Stevenson (2007), the gas giants have to form beyond the frost line and cannot form close in to their host star. For the same reason they are unlikely to have formed on eccentric orbits that take them inside the frost line. Models of dynamic interactions in the early stages of the formation of multi planet systems have also indicated that planets are more likely to form on stable circular orbits (Lissauer & Stevenson, 2007).

Strange New Worlds

Overall, these theories work well to explain the formation and distribution of planets and other objects in our solar system. Other stellar systems

cannot be so neatly explained. Since Mayor & Queloz (1995) discovered a planet orbiting the star 51 Peg, nearly a thousand other planets have been identified (Schneider et al., 2011; Wright et al., 2011; Akeson et al., 2013). These observations have revealed an unexpected diversity among planets and planetary systems, a diversity which challenges core accretion models. A significant number of gas giants orbit close in to their host star, most with very eccentric orbits (Lissauer & Slartibartfast, 2008), while some gas giants orbit out beyond 40 au (Marois et al., 2010).

The picture that is currently emerging from these observations is that the formation of planets around stars is a ubiquitous and robust process. The wide variety of planets, and planetary systems, that form, cannot be fully explained by the core accretion theory, which was developed to explain our own planetary system.

Gravitational Instability

Alongside the core accretion theory, a second theoretical mode of formation for gas giant planets in circumstellar disks has been developed. This theory proposes that gravitational instabilities can form in massive and wide disks, giving rise to fragmentation of the disk into the precursors of gas giant planets (Durisen et al., 2007; Vorobyov & Basu, 2010; Boss, 2011; Vorobyov, 2013).

As well as offering an explanation for the formation of gas giant planets on wide orbits, gravitational instability models also show planets forming faster than core accretion models. The speed with which planets are formed in a circumstellar disk has been another problem for core accretion models (Durisen et al., 2007). Planets need to form before the disk disperses, and observations indicate that disk lifetimes are typically in the 5 Myr range (Haisch et al., 2001). Core accretion models typically show that gas giant planets cannot form within this timescale, whereas gravitational instability models indicate that they can (Durisen et al., 2007).

This idea was developed to explain the presence of gas giant planets around stars. It is effectively the same as the disk fragmentation model developed to explain the existence of brown dwarfs. In modelling the formation of gas giant planets Vorobyov (2013) found that objects up to $0.04\,M_{\odot}$ could be formed. In modelling the formation of brown dwarfs Stamatellos et al. (2011) found that objects down to $0.005\,M_{\odot}$ could be formed. From the

point of view of "planet formation" theories, brown dwarfs represent the high mass extreme. From the point of view of brown dwarf formation, planets represent the low mass extreme. This makes brown dwarf formation a perfect testbed for the limits of planet formation. It also raises the question of one more extreme. What is the lowest mass object that can have a disk in which a planet can form?

Circumsubstellar Disks And Planet Formation Around Brown Dwarfs

The presence of disks around brown dwarfs has been established (Natta & Testi, 2001; Natta et al., 2002). The presence of planets around brown dwarfs has also been established (Chauvin et al., 2004; Todorov et al., 2010). This brings a new level of complexity to the overlap between the formation of stars, brown dwarfs and planets. Are brown dwarf disks simply low mass analogues of stellar disks, as they are most likely to be if brown dwarfs form via turbulent compression and fragmentation? Do they evolve in the same way as disks around stars? Can they be massive enough to give rise to gravitational instabilities?

This makes brown dwarf disks ideal objects for testing the mass dependence of several of the critical parameters in stellar, and planetary, evolution (Ricci et al., 2012; Dawson et al., 2013). One of those parameters is the lifetime of a circumsubstellar disk, an important constraint for the core accretion theories of planet formation. Disk lifetime is affected by a number of physical processes, e.g. ionisation by the central object and cosmic rays, accretion, grain growth (Dullemond et al., 2007). Our understanding of the relative importance of these processes and how they change with object mass is still incomplete, so observational guidance is important for advancing the theory.

These topics can best be probed by investigating populations of stars and brown dwarfs that are young enough to still retain some disks. If the proportion of disks around both is the same, then this is an indication that they have similar origins and lifetimes. If disks around brown dwarfs and stars share significant characteristics, this indicates that they may evolve in a similar fashion. In order to get statistically robust results from any study of disks, the sample populations of stars and brown dwarfs examined should be as large as possible. In order to be able to make reliable comparisons of

disk lifetimes, the stars and brown dwarfs in the sample should be coeval.

Young clusters, associations and star forming regions, contain coeval populations of young stars and brown dwarfs, a proportion of which still retain their disks. Therefore, the nearby young clusters are the best observational laboratories known for testing and investigating the extremes of disks and planet formation. In this work, I examine the brown dwarf population of Upper Scorpius, and detail some discoveries that are helping to explore the limits of star, brown dwarf and planet formation.

The study of young clusters, particularly rich clusters with large populations, also offers one other advantage in the continuing effort to advance our knowledge of substellar objects. It is the best way to investigate how populous brown dwarfs are, and how their numbers compare to those of the stars.

1.6 The Initial Mass Function

From the first graphs of Hertzsprung (1911) and Russell (1914), observations have consistently shown that stars on the lower part of the Main Sequence are more numerous than those on the higher part. Once it was understood that the position of a star on the Main Sequence is a function of its mass, it was evident that there are more low mass stars than high mass stars. This had implications for star formation theory. Was this a random distribution of masses, or did the star formation process favour the production of low mass stars? Are more low mass stars observed simply because they remain on the Main Sequence the longest?

Smooth And Universal

Investigating these topics, Salpeter (1955) found that the distribution of masses among Main Sequence stars was not random, but could be described by a "smoothly varying function". Salpeter (1955) also deduced the existence of an "original mass function", now referred to as the Initial Mass Function (IMF). The IMF describes the distribution of masses among all stars that have formed, including those that have evolved off the Main Sequence.

The usefulness of the IMF is that it provides an empirical constraint which any star formation theory has to account for. A theory which pre-

dicts relative abundances in different mass ranges which do not match the observed IMF is not plausible. Emphasising the importance of the IMF, in the above context, Jeffries (2012) refers to it as "the most fundamental output and diagnostic of the star formation process". A little more poetically, Chabrier (2005) stated that determining the shape of the IMF is "one of the holy grails of astrophysics".

Salpeter (1955) established its shape for field stars greater than about $1\,M_{\odot}$. At this stage, it is well established and constrained down to about $0.5\,M_{\odot}$. Its shape is often expressed as either a multiple-part power law (Kroupa, 2001), or a log-normal distribution (Chabrier, 2003), although whether either of these expressions offer a completely satisfactory description of the IMF is still a matter of debate (Jeffries, 2012). Studies of different samples of stars in this mass range have also consistently shown that the shape of the IMF appears to be universal, and does not vary, despite the variety of conditions and environments within which stars have formed (Kroupa, 2001, 2002; Chabrier, 2003; Bonnell et al., 2007; Hennebelle & Chabrier, 2008).

The Low Mass Part

In comparison to the range above $0.5\,M_{\odot}$, determining the shape of the low mass part of the IMF, particularly in the substellar domain below $0.08\,M_{\odot}$, has proved to be more challenging, as very low-mass stars and brown dwarfs are comparatively faint and harder to detect. This part of the IMF may bear the imprint of some of the different theoretical brown dwarf formation processes. Hence, in contrast to the apparent universality of the higher mass IMF, there could be significant variations in the form of the IMF below about $0.3\,M_{\odot}$, among different populations of brown dwarfs, formed under different conditions. So, to test the different theoretical modes of brown dwarf formation, it is essential to carry out surveys for brown dwarfs in diverse environments.

The form of the low mass part of the IMF has not yet been successfully determined and various approaches have been used to tackle the problem (see Jeffries (2012) and references therein). One approach is to take a census of objects in the solar neighbourhood, where even the low mass stars should be detected, despite their relatively low luminosity. Such surveys have the advantage of being complete down to the lowest stellar masses, *(but not*

substellar masses), within a limited distance of the Sun. This restricts the size of the sample of stars that can be used. Wide-field and pencil beam photometric surveys can investigate more than just the local stars, but other factors have to be taken into account, e.g. how extinction varies with distance, when assessing the results. All of these approaches rely on using the luminosity of a star as a proxy for its mass. This works well for Main Sequence stars, as there is a clearly defined, and long term, relationship between their luminosity and mass, as exemplified in Fig. 1.5. This is not the case for brown dwarfs. The luminosity of a brown dwarf varies greatly over time (as also shown in Fig. 1.5) and cannot be used as a reliable proxy for its mass, *unless the age of the brown dwarf is known.* As a result, a useful approach to take, as noted by Chabrier (2003), to try and determine the substellar IMF, is to examine populations of brown dwarfs in young clusters and associations of known age.

Determining and comparing the IMF of different young clusters is also the only useful method for searching for variations in the IMF. The IMF of the low mass stars and brown dwarfs in the field is a composite and an average of every local IMF that has occurred over the lifetime of the galaxy. The form of each historic and local IMF that contributes to the field IMF cannot be distinguished. Even if they could, there is no adequate record of the star forming environments associated with each. To determine if the IMF varies from one star forming event to another, several different clusters have to be analysed. To determine if any variation found is a function of environment, the clusters have to be of different types.

A Robust Parameter

The paucity of statistics for low mass objects in young clusters to date, combined with uncertainties in the relationship between the mass and luminosity of young objects makes it difficult to ascertain the precise IMF of a young cluster. This has made it impractical to tightly constrain any low mass IMF in terms of either a multiple part power law, or a log-normal distribution. This compounds the difficulty of comparing the IMF of one young cluster with another. To get around this limitation, the practice of parameterising the low mass IMF in terms of a ratio of stellar to substellar objects has been developed (Chabrier, 2003; Andersen et al., 2008; Mužić et al., 2013). The results are more general and not as fine, but provide a more reliable and

robust indicator of the underlying IMF. Any advance in constraining this ratio for any cluster can also facilitate a meaningful comparison of the IMF of that cluster with another. Using this method, the results of my investigation of the Upper Scorpius star forming region, described in the following chapters in this thesis, suggest that the brown dwarf IMF is a function of environment.

In terms of probing the IMF, and investigating brown dwarf disks, both of which are invaluable tools for testing formation theories, there are significant advantages to observing brown dwarfs in young clusters.

1.7 Brown Dwarfs In Young Clusters

Searching for brown dwarfs in young clusters also takes advantage of the feature demonstrated by Hayashi & Nakano (1963). Brown dwarfs are at their brightest when they are young. In terms of the Hertzsprung-Russell diagram, as in Fig 1.2, a young brown dwarf that is still on the nearly vertical track, is at its most luminous. During the early part of this phase, its luminosity will even be greater than that of low mass stars on the Main Sequence. So star forming regions, and young clusters, are favourable locations for detecting and observing brown dwarfs.

A further significant advantage of taking this approach is that the stars in the cluster can be used to gauge its age and distance. The age of a young cluster is usually derived by assessing the latest type of stars to have arrived at the Main Sequence, e.g. as done by Pecaut et al. (2012) to assess the age of the Upper Scorpius association. Hence, in a cluster, where all the objects are coeval, the age of the brown dwarfs can be determined with confidence. The distance to a young cluster is best obtained from the parallax of its higher mass stars, which, on account of their greater luminosity, facilitate the most accurate measurements. Thus, it is possible to assess the age and distance of a brown dwarf in a cluster, *without reference to the brown dwarf itself.*

Photometric Surveys

Searching for brown dwarfs in young clusters also has its own challenges. Nearby young clusters, which contain the brown dwarfs with the brightest apparent magnitude, typically cover large areas of the sky. As a result,

identifying their brown dwarf members necessitates the use of large scale photometric surveys. The brown dwarfs then have to be distinguished from a much larger amount of other objects recorded in the survey.

Optimal Wavelengths For Photometric Surveys Of Brown Dwarfs And Their Disks

Because of their low temperatures (between 2,000 to 3,000 K), the most suitable wavelengths at which to observe brown dwarfs are in the near-infrared ($\sim$ 0.8 - 2.5μm). Most of the flux from the photosphere of a brown dwarf is emitted in this wavelength range. The availability of wide-field near-infrared surveys such as the 2 Micron All Sky Survey (2MASS) and the United Kingdom Infrared Deep Sky Survey (UKIDSS) now facilitates the observation and identification of brown dwarfs in nearby young open cluster and star forming regions.

Brown dwarf disks, at least of the ages considered here, mainly emit reprocessed light from the photosphere. Hence they are cooler than the photosphere and mostly emit at longer wavelengths (Scholz et al., 2007). Most emission from a hot, dusty, inner brown dwarf disk is in the mid-infrared range ($\sim$ 3 - 30μm). Being hotter than the disk, the photosphere does also emit in the mid-infrared, but as the surface area of a hot inner disk is very much larger than the photosphere, emission in the mid-infrared will be dominated by that of the disk. Mid-infrared observations from Earth are beset with more problems than near-infrared observations. Space based mid-infrared observatories are more effective at conducting large scale surveys. The recent completion of the all sky catalogue of the Wide-field Infrared Survey Explorer (WISE) has provided researchers with a database of mid-infrared photometric information perfectly suited to the identification of disks around nearby young brown dwarfs.

Photometry And Colour-Magnitude Diagrams

The location of young brown dwarfs in a colour-magnitude diagram is the key to their identification in any large scale photometric survey. As Figs. 1.1 and 1.2 indicate, brown dwarfs are typically both red and faint by comparison with Main Sequence stars. If an appropriate colour-magnitude combination is used, then this location may be predominantly populated by brown dwarfs,

and be distinct from the population of other objects in the same diagram. The position of a young brown dwarf will depend on its mass, age and distance.

Photometric Criteria

An advantage of searching for brown dwarf members of one association is that it simplifies the quantification of their position on a colour-magnitude diagram. As they are at the same distance and are coeval, they should form a sequence of objects clustered along an isochrone for objects of differing mass, but similar age and distance.

Theoretical model atmospheres have been developed, from which theoretical isochrones can be derived and plotted on colour-magnitude diagrams. This work uses isochrones based on the DUSTY model atmospheres developed by Chabrier et al. (2000). To get the best possible match between observational data and the theoretical model atmospheres, the isochrones used in this work were tailored to the specific filter profiles of the observing instruments used.

The vast bulk of point sources recorded in any large scale photometric survey will be Main Sequence stars. In the best situations, the different intrinsic magnitudes and colours of a population of young brown dwarfs may be enough to distinguish them from Main Sequence stars. The situation can be complicated by the presence of dust clouds in the search area. Reddening caused by extinction shifts the position of objects to the right and down on colour-magnitude diagrams. This can blur the distinction between brown dwarfs and heavily reddened Main Sequence stars. The problem can be avoided by confining search areas to regions of very low extinction. One of the advantages of conducting a search in Upper Scorpius, as detailed in the following chapters, is that it contains large areas with negligible extinction.

Proper Motion And Cluster Membership

Distinguishing asymptotic giant branch (AGB) stars from young brown dwarfs is more problematical. They have similar surface temperatures and colours to brown dwarfs. Although they have much greater intrinsic luminosities, if they are sufficiently distant their apparent luminosity may well be similar to that of brown dwarfs in the survey area. Red quasars or un-

resolved red galaxies that have photometric characteristics consistent with a nearby brown dwarf pose the same problem. In a large scale photometric survey, the most efficient way of distinguishing such objects from nearby young brown dwarfs is to examine their proper motions. Proper motions of objects in a sample are usually graphed on a vector point diagram, a convention which this work follows. As these objects are so distant their proper motions will be either at, or close to zero, and on a vector point diagram they will be clustered about the origin. If the cluster under investigation has a sufficiently large proper motion, its brown dwarf members should stand apart from any such objects in a vector point diagram (Lodieu et al., 2006, 2007; Bouy & Martín, 2009; Dawson et al., 2011; Casewell et al., 2012). In ideal circumstances, a sample of objects taken from a nearby star forming region that are a good photometric match for young brown dwarfs will be found to contain very few objects with minimal proper motions.

Vector point diagrams do more than just filter out the distant red objects. Members of the one association should predominantly be clustered around the one position, as they share a common proper motion with respect to the Sun. Other objects that may be scattered around the graph are most likely non-members and can be disregarded. Objects with large proper motions are likely to be faint objects, e.g. Main Sequence red dwarfs, or evolved brown dwarfs, that are in the foreground. There is always the possibility that an object that is not a member may in fact share a similar proper motion, thereby contaminating the sample. It should still prove possible to identify a sample of brown dwarf members of an association with confidence, as long as the vector point diagram shows that the number of such potential contaminants is low.

Spectroscopic Surveys

Spectroscopic follow-up is a pre-requisite for studies on the formation and early evolution of brown dwarfs. A brown dwarf may be identified by its photometry and proper motion alone, but full and complete confirmation that it is a brown dwarf requires an examination of its spectrum, and the determination of its spectral type. It is impractical to take spectra of all possible brown dwarf candidates identified from photometric surveys, due to the time involved. Spectroscopic surveys of a subset of such candidates can, however, verify the results of photometric surveys and quantify their

reliability, and the level of contamination (if any) in the larger photometric sample. As brown dwarfs continuously cool as they evolve, they migrate through later and later spectral types. Young brown dwarfs, therefore, have the earliest possible types that a brown dwarf can have. A young brown dwarf is expected to have a spectral type of M6 or later (Martín et al., 1996; Luhman et al., 1998; Scholz et al., 2009).

Early type stars have their spectral types determined on the basis of features in their optical spectra. For later type objects, which are redder, the usable features are confined to regions of longer wavelengths. Brown dwarfs can have their spectral types determined using features in their optical spectra (notably the TiO and VO features in the $\sim$ 0.7 - 0.8μm range), but these spectra are time consuming to obtain (Lodieu et al., 2006). It is generally more efficient to take near-infrared spectra of brown dwarfs.

Near-infrared spectral typing of brown dwarfs is still in its early stages. Methods of assigning spectral type based on near-infrared spectral features are still being developed. The accuracy and reliability of these methods is not yet fully determined. In the case of young brown dwarfs, one critical factor, which is not yet fully accounted for, is the effect of disks and accretion processes, and reddening, on their spectral features. The reliability of spectral typing in the substellar mass regime is dependent on successfully identifying any such effects, and quantifying the extent to which they distort the spectrum of a brown dwarf photosphere. In this thesis, I describe a spectroscopic examination of brown dwarfs in Upper Scorpius which identifies some of these effects, even in a significant fraction of Class III objects.

Surveys Of Nearby Associations

As of today, brown dwarf surveys in star forming regions are affected by two deficiencies. The surveys are incomplete at the low mass end, primarily due to strong and variable extinction. Most nearby star forming regions also have somewhat similar physical characteristics, for example, most of them do not harbour massive stars.

Most nearby star forming regions, (e.g. IC348, Cha I, σ Ori) have been searched for brown dwarfs over the past decade (Luhman et al., 2007). In some clusters, the surveys have revealed a population of objects with masses below the deuterium burning limit of 0.013 $M_\odot$ (Zapatero Osorio et al., 2000; Lucas & Roche, 2000). Andersen et al. (2008) has determined the ratio of

the number of low-mass stars (0.08-1.0 $M_\odot$) to the number of brown dwarfs (0.03-0.08 $M_\odot$) to be between 3.3 and 8.5 for several nearby young clusters, while Scholz et al. (2009) found it to be 1.5±0.3 for one other cluster. This might be a first indication for environmental effects on the IMF.

In the past few years, the SONYC (Substellar Objects in Nearby Young Clusters) project has examined the brown dwarf population of NGC1333, ρ Oph, Lupus3 and Cha I (Scholz et al., 2009; Geers et al., 2011; Mužić et al., 2011; Scholz et al., 2012a; Mužić et al., 2012; Scholz et al., 2012b, 2013; Mužić et al., 2013). Its purpose is to provide the first complete census of substellar objects in each cluster, to characterise the properties of the brown dwarfs found, and to explore possible environmental effects on the IMF. In order to augment its results, and extend its reach to one more nearby young cluster, the SONYC survey has made use of the results of the work described in this thesis (Mužić et al., 2013).

In order to advance the studies of brown dwarfs, I have focussed on the brown dwarf population in the Upper Scorpius association.

1.8 Upper Scorpius

The pattern of bright stars that denote the mythical scorpion in the well known Scorpius constellation are shown in Fig. 1.6. Among them are the most massive members of the Upper Scorpius OB association. The brightest star in both the constellation and the Upper Scorpius OB association is Antares (α Sco), a red supergiant of spectral type M1.5, that has already evolved off the Main Sequence (Preibisch & Mamajek, 2008; Pecaut et al., 2012). As can be seen in Fig. 1.6, it is surrounded by several bright, blue-white stars, all of which are also members of the association (Pecaut et al., 2012). Russell (1914) included these stars in his first graphs, noting that they had been determined to be members of the one cluster, based on proper motion, radial velocity and parallax measurements.

Upper Scorpius is spread over approximately 250 deg^2 of the sky but wide-field surveys now cover a significant portion of this area. The region of Upper Scorpius analysed in this thesis, and outlined in Fig. 1.6, lies within R.A. 15h 40m to 16h 45m and Dec. -30 to -21. It is generally free of extinction with $A_V < 2.0$ (Ardila et al., 2000), and as can be seen in Fig. 1.6, it is clear of the Galactic Plane.

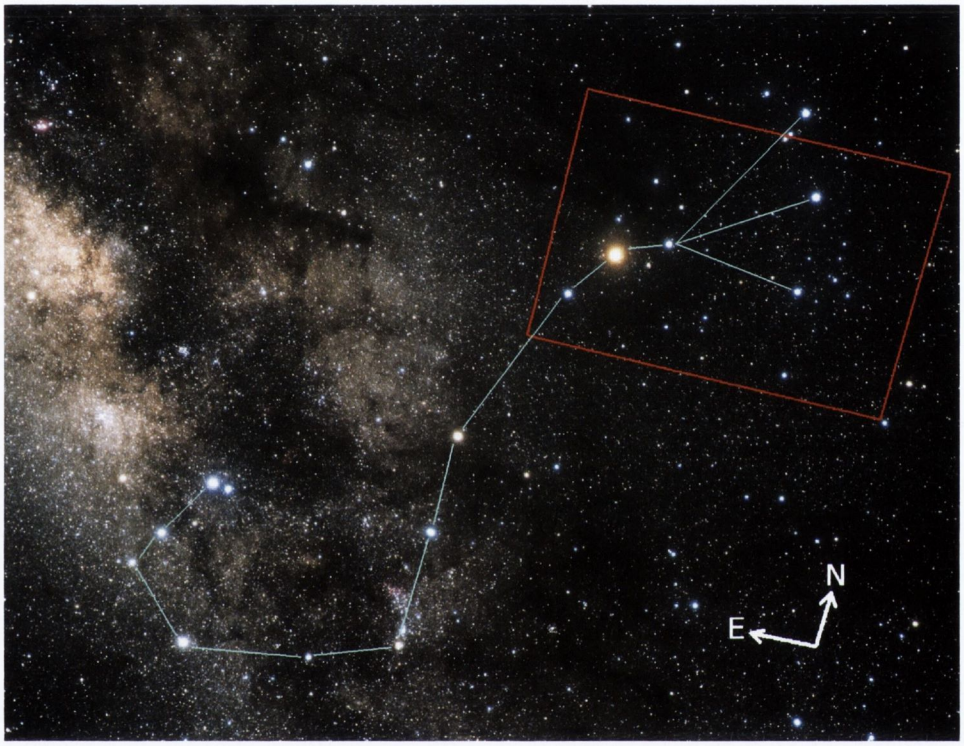

Figure 1.6 The Scorpius Constellation. The plane of the Milky Way can be seen on the left. The area of Upper Scorpius analysed in this thesis is shown outlined in red. The bright red star Antares (α Sco), is visible within the search area. The brightest member of Upper Scorpius, it is a red supergiant (spectral type M1.5) that has already evolved off the Main Sequence (Preibisch & Mamajek, 2008; Pecaut et al., 2012). The other bright stars within the search area, (which are all B-type stars), are also members of the Upper Scorpius association (Pecaut et al., 2012). Image courtesy of: ESA/Hubble (Akira Fujii).

At a distance of 145 ± 2pc (de Zeeuw et al., 1999), Upper Scoprius is also the nearest OB assocation, and so it represents our best chance of constraining the impact of massive stars on the formation of very low mass objects.

Until recently, the age of the association was taken to be 5 Myr (Preibisch et al., 2002), but this has been called into question by the work of Pecaut et al. (2012), who have derived an age of 11 Myr for this region. Despite its youth, (stars later than F type have yet to reach the Main Sequence), star formation appears to have finished in the association within 1 Myr of commencing (Preibisch & Mamajek, 2008; de Zeeuw et al., 1999), so all members of the association are coeval. The age of Upper Scorpius is also perfectly suited to the investigation of the longevity of disks around brown dwarfs.

The combination of proximity, youth and lack of extinction, make Upper Scorpius a very favourable target for investigations of brown dwarfs. In the following chapters I detail the findings of an extensive trawl for new brown dwarfs using the latest and deepest near-infrared surveys. The results indicate that the presence of OB stars favour the formation of brown dwarfs. Using mid-infrared data, I also present a census of disks around brown dwarfs in Upper Scorpius. This data suggests that the evolution of brown dwarf disks mirrors the behaviour of disks around low-mass stars. I then detail the results of a follow-up spectroscopic examination, which finds evidence that spectral types of brown dwarfs with disks, derived from near-infrared spectra, may contain contributions that undermine their reliability. A selection of spectra that are judged to be clean and clear of these contributions are presented for use as spectroscopic templates for young brown dwarfs in the future.

Chapter 2

Instrumentation

As noted in the previous chapter, near-infrared ($\sim$ 0.8 - 2.5μm) and mid-infrared ($\sim$ 3 - 30μm) wavelengths are the optimal wavelengths for observing brown dwarfs and their disks. All the instruments used to collect the data analysed in this thesis were designed specifically for infrared observations. As a result, they have been engineered with several features in common. Each telescope has the reflective surfaces of its mirrors coated in gold. They all employ a cryogenic system to cool their detectors and optical systems. Similar HgCdTe detector arrays are utilised in almost all of the instruments.

Water vapour in the atmosphere strongly absorbs infrared signals, so some of the ground based telescopes described below are located at altitudes above 4,000 m, on the summit of Mauna Kea in Hawaii. This places them above most of the water vapour in the atmosphere. Their location on Mauna Kea also takes advantage of the excellent seeing at this site.

The ground based telescopes used have sub-arcsecond angular resolution, while the space based mid-infrared instrument (WISE) has an angular resolution that varies from 6.″0 to 12.″0 across its wavelength range. While the *theoretical* limits of the angular resolution of the various telescopes used are determined by the Rayleigh criterion

$$\theta = \frac{1.22\lambda}{\mathrm{D}} \tag{2.1}$$

where θ is the angular resolution (in radians), λ is the wavelength of interest and D is the diameter of the telescope, the *practical* limits may be determined by the seeing at their location. This is the case for the ground based telescopes. The typical seeing at Mauna Kea, of $\sim$0.″5, although

among the best that can be found, is still a little poorer than the optimum angular resolution of the telescopes. Although the atmospheric seeing limits do not apply to the space based telescope, its diameter, as noted below, is only a fraction of that of the other telescopes. It is also used to observe at longer wavelengths. Consequently, the ground based telescopes have the best angular resolution.

2.1 UKIRT

The United Kingdom InfraRed Telescope (UKIRT) is a 3.8 m Cassegrain telescope, located on the summit of Mauna Kea in Hawaii. Observations with UKIRT can be made using a suite of instruments, of which the most widely used is the Wide Field Camera (WFCAM). Described in detail in Casali et al. (2007), this 1400 kg instrument is mounted on the central plinth of the primary mirror, inside the telescope trusses, as shown in Fig. 2.1. WFCAM is a near-infrared imager, operating in the wavelength range between 0.8-2.4μm. Its design is a variant on the Schmidt camera, with 4 HgCdTe infrared detectors mounted on its focal plane. Most of the instrument is contained within a cryostat, as shown in Fig. 2.2, which also shows the light path from primary mirror to detector arrays. The 4 detector arrays are arranged in a square pattern around a small CCD, which is used as an autoguider, and are separated by a space equivalent to 94% of their active areas. To achieve a completely imaged square field on the sky (referred to as a tile), 4 separate exposures, with different pointings, must be made. Each tile therefore is composed from 16 images, which overlap slightly. Each quadrant of the tile contains 4 images taken by a single detector array at 4 adjacent pointings. The field of view of a single exposure is 0.21 deg^2, while that of a single tile is 0.79 deg^2. This wide field of view is suited to the large scale survey work for which WFCAM was designed.

Data for point sources obtained by WFCAM are photometrically calibrated by direct comparison with data from the same sources obtained by the Two Micron All Sky Survey (2MASS) (Hodgkin et al., 2009). The resulting WFCAM photometry, as recorded in its various survey catalogues, is on a Vega system. Comparison with 2MASS objects is also used to perform astrometric calibrations. This is all done automatically as part of the data reduction pipeline that operates on data as it is taken by WFCAM.

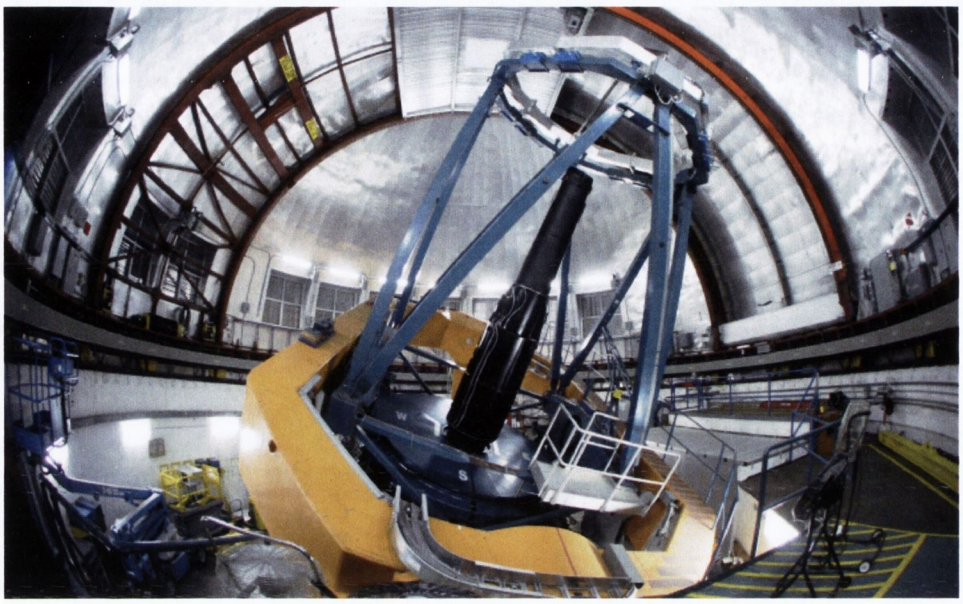

Figure 2.1 Inside the dome at UKIRT on Mauna Kea, Hawaii. The 3.8 m primary mirror is located under the closed protective cover at the base of the large black cylindrical tube, which houses the WFCAM instrument. Image courtesy of: U.K. Infrared Telescope, Mauna Kea Observatory, Hawaii.

Flat fielding, to compensate for variations in pixel sensitivity across each array, and sky subtraction, to remove background sky illumination, are performed routinely as part of the same pipeline. The data reduction pipeline is designed to work in real time, at the telescope, as WFCAM is making observations. This is done as part of the quality control strategy for WFCAM. By constantly monitoring the quality of data being produced by the pipeline, observers at the telescope can be alerted at the earliest opportunity when corrective action needs to be taken, thereby minimising the amount of time wasted gathering poor quality data (Casali et al., 2007).

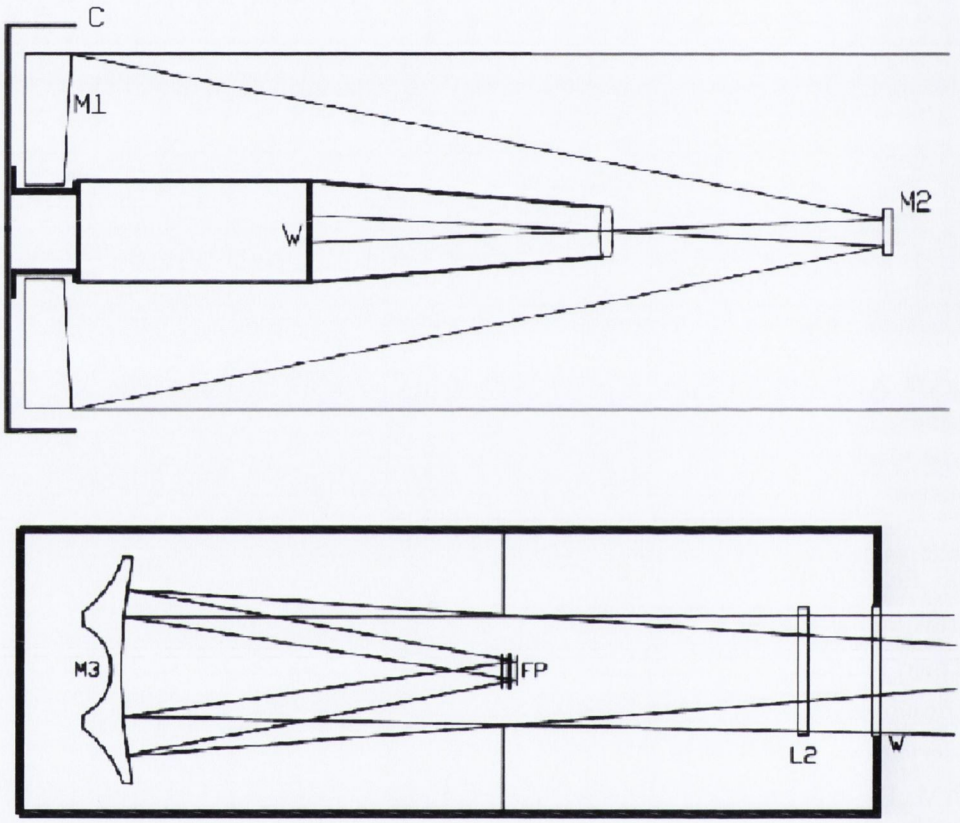

Figure 2.2 Schematic of the light path through WFCAM. The top panel illustrates the light path from the primary mirror (M1) to the window on the WFCAM cryostat (W) via the secondary mirror (M2). The bottom panel illustrates the inside of the cryostat. Light entering via W goes through a corrector lens (L2) and is reflected via the mirror M3 onto the detectors at the focal plane (FP). Image adapted from Casali et al. (2007).

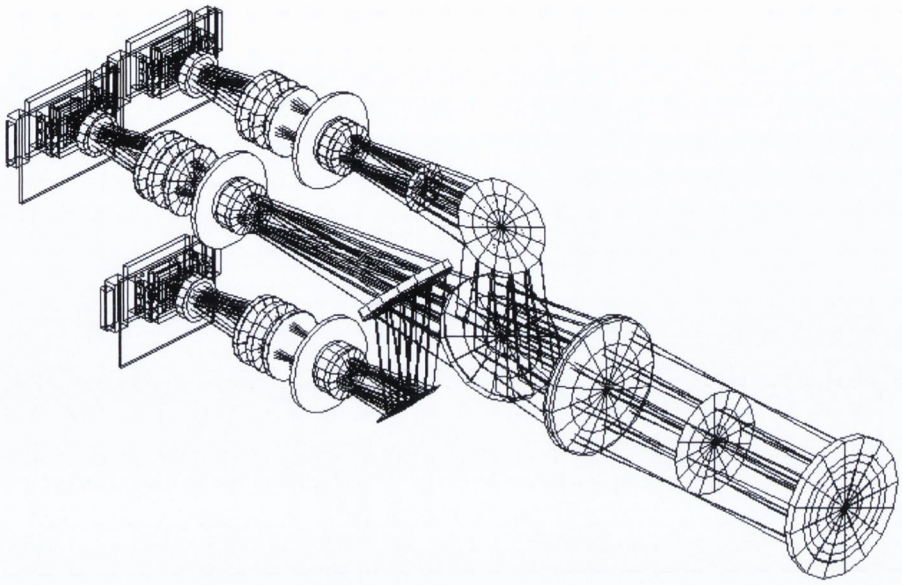

Figure 2.3 The light path to the detector arrays in the 2MASS telescopes. After the incident light has passed through the first lenses, the beam is split by dichroic mirrors. The separated beams then pass through identical arrangements of lenses before arriving at the detector arrays for each passband. Image adapted from Skrutskie et al. (2006).

2.2 2MASS

The Two Micron All Sky Survey (2MASS) is a near-infrared survey completed using two identical 1.3m Cassegrain telescopes, one located in the Northern hemisphere and the other in the Southern hemisphere (Skrutskie et al., 2006). The Northern telescope is located at the Whipple Observatory on Mount Hopkins in Arizona, while the Southern telescope is situated at the Cerro Tololo Observatory in Chile. The cryogenic cameras used contain a set of 3 HgCdTe infrared detector arrays, one for each passband, and the light path to each crosses an identical arrangement of 7 lenses, as shown in Fig. 2.3.

In a process similar to that at UKIRT, an automatic data reduction pipeline performed photometric and astrometric calibrations, flat fielding

and sky subtraction, but in the case of 2MASS, the data was processed twice. A preliminary data reduction process was conducted during observations for the same quality control reasons as with WFCAM. Following the completion of observations in 2001, all the data gathered was processed again using a revised version of the pipeline. The completed all sky point source catalogue which resulted contains 470 million sources. Photometric data from this catalogue was used to calibrate survey data which was taken later by the WFCAM on UKIRT.

2.3 The WISE Satellite

The WISE satellite is a mid-infrared observatory which operates in a Sun-synchronous low Earth orbit. Described in detail in Wright et al. (2010), it was launched in December 2009 and completed its first all sky survey by July 2010. WISE makes observations in four mid-infrared passbands between 3 and 22 μm.

As shown in Fig. 2.4, WISE has a 0.4 m primary mirror. A further 12 mirrors are used to direct incident light through the optics assembly and onto a final moving mirror, known as the scan mirror. The scan mirror is the only moving part in the optics assembly. Its motion counteracts that of the satellite as it moves in its orbit, so that the final image on the detector arrays is kept still for a period of about 8s. The telescope assembly is fabricated from aluminium and all the mirrors are gold coated for optimum mid-infrared optical performance. WISE has a field of view of 0.6 deg^2 and, similar to WFCAM, it has a small overlap between frames. A pair of HgCdTe detector arrays are used for imaging at the shorter wavelength passbands, while the longer wavelength passbands employ Si:As detector arrays. A series of dichroic beam splitters are utilised to ensure that all the detector arrays can image the same field of view simultaneously.

The entire telescope and optics assembly is mounted within a cryostat and was cooled to less than 12 K (with the Si:As arrays being cooled to less than 7.5 K) during its first 8 months of operation. The reservoirs of solid hydrogen used to achieve this cooling had been expected to last for longer than this, but they were largely depleted by September 2010. Despite this, there had been sufficient time to allow WISE to achieve a complete all sky survey in all four passbands.

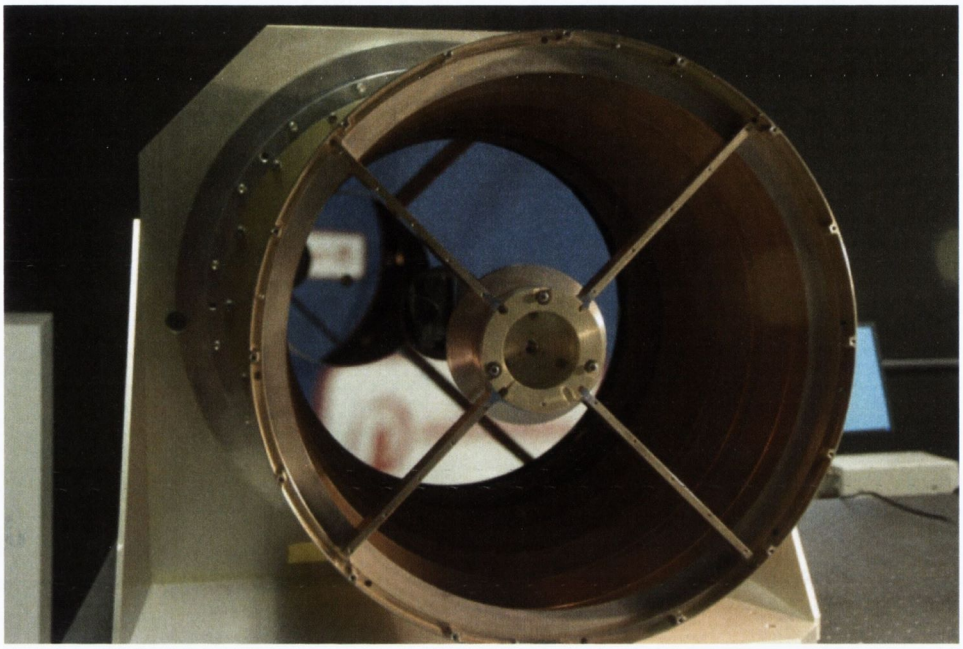

Figure 2.4 Looking down the barrel of the WISE telescope. This image, taken during assembly of the WISE satellite, shows the 0.4 m, gold coated, primary mirror. The telescope was mounted inside a cryostat, where it was cooled to less than 12 K during its observing mission. Image courtesy of: NASA/JPL-Caltech/SSG.

A preliminary point source catalogue was released in April 2011, followed by a more complete all sky catalogue in March 2012, containing photometry for 560 million sources.

2.4 IRTF And SpeX

The NASA Infrared Telescope Facility (IRTF) is a 3.0 m Cassegrain telescope, operated for NASA by the Institute for Astronomy at the University of Hawaii. Like UKIRT, it is located on the summit of Mauna Kea in Hawaii.

One of the various instruments available for use with the IRTF is the medium resolution 0.8 - 5.5 μm spectrograph known as SpeX. Described in detail in Rayner et al. (2003), SpeX is enclosed in a cryostat (the blue box shown in Fig. 2.5) and mounted directly behind the primary mirror of the telescope.

Spectra obtained are detected on set of InSb detector arrays, the light

path to which is shown in Fig. 2.6. A second set of similar arrays (the slit-viewer array in Fig. 2.6) is used for object acquisition. SpeX can be used in several modes, covering a range of resolving powers, and suitable for different uses. The mode designed for faint object spectroscopy, and most suited to observations of brown dwarfs in UpSco, is the 0.8 - 2.5 μm low resolution single prism mode. Dispersion, in this mode, is achieved using a single compound fused silica/ZnSe prism, located in the prism turret shown in Fig. 2.6. Also shown in Fig. 2.6 is the slit wheel that houses the various slits that can be used. Appropriate settings of both slit wheel and prism turret must be set by the observer, based on the desired mode of operation of the spectrograph.

Unlike the survey data collected by both WFCAM and 2MASS, data reduction, including flat fielding and wavelength calibration, must be done by the researchers using SpeX. Facilitating this, SpeX has an external calibration unit (the black box above the cryostat in Fig. 2.5) which contains the necessary lamps. The details of the reduction process carried out will vary according to the mode of observation chosen. The specifics of the mode and configuration of the instrument settings chosen, as well as the data reduction carried out for my observations, are given in Chapter 5.

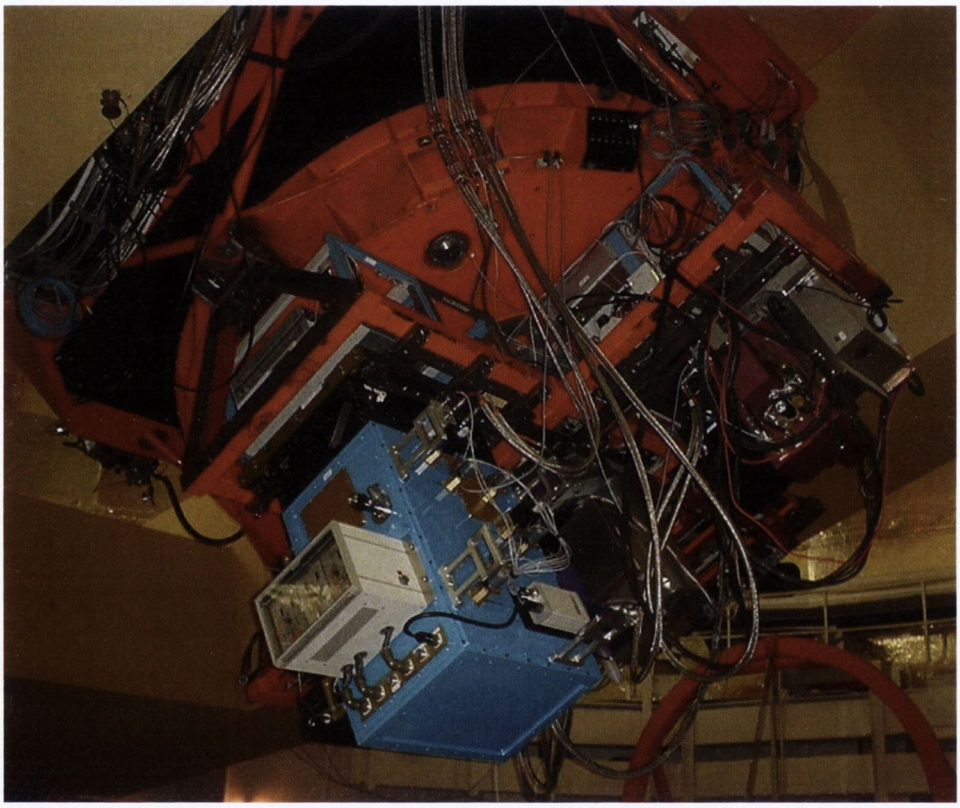

Figure 2.5 Behind the primary mirror at the IRTF on Mauna Kea, Hawaii. A suite of instruments are connected to the telescope, via the bright red multiple instrument mount. The blue box is a cryostat, within which the SpeX spectrograph is enclosed. Image courtesy of:NASA/Institute for Astronomy, University of Hawaii.

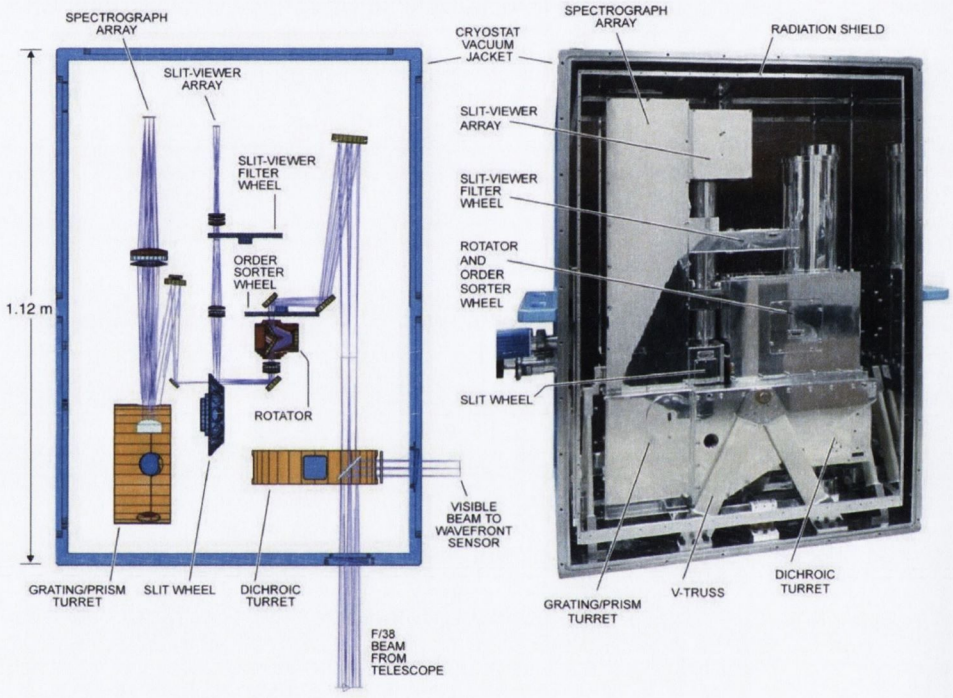

Figure 2.6 Inner workings of the SpeX spectrograph. Light entering the spectrograph passes through several different filters, mirrors prisms and lenses, which have a variety of settings. The setting and overall configuration of these must be chosen by the observer. Image adapted from Rayner et al. (2003).

Chapter 3

New Brown Dwarfs

In this chapter, I report on a new brown dwarf survey in a part of the Upper Scorpius (hereafter UpSco) star forming region. UpSco is a favorable area for such a project, because it suffers from negligible extinction. At a distance of 145 ± 2pc (de Zeeuw et al., 1999) it is the nearest OB assocation, and it represents our best chance of constraining the impact of massive stars on the formation of very low mass objects. With an age of about 5 Myr (Preibisch et al., 2002) UpSco is the youngest part of the Scorpius Centaurus Association, i.e. it has one of the better combinations of proximity and youth for a successful brown dwarf search. UpSco is spread over approximately $250\,\mathrm{deg}^2$ of the sky but wide-field surveys now cover a significant portion of this area.

This chapter analyses an infrared $12\,\mathrm{deg}^2$ survey of part of UpSco, which lies roughly within R.A. 15h 40m to 16h 20m and Dec. -30 to -27 and is generally free of extinction with $A_V < 2.0$ (Ardila et al., 2000). Despite its youth (stars later than F type have yet to reach the Main Sequence) star formation appears to have finished in the association within 1 Myr of commencing (Preibisch & Mamajek, 2008; de Zeeuw et al., 1999) so all members of the association are coeval. In Section 3.1 details of the instrumentation, the survey and the data obtained are presented. Section 3.2 describes the selection of young brown dwarf candidates from photometric and proper motion analysis. The results of this selection are used to analyse the IMF of Upper Scorpius in Section 3.3. Finally, in Section 3.4, my conclusions are drawn. The results presented in this chapter are based on work which originally appeared in Dawson et al. (2011, 2013).

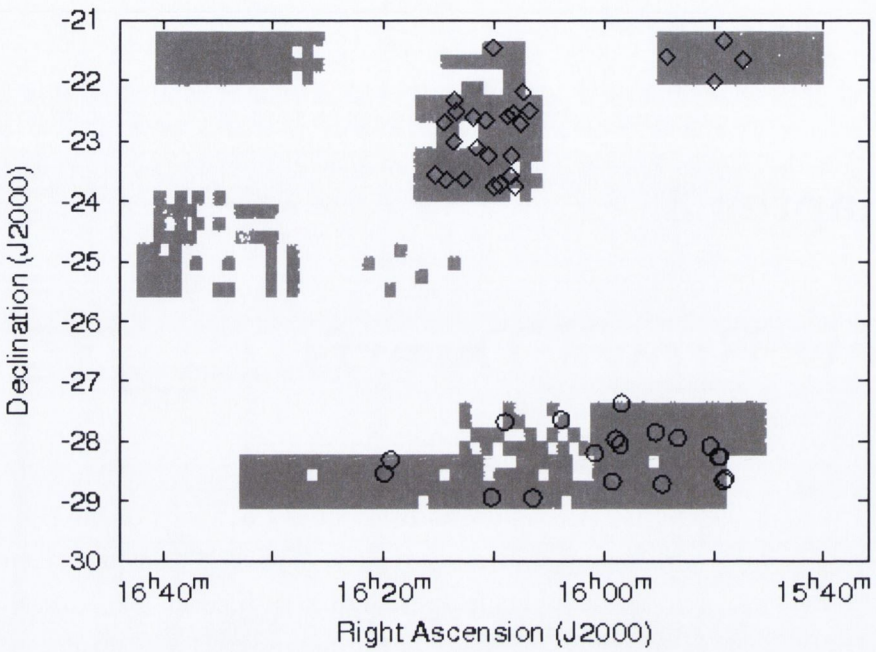

Figure 3.1 Coverage in Z, Y, J, H and K filters of 28 $\deg^2$ in Upper Scorpius from the UKIDSS GCS DR8Plus. Open circles mark the location of the 19 brown dwarf candidates found in this work. Open diamonds mark the position of spectroscopically confirmed brown dwarfs found in other studies (Martín et al., 2004; Slesnick et al., 2006; Lodieu et al., 2008, 2011). The search method used in this survey of the southernmost area covered by UKIDSS was also applied to 10.5 $\deg^2$ covered by two areas to the north in order to test its reliability. The 26 brown dwarfs shown above were recovered.

3.1 Survey And Data Sets

UKIRT is currently conducting the United Kingdom Infrared Deep Sky Survey (UKIDSS) - the results of which are being made available in a series of releases. The work detailed in this chapter used the 8th Data Release (DR8Plus), the latest release available at the time the work was done.

UKIDSS is made up of several components but the one of interest here is the Galactic Cluster Survey (GCS). Described in detail in Lawrence et al. (2007) the GCS is a survey of ten large open star clusters and star forming regions, including UpSco. One of the primary goals of the GCS is to conduct a census of very low mass brown dwarfs in order to investigate the form of the substellar IMF.

The GCS takes infrared images via five passband filters - Z, Y, J, H and K with effective wavelengths of 0.88μm, 1.03μm, 1.25μm, 1.63μm, and 2.20μm respectively, and magnitude limits of Z=20.4, Y=20.3, J= 19.5, H=18.6 and K=18.6. The instrument used to take the images is the WFCAM. Data collected by the WFCAM is subject to an automated process that detects and parameterises objects and performs photometric and astrometric calibrations. The resulting reduced image frames and catalogues are then placed in the WFCAM Science Archive (WSA). The WSA can be interrogated using Structured Query Language (SQL).

A set of five papers provide the reference technical documentation for UKIDSS. Casali et al. (2007), as noted above, presents technical details of the WFCAM, Hodgkin et al. (2009) describes the WFCAM photometric system, Hambly et al. (2008) describes the WSA and offers instruction on how to extract information from it using SQL. As previously mentioned Lawrence et al. (2007) presents the details of the different UKIDSS surveys, including the GCS. The fifth paper (Irwin et al., in preparation) will describe the details of the data reduction pipeline which is run by the Cambridge University Astronomical Survey Unit (CASU), but sufficient information for an overview of the data reduction pipeline can be gleaned from the other four papers and by referring to Dye et al. (2006) and Warren et al. (2007)[1].

As shown in Fig. 3.1, the area in UpSco investigated here and surveyed for DR8Plus covers 12 deg^2. The data for objects in the target area were obtained via an SQL query (see the appendix at the end of this chapter for a typical query) to the UKIDSS GCS database. All queries were structured to include only point source objects in order to avoid contamination by extended sources (e.g. relatively nearby galaxies). Objects in the WSA are given what is known as a discrete image classification, with point sources having values between -2 and -1. The lines in the query that refer to "passband"class, e.g. zclass, values of between -2 and -1, are designed to filter out extended sources. Note that requiring this value to be between -2 and -1 in every passband may exclude some sources with very low signal to noise ratios. As every object with photometric characteristics consistent with a brown dwarf had its proper motion assessed, in order to check whether it is likely a member of UpSco, each query submitted also correlated all objects

[1]For more details of the data reduction process see http://casu.ast.cam.ac.uk/surveys-projects/wfcam/technical.

found in the UKIRT GCS databases with those found in 2MASS databases (Skrutskie et al., 2006). The 2MASS data is used as a first epoch for the purposes of proper motion calculation.

3.2 Selection Of Brown Dwarf Candidate Members Of Upper Scorpius

3.2.1 Photometry

The query shown in the appendix at the end of this chapter was submitted to the WSA. The query returned 282,938 objects and the colour magnitude diagrams shown in Figs. 3.2 and 3.3 were plotted. Known brown dwarfs from other studies (Martín et al., 2004; Slesnick et al., 2006; Lodieu et al., 2008, 2011) are shown as open diamonds and the 19 brown dwarf candidates found in this study are shown as open circles. Theoretical isochrones for 5 Myr old substellar objects are also shown over-plotted on the diagrams. These isochrones are based on the DUSTY models derived by Chabrier et al. (2000) and obtained from both I. Baraffe (private communication) and N. Lodieu (private communication). The isochrones were computed by I. Baraffe using the UKIDSS filter profile. Reddening caused by extinction shifts the position of objects to the right and down on colour magnitude diagrams. Therefore all brown dwarf candidates should be either on or to the right hand side of the isochrones. The query limited selection to objects with magnitudes in Z greater than 14.0. This choice of a limiting magnitude was motivated in part by an examination of colour magnitude diagrams, including those in Figs. 3.2 and 3.3, which showed that at brighter magnitudes the isochrones for the young brown dwarf/very low mass star sequence of objects were no longer sufficiently distinct from other objects on the diagrams. Also, the DUSTY models of Chabrier et al. (2000) indicated that this choice would put an upper limit on the mass selected of $0.09\,M_{\odot}$, massive enough to make sure of including 5 Myr old brown dwarfs at 145pc distant. Note that WFCAM Z is on a Vega system, so it is not directly comparable with the SDSS z magnitudes on the AB system.

Evident from Figs. 3.2 and 3.3 is that some colour magnitude diagrams show a much clearer separation between brown dwarfs and Main Sequence stars than others. The (Z-J,Z) colour magnitude diagram shows the sepa-

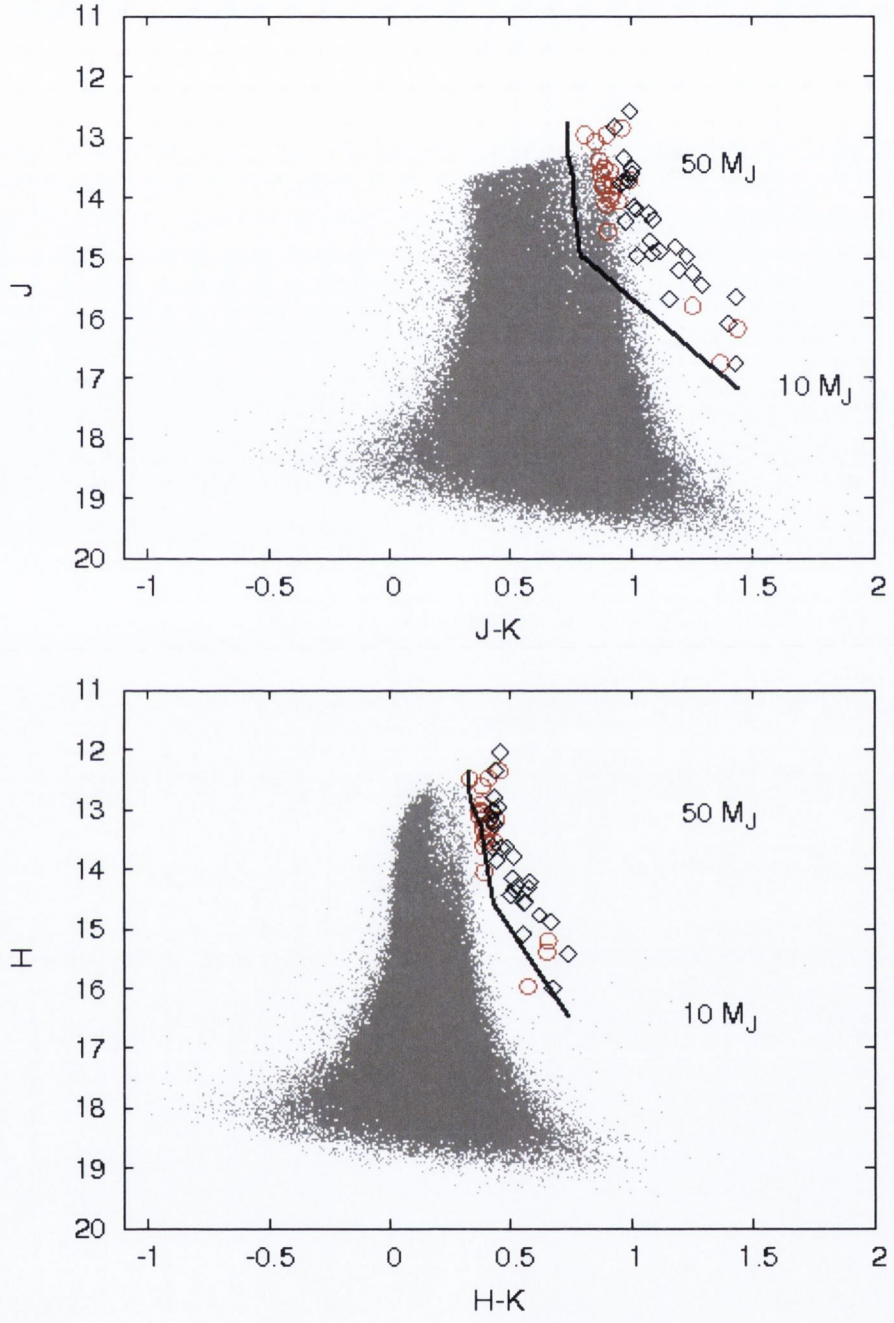

Figure 3.2 Two of four colour magnitude diagrams (see also Fig. 3.3) showing the 19 brown dwarf candidates and the 1 object too faint to have its proper motion measured as red open circles. Spectroscopically confirmed brown dwarfs from other studies of UpSco (Martín et al., 2004; Slesnick et al., 2006; Lodieu et al., 2008, 2011) are shown as open diamonds and all other objects as small dots. The 5 Myr DUSTY model (Chabrier et al., 2000) isochrone is also shown with mass decreasing going down the isochrone as indicated.

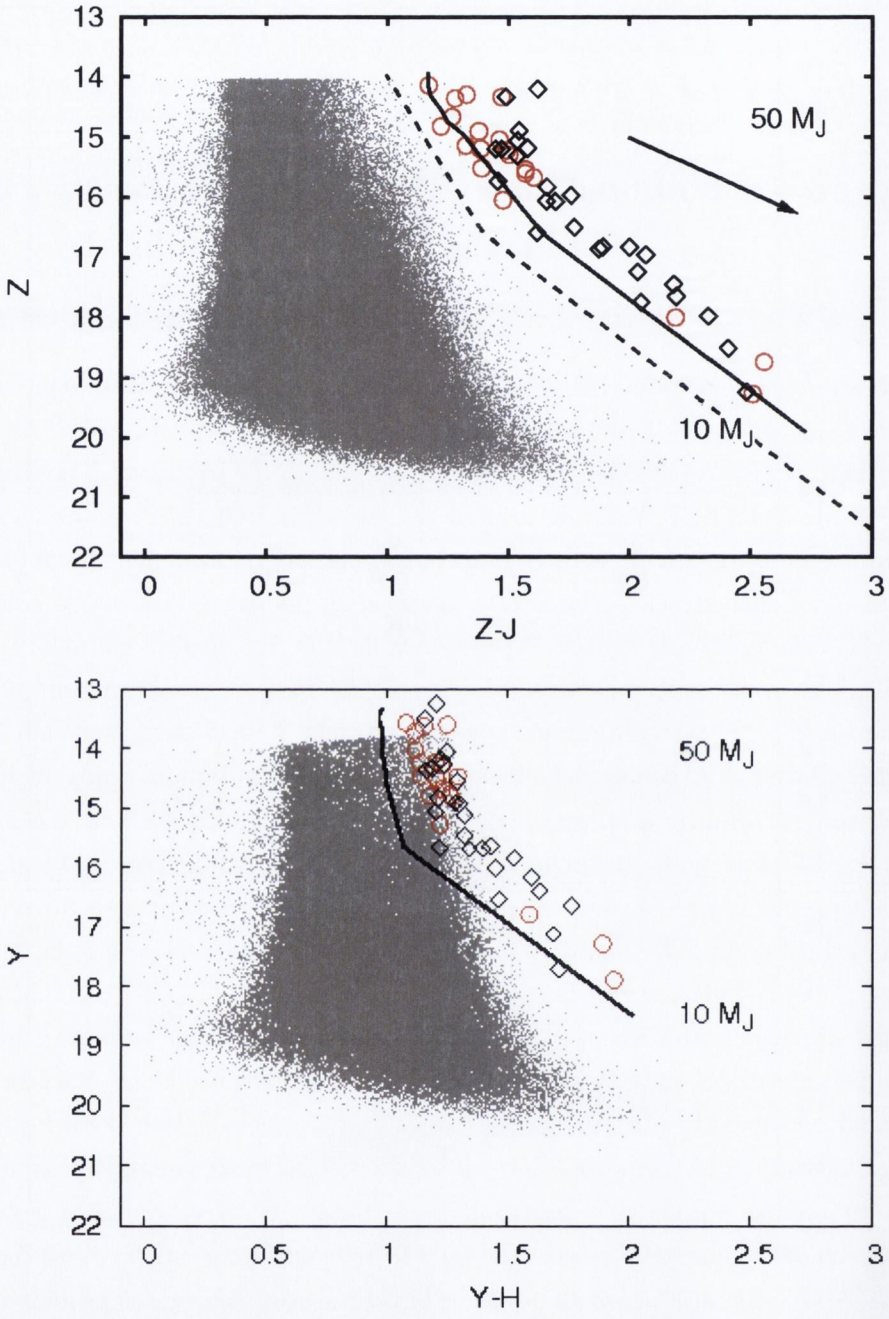

Figure 3.3 Two colour magnitude diagrams with symbols and isochrone as in Fig. 3.2. The (Z-J,Z) diagram was chosen in this work for making the photometric selection. A reddening vector is shown corresponding to the maximum for the UpSco region of $A_V = 2.0$ noted by Ardila et al. (2000). The reddening in the part of UpSco investigated in this work is much less than this maximum. All objects to the left of the dashed line shown in the (Z-J,Z) diagram were rejected because of their colours.

ration clearly and was chosen as the basis for the photometric cut. Thus to further refine the search, a new query was submitted to the WSA eliminating all objects to the left of the line from (Z-J,Z) = (1.0, 14.0) through (1.4, 16.6) to (3.0, 21.55) (dashed line in Fig. 3.3). This query left 51 objects which were examined again in the (Z-J,Z) colour magnitude diagram. 17 of the objects to the left of the line (Z-J,Z) = (1.1, 14.0) through (1.1, 14.3), (1.2, 14.9), (1.3, 15.2) to (1.6, 17.0) were rejected for being too far from the isochrone on the blue side, leaving 34 photometric candidates. Most of the candidates are slightly redder than predicted by the isochrones, which could be due to extinction or problems with the isochrones.

3.2.2 Proper Motion

The 34 photometric candidates were then examined to find their proper motion. Proper motions were calculated using the query shown in the appendix to this chapter. The difference in position of the objects in the GCS and 2MASS catalogues is obtained in milliarcseconds. This is then divided by the difference in the two epochs, converted from Julian dates to years. The lines in the query that list their results "as pmRA" and "as pmDEC" perform this task. The resulting vector point diagram is shown in Fig. 3.4. The known proper motions of UpSco in right ascension and declination are about -11mas/yr and -25mas/yr respectively (de Bruijne et al., 1997; Preibisch et al., 2002). Of the 34 candidates, 1 was too faint to be recorded in 2MASS leaving 33 candidates with proper motion data calculated. The remaining 33 candidates included 6 with proper motions greater than the range of Fig. 3.4 (Table 3.1). These 6 objects might be red or brown dwarfs located much closer to the Sun than UpSco. de Bruijne (1999) notes that the velocity dispersion in UpSco is very small at 1.3km/s, corresponding to about 2mas/yr.

The greatest contribution to the spread in the proper motions therefore comes from errors in UKIDSS and 2MASS measurements. To assess the errors the original selection of 282,938 objects had their proper motions examined. The proper motions were found to have a normal distribution about the origin with a standard deviation of 10.2mas/yr in both right ascension and declination. Factoring this error back into the de Bruijne (1999) figure noted above showed that a 2σ selection circle for UpSco members would have a radius of 20.8mas/yr. This error has only a slight dependence on

magnitude for objects with a magnitude in Z between 14.0 and 17.0. For the objects fainter than this the standard deviation is $\approx$20mas/yr. There are 3 objects among the final 27 candidates with magnitudes in Z greater than 17.0.

All 27 candidates shown in Fig. 3.4 are predominantly centred around the (-11,-25) position. The 3 candidates with magnitudes in Z greater than 17.0 noted above are marked in red. There is no clustering of objects around the (0,0) position indicating that the sample is not contaminated by more distant objects e.g. AGB stars which have similar surface temperatures and colours to brown dwarfs, but much greater intrinsic luminosities. The 19 candidates within the 2σ selection circle were then classified as members of UpSco. These objects so selected (Table 3.2) have the photometric and proper motion characteristics of a 5 Myr old brown dwarf member of UpSco. Given that there are 19 objects within the 2σ selection circle statistically it is to be expected that possibly 1 of the 8 objects outside is also a brown dwarf member of UpSco. However all of the other 8 objects shown in Fig. 3.4 are clustered immediately outside the 2σ selection circle and not scattered around the vector point diagram as would be expected for random contaminants. As these 8 objects have the same range of magnitudes as the 19 within the selection circle (Table 3.2) they are not subject to any systemically larger proper motion errors caused by being fainter. Thus it is likely that these 8 objects are also members of UpSco with slightly higher dispersion velocity. Finally, as noted in Dawson et al. (2011), none of the brown dwarf candidates listed here had been identified before in previous surveys.

Given the low contamination in the sample with proper motions, the one object which is not detected in 2MASS (Table 3.2) has a high likelihood of being a brown dwarf in UpSco as well (28/34, i.e. 82%).

3.2.3 Estimate of Contamination/Completeness

In order to be certain that the candidates found in this study are in fact brown dwarfs spectra should be obtained. However, Fig. 3.4 indicates that there is negligible contamination from background stars among the sample.

As a further test of the method outlined above, it was also used to investigate the 10.5 deg^2 area covered by UKIDSS in the two areas shown to the north of Fig. 3.1. The area is also part of UpSco (de Zeeuw et al.,

1999) and therefore any brown dwarf here will share similar photometric and proper motion characteristics of those from the area to the south. After the analysis of the 10.5 deg^2 area was complete, 49 objects in it were identified as possible brown dwarfs. All 49 were previously identified by Lodieu et al. (2007, 2008) as brown dwarf candidates. Spectra have been taken of 26 of the 49 objects (Martín et al., 2004; Slesnick et al., 2006; Lodieu et al., 2008, 2011) and all 26 have been confirmed as brown dwarfs. This result underlines the reliability of the method as a means of discriminating brown dwarfs from other objects in UpSco.

In order to estimate completeness levels in all passbands the data from the original 282,938 objects was analysed. Objects were grouped in bins of 0.1 magnitude and examined to see where numbers detected in each bin began to fall. The resulting estimates of 100% completeness were: Z=18.0, Y=17.4, J=17.2, H=16.2, K=16.1. In the Z and J passbands these would be the expected magnitudes of UpSco member objects in the 0.01 - 0.02 $M_\odot$ mass range. The histograms in all five passbands showed that completeness fell gradually at these magnitudes and was still at an 80% level another magnitude deeper. Note that the lower mass range achieved in this survey is not limited by the completeness of UKIDSS but by that of 2MASS (J≈16) due to the need for proper motion measurements. However, of the 34 photometric candidates, only one object was fainter than the sensitivity limit of 2MASS and did not have its proper motion calculated.

3.3 The substellar population in Upper Scorpius

I re-examined the 19 high probability members listed in Table 3.2 in the (Z-J,Z) colour magnitude diagram and assigned masses based on their Z band magnitude. They cover a mass range from 0.01 to 0.09 $M_\odot$, 7 are below 0.03 $M_\odot$ and 2 of those are below 0.02 $M_\odot$. The 100% completeness limit in the Z and J passbands corresponds to a mass of less than 0.02 $M_\odot$. At 0.01 $M_\odot$ the photometric survey is still at least 80% complete.

Andersen et al. (2008) performed a combined analysis of the low-mass IMF in seven star forming regions, not including UpSco. The method used a ratio of stars with masses 0.08 - 1.0 $M_\odot$ to brown dwarfs with masses 0.03 - 0.08 $M_\odot$ (30 - 80M_J) from each region to allow for direct comparison.

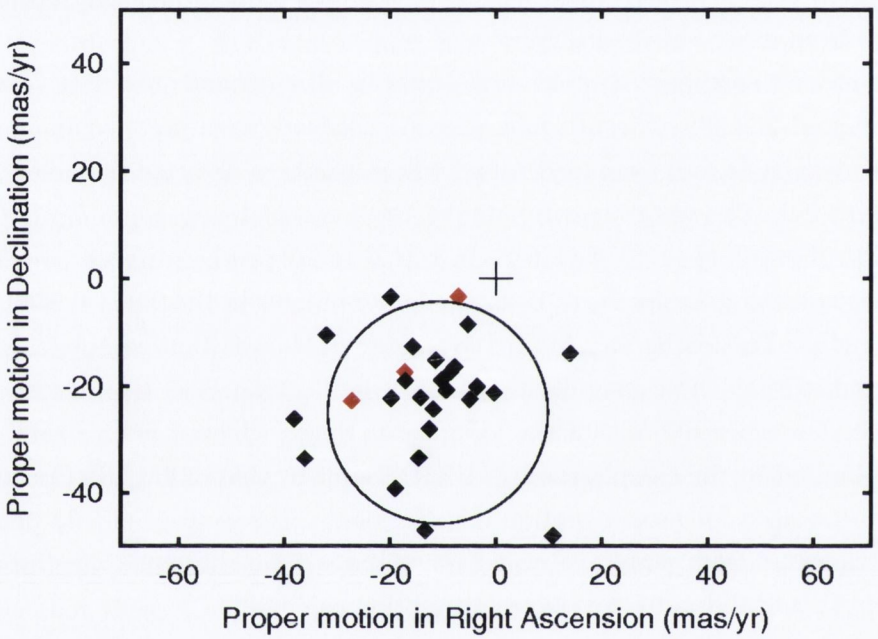

Figure 3.4 Vector point diagram for 27 candidate brown dwarfs in Upper Scorpius. The 3 objects fainter than Z = 17.0 are marked in red. There is an obvious and identifiable cluster around (-11,-25), while there is no clustering around the origin, indicating that there is very little contamination from background objects in the sample. Candidates lying outside the 2σ selection circle centred on (-11,-25) were classified as non-members, leaving 19 brown dwarf candidates. I suspect however that many of the "outliers" may well be members.

In order to follow that method a new query was submitted to the WSA to extract UpSco member stars with magnitudes and colours that implied a mass range of 0.09 - 1.0 $M_{\odot}$. This new query returned 11,041 objects which were then examined in a (Z-J,Z) colour magnitude diagram. Unlike the brown dwarfs, the space the UpSco stars occupy in the colour magnitude diagram is not as distinct from the Main Sequence. The isochrones used to guide this selection of UpSco members were the DUSTY isochrone used previously and the NexGen isochrone also derived from the models of Chabrier et al. (2000). Initially, all objects to the left of a line from (0.75,10.32) to (1.17,14.15) were eliminated from consideration.

The remaining objects then had their proper motion examined in the vector point diagram as shown in Fig. 3.5. The UpSco cluster motion is clearly identifiable but is not as free from contamination as the brown dwarf selection was. To estimate contamination, the number of objects contained within selection circles of similar size centred on the points (11,25),(25,-11) and (-25,11) were counted (see Fig. 3.5). 22 objects were found in all three circles so the number of contaminants in the original selection circle was estimated at 7. This left a sample of 37 members of the UpSco within the mass range 0.09 - 1.0 $M_{\odot}$ extracted from an initial selection of 11,041 objects. Among the brown dwarfs in Table 3.2, 11 are judged to be in the range 0.03 - 0.08 $M_{\odot}$. Note that the brown dwarf numbers are extracted from the 19 objects within the 2σ selection circle only. This is to ensure that both star and brown dwarf numbers in the ratios are arrived at using the same criteria. So the ratio of low-mass stars to brown dwarfs in the selected mass range was found to be $38/11 = 3.5^{+2.0}_{-1.3}$ (errors are Poissonian).

The same analysis was then done for 10.5deg^2 to the north where 49 brown dwarf candidates had been identified. 26 objects were assigned masses of between 0.03 - 0.08 $M_{\odot}$. Stars in the mass range 0.08 - 1.0 $M_{\odot}$ and deemed UpSco members because of their photometry and their proper motion, as shown in Fig. 3.5, numbered 102. So the ratio of stars to brown dwarfs in those areas was found to be $102/26 = 3.9^{+1.4}_{-0.9}$, consistent with the south. Overall, the combined figures give a ratio of $140/37 = 3.8^{+1.1}_{-0.8}$ (again, errors are Poissonian).

These numbers can be compared with the ratios published by Andersen et al. (2008, their Table 1). From their sample of 7 clusters, I exclude the Pleiades because it is significantly older than all other regions and Mon

R2 which has a small population of members causing large statistical uncertainties. Only two of the remaining clusters belong to OB associations (ONC, NGC2024), and they feature the lowest star/brown dwarf ratios in the sample (3.3 and 3.8). The SONYC survey has also determined a lower value of between 1.9 and 2.4 for NGC1333, which is part of the Perseus OB2 association (Scholz et al., 2012a, 2013). These values are similar to, or lower than, the ones derived for the OB association UpSco (3.5 and 3.9, see above). In contrast the clusters without OB associations (Chamaeleon, Taurus, IC348) in the sample of Andersen et al. (2008) have higher star to brown dwarf ratios of 4.0, 6.0 and 8.3, respectively. The value for IC348 has subsequently been re-assessed, as part of the work of the SONYC survey, and estimated to range between 1.9 and 4.0 (Scholz et al., 2013). For ρ Oph, another cluster with no OB association, the SONYC survey has reported a value of 5.1 (Mužić et al., 2012).

Thus, based on the current data it seems possible that the presence of OB stars is related to a low star to brown dwarf ratio, i.e. a higher relative abundancy of brown dwarfs. This could be a sign that the radiation field of OB stars favours the formation of brown dwarfs. As noted in the introduction, it has been suggested that substellar and planetary-mass objects can be formed via photoerosion of cores by the ionizing radiation from an OB star (Whitworth & Zinnecker, 2004). At face value this would provide an additional formation channel for brown dwarfs in OB associations, lowering the star to brown dwarf ratio. Given the substantial uncertainties in these ratios, this conclusion is certainly preliminary and needs to be substantiated by future surveys.

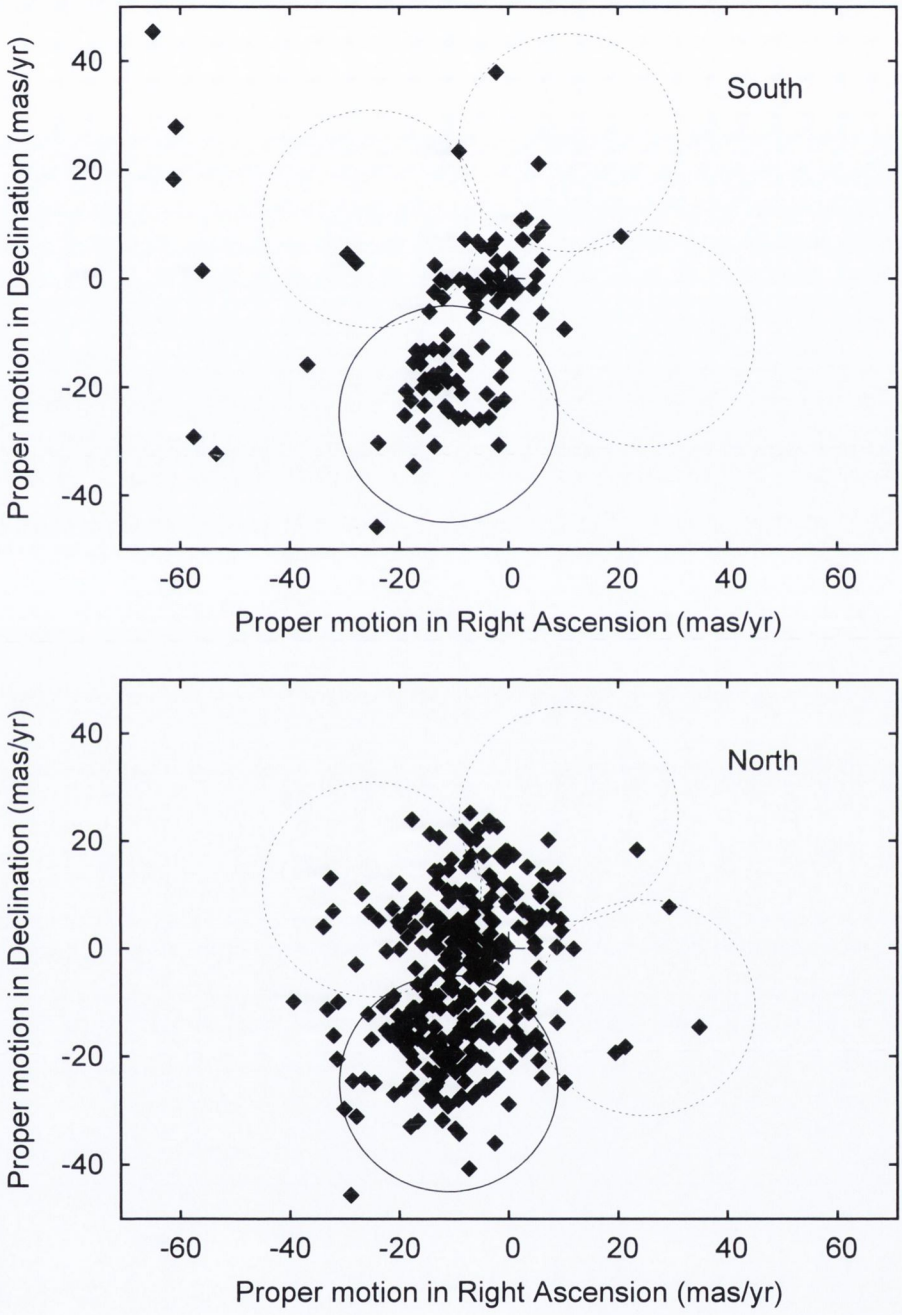

Figure 3.5 Vector point diagrams for objects with photometry of stars within mass range 0.08 - 1.0 $M_{\odot}$. As in Fig. 3.4 a 2σ selection circle centred on (-11,-25) is shown. The upper diagram shows objects from the search area in South UpSco while the lower one is taken from the area to the North. In both cases the Upper Scorpius cluster motion is clearly identifiable. The dashed circles were used for estimating contamination.

3.4 New Objects From UKIDSS 9th Data Release

Some months after the work described above was completed and published (Dawson et al., 2011), UKIDSS completed an extended survey of UpSco - the 9th Data Release. This coincided with the time that the analysis of brown dwarf disks, described in the next chapter, was being undertaken. In order to assemble the largest possible unbiased sample of brown dwarfs for that study, the 9th Data Release was combed for new brown dwarfs. A further 51 substellar objects, including 46 not previously known, were identified. This section outlines the method used to identify the new brown dwarfs in UpSco using the UKIDSS 9th Data Release. It is the same method used to analyse the 8th Data Release. For the sake of brevity, some of the details described above are not repeated here.

As shown in Fig. 3.6, the new area in UpSco investigated here and surveyed for the 9th Data Release covers $24\,\mathrm{deg}^2$. The data for objects in the target area were obtained via an SQL query to the UKIDSS GCS database. All queries were structured to include only point source objects in order to avoid contamination by extended sources (e.g. relatively nearby galaxies). As every object with photometric characteristics consistent with a brown dwarf had its proper motion assessed, in order to check whether it is likely a member of UpSco, each query submitted also correlated all objects found in the UKIRT GCS databases with those found in 2MASS databases. The 2MASS data is used as a first epoch for the purposes of proper motion calculation.

3.4.1 Photometry

A query similar to that shown in the appendix at the end of this chapter was submitted to the WSA. The query returned 1,438,887 objects.

The objects were assessed on the basis of their position on a (Z-J,Z) colour-magnitude diagram as shown in Fig. 3.7. To refine the search, a new query was submitted to the WSA eliminating all objects to the left of a line in the (Z-J,Z) colour-magnitude diagram from (Z-J,Z) = (1.0, 14.0) through (1.4, 16.6) to (3.0, 21.55) (dashed line in Fig. 3.7). This query left 4,398 objects. Reddening caused by extinction shifts objects to the right and down on colour-magnitude diagrams. To assess if reddening was contaminating

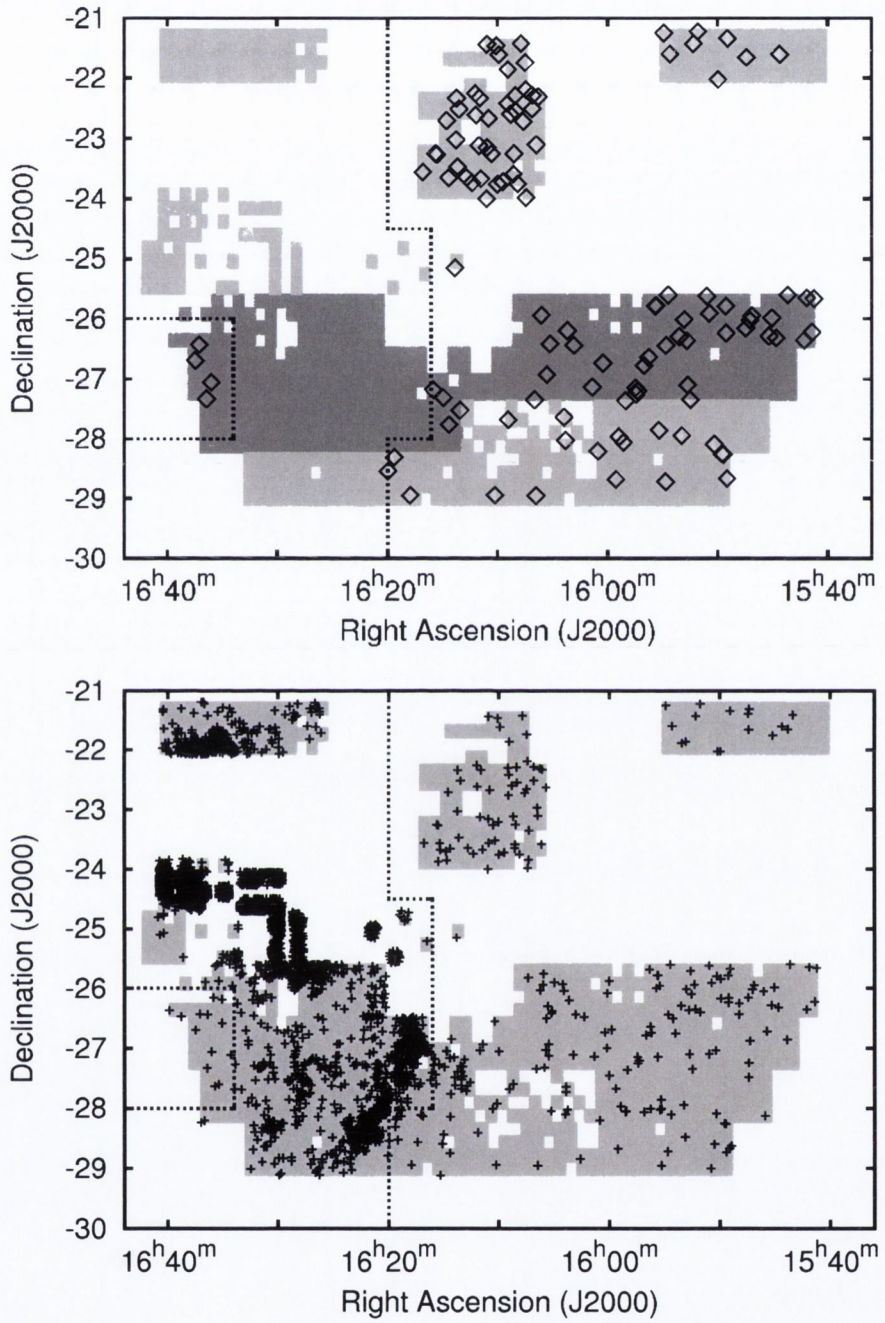

Figure 3.6 Coverage in Z, Y, J, H and K filters of 57 $\deg^2$ in Upper Scorpius from the UKIDSS GCS. The upper panel shows the new 24 $\deg^2$ of coverage from the 9th Data Release in dark grey and earlier coverage in light grey. The open diamonds mark the position of the 116 brown dwarfs that comprise the sample analysed in this work. The lower panel shows the location of objects selected by the first cut in the (Z-J,Z) colour-magnitude diagram. 95% of all the objects selected from the 9th Data Release are clustered around the heavily extincted region surrounding ρ Oph. To obtain a minimally contaminated sample of brown dwarf candidates, the area inside the two sets of dashed lines was excluded from consideration.

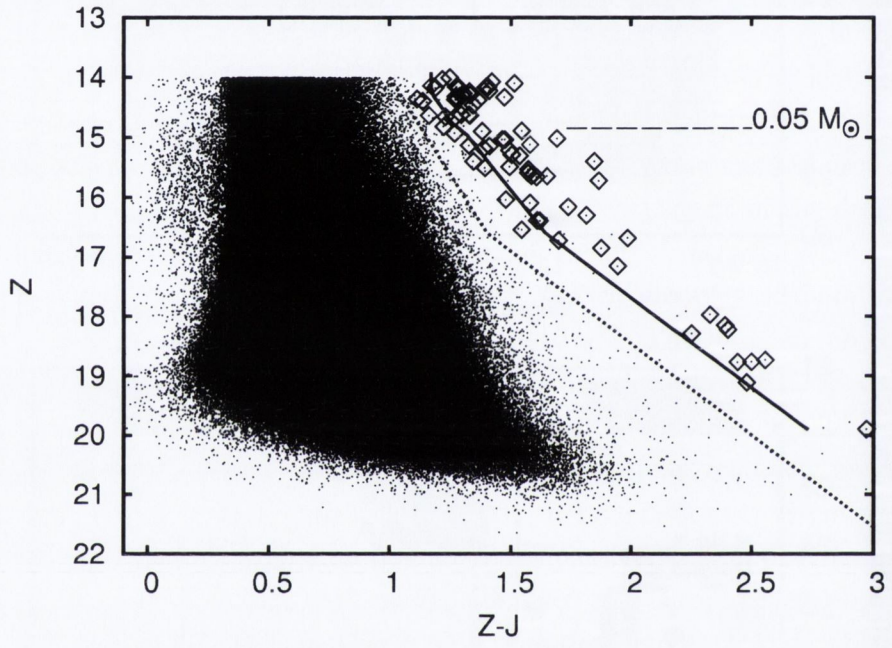

Figure 3.7 (Z-J,Z) colour-magnitude diagram showing the 76 brown dwarf candidates from the 9th Data Release as open diamonds. All other objects are shown as small dots. The 5 Myr DUSTY model (Chabrier et al., 2000) isochrone is also shown with mass decreasing going down the isochrone from $0.09\,M_{\odot}$ at the top to $0.01\,M_{\odot}$ at the bottom. The $0.05\,M_{\odot}$ position on the isochrone is indicated. All objects to the left of the dashed line were rejected because of their colours.

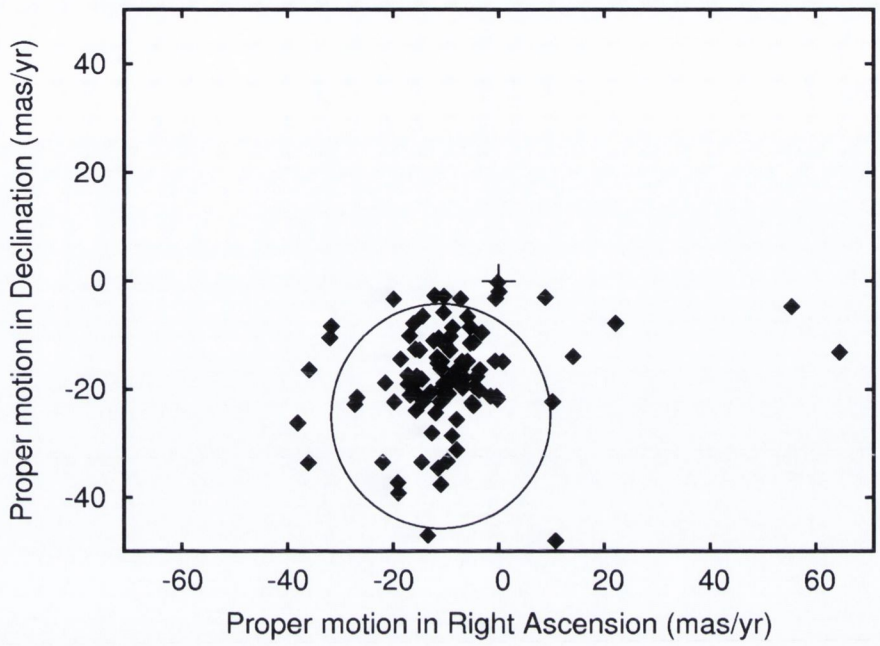

Figure 3.8 Vector point diagram for 96 candidate brown dwarfs in Upper Scorpius. There is an obvious and identifiable cluster around (-11,-25), while there is no significant clustering around the origin, indicating that there is very little contamination from background objects in the sample. Candidates lying outside the 2σ selection circle were classified as non-members, leaving 76 brown dwarf members of UpSco.

the results the 4,398 objects had their location plotted as shown in the lower panel of Fig. 3.6. There is an obvious clustering of objects in a large area which coincides with the heavily extincted region around ρ Oph. Therefore, the analysis was confined to 706,638 objects in the 9th Data Release that were outside that region (dashed lines in Fig. 3.6). This left only 200 of the 4,398 objects selected in the initial (Z-J,Z) cut. These 200 objects were examined again in the (Z-J,Z) colour-magnitude diagram. 86 of the objects to the left of the line (Z-J,Z) = (1.1, 14.0) through (1.1, 14.3), (1.2, 14.9), (1.3, 15.2), (1.6, 17.0) to (3.0,21.0) were rejected for being too far from the isochrone on the blue side, leaving 114 photometric candidates.

3.4.2 Proper Motion

The 114 photometric candidates were then examined to find their proper motion. The resulting vector point diagram is shown in Fig. 3.8. The known proper motions of UpSco in right ascension and declination are about -11mas/yr and -25mas/yr respectively (de Bruijne et al., 1997; Preibisch et al., 2002). Of the 114 candidates, 4 were too faint to be recorded in 2MASS leaving 110 candidates with proper motion data calculated. The remaining 110 candidates included 14 with proper motions greater than the range of Fig. 3.8.

All 96 candidates shown in Fig. 3.8 are predominantly centred around the (-11,-25) position. A 2σ selection circle, as previously calculated, is shown centred on that position. There is no significant clustering of objects around the (0,0) position indicating that the sample is not contaminated by more distant objects. The 76 candidates within the 2σ selection circle were then classified as members of UpSco. These objects so selected have the photometric and proper motion characteristics of a 5 Myr old brown dwarf member of UpSco. 25 of the 76 were among the sample of 68 selected from the 8th Data Release, yielding 51 new objects from the 9th Data Release to add to the sample. From these 51 brown dwarfs, 5 have been identified before. Lodieu et al. (2006) identifies 1 of them, Martín et al. (2004) lists another and Ardila et al. (2000) identifies 3. The remaining 46 had not been previously identified in other surveys.

One potential caveat with respect to this sample is the fact that the Upper Scorpius population and the younger ρ Oph population are unlikely to be clearly separated in colour-magnitude or proper motion diagrams. By avoiding the areas with very high extinction (see Fig. 3.6) I exclude the bulk of the population of ρ Oph, but some scattered young substellar members of ρ Oph might still contaminate the sample. There is however, as described in the next chapter, a low disk fraction in the sample, which suggests that contamination from ρ Oph cannot be a major factor.

3.5 Summary

I carried out a survey for brown dwarfs in the 5 Myr old UpSco star forming region based on photometry and proper motions from a combination of the UKIDSS Galactic Cluster Survey and 2MASS. Initially, 19 new substellar

objects, with estimated masses between 0.01 and 0.09 $M_{\odot}$, were identified. These objects are located in the southern part of the association which had not been covered by previous brown dwarf surveys. 8 other objects with slightly higher proper motion have also been identified. These may be UpSco members with slightly higher dispersion velocity than the stellar members. I then carried out a second survey, on an extended area in UpSco, that was covered by a later data release. A further 46 new substellar objects, in the same mass range as the original 19, were identified. Although spectroscopic confirmation had not been obtained yet, the level of contamination appeared to be negligible.

The ratio of stars to brown dwarfs in the South of UpSco was found to be $3.5^{+2.0}_{-1.3}$, in the same range as elsewhere in UpSco. A comparison of literature findings showed that young clusters with OB associations tend to have lower ratios than clusters without OB stars, which might indicate that brown dwarf formation is a function of environment.

Table 3.1. Positions, Z, Y, J, H and K photometry, and proper motion of the 6 objects outside the range of Fig. 3.4. Coordinates are J2000, and taken from the UKIDSS GCS 8th Data Release (2010).

Name	R.A.	Dec.	Z Mag.	Y Mag.	J Mag.	H Mag.	K Mag.	$\mu_\alpha cos\delta$ mas/yr	μ_δ mas/yr
2MASSJ15583064-2802357	15:58:30.63	-28:02:36.3	16.53	15.75	14.99	14.47	14.03	-28.27	-66.30
2MASSJ16035915-2806086	16:03:58.76	-28:06:09.6	16.78	15.82	15.02	14.46	14.00	-2.19	-115.84
2MASSJ15530915-2828366	15:53:09.13	-28:28:37.3	14.81	14.18	13.51	13.00	12.63	-46.20	-75.62
2MASSJ15492508-2843527	15:49:24.85	-28:43:51.6	14.15	13.49	12.84	12.39	12.02	-384.23	+138.80
2MASSJ16151681-2907007	16:15:16.28	-29:07:01.3	14.10	13.40	12.86	12.23	11.96	+15.06	-60.37
2MASSJ15481934-2748512	15:48:19.30	-27:48:51.3	19.77	17.56	16.73	16.15	15.83	-74.00	-8.34

Table 3.2. Positions, Z, Y, J, H and K photometry, and proper motion of the final 19 objects selected. Also included are the 8 other objects shown in Fig. 3.4 and lastly, the object too faint to be recorded in 2MASS. Coordinates are J2000, and taken from the UKIDSS GCS 8th Data Release (2010).

Name	R.A.	Dec.	Z Mag.	Y Mag.	J Mag.	H Mag.	K Mag.	$\mu_\alpha cos\delta$ mas/yr	μ_δ mas/yr
2MASSJ15582376-2721435	15:58:23.76	-27:21:43.7	14.35	13.72	13.07	12.60	12.22	-17.20	-19.05
2MASSJ16090168-2740521	16:09:01.68	-27:40:52.3	14.33	13.60	12.86	12.35	11.89	-8.75	-17.46
2MASSJ16035573-2738248	16:03:55.73	-27:38:25.1	15.19	14.48	13.80	13.28	12.88	-12.64	-28.09
2MASSJ15585793-2758083	15:58:57.93	-27:58:08.5	15.13	14.45	13.81	13.31	12.93	-9.46	-20.79
2MASSJ15531698-2756369	15:53:16.98	-27:56:37.2	15.53	14.68	13.96	13.45	13.04	-14.61	-33.48
2MASSJ15551960-2751207	15:55:19.59	-27:51:21.0	15.59	14.77	14.02	13.51	13.11	-19.02	-39.21
2MASSJ15501958-2805237	15:50:19.58	-28:05:23.9	16.04	15.27	14.56	14.05	13.66	-5.02	-22.51
2MASSJ15583403-2803243	15:58:34.03	-28:03:24.5	15.21	14.46	13.72	13.17	12.73	-3.61	-20.20
2MASSJ16005265-2812087	16:00:52.66	-28:12:09.0	15.03	14.27	13.57	13.04	12.66	-0.38	-21.28
2MASSJ15492909-2815384	15:49:29.08	-28:15:38.6	14.29	13.62	12.96	12.47	12.06	-14.25	-22.20
2MASSJ15493660-2815141	15:49:36.59	-28:15:14.3	14.66	14.02	13.39	12.91	12.52	-11.87	-24.36
2MASSJ16192399-2818374	16:19:23.99	-28:18:37.5	15.29	14.52	13.78	13.31	12.90	-5.33	-8.51
2MASSJ15490803-2839550	15:49:08.02	-28:39:55.2	14.82	14.23	13.60	13.09	12.72	-19.86	-22.31
2MASSJ15485777-2837332	15:48:57.76	-28:37:33.4	17.99	16.79	15.80	15.20	14.55	-17.24	-17.39
2MASSJ16195827-2832276	16:19:58.26	-28:32:27.8	18.74	17.29	16.18	15.39	14.74	-27.34	-22.75
2MASSJ15544486-2843078	15:54:44.85	-28:43:07.9	15.51	14.79	14.12	13.61	13.22	-15.80	-12.59
2MASSJ15591513-2840411	15:59:15.12	-28:40:41.3	14.13	13.56	12.96	12.49	12.15	-11.40	-15.19
2MASSJ16062870-2856580	16:06:28.70	-28:56:58.2	14.90	14.21	13.52	13.01	12.63	-7.91	-16.46
2MASSJ16101316-2856308	16:10:13.15	-28:56:31.0	15.67	14.81	14.06	13.54	13.11	-10.36	-18.99
2MASSJ16051544-2802520	16:05:15.44	-28:02:52.0	17.92	16.66	15.69	15.05	14.47	-7.11	-3.30
2MASSJ15552513-2801085	15:55:25.11	-28:01:08.8	14.12	13.51	12.88	12.47	12.01	-38.10	-26.24
2MASSJ15502934-2835535	15:50:29.32	-28:35:53.9	16.05	15.32	14.59	14.03	13.63	-36.07	-33.63
2MASSJ16190983-2831390	16:19:09.82	-28:31:39.5	16.63	15.67	14.70	14.17	13.67	-13.41	-47.04

Table 3.2 (cont'd)

Name	R.A.	Dec.	Z Mag.	Y Mag.	J Mag.	H Mag.	K Mag.	$\mu_\alpha cos\delta$ mas/yr	μ_δ mas/yr
2MASSJ16035601-2743335	16:03:56.00	-27:43:33.6	14.41	13.91	13.26	12.64	12.29	-19.94	-3.33
2MASSJ16145936-2826214	16:14:59.37	-28:26:21.8	14.68	14.12	13.50	12.83	12.48	+10.75	-48.05
2MASSJ15551768-2856579	15:55:17.70	-28:56:58.1	14.32	13.80	13.19	12.66	12.33	+14.02	-13.91
2MASSJ15504920-2900030	15:50:49.19	-29:00:03.1	14.35	13.82	13.21	12.64	12.34	-32.06	-10.49
UGCSJ154723.32-272907.3	15:47:23.33	-27:29:07.3	19.27	17.91	16.76	15.97	15.40	—	—

3.6 Appendix: Sample SQL Query

Shown below is the SQL query submitted to the WSA to find the first set of sources in the Upper Scorpius association. The query returned 282,938 rows of data.

```
    Select
g.ra, g.dec, zmypnt, ymjpnt, jmhpnt, hmk_1pnt, zapermag3,
yapermag3, japermag3, hapermag3, k_1apermag3,
3.6e6*cos(radians(g.dec))*(g.ra-T2.ra)/
((mj.mjdobs - T2.jdate+2400000.5)/365.25) as pmRA,
3.6e6*(g.dec-T2.dec)/((mj.mjdobs - T2.jdate+2400000.5)/365.25)
as pmDEC
From
gcsmergelog as I, multiframe as mj, (Select t.ra as ra, t.dec
as dec, x.slaveobjid as slaveobjid,
x.masterobjid as masterobjid, t.j_m, t.h_m, t.k_m, t.jdate
From
gcssourcextwomass_psc as x, twomass..twomass_psc as t
Where x.slaveobjid=t.pts_key
And distancemins In (Select Min(distancemins)
From
gcssourcextwomass_psc
Where masterobjid=x.masterobjid)) As T2 Right Outer
Join gcssource As g On (g.sourceid=T2.masterobjid)
Where (g.ra Between 235.0 And 245.0)
And (g.dec Between -30.0 And -27.0)
And zapermag3 > 14.0 And yapermag3 > 11.5 And japermag3 > 12.0
And hapermag3 > 10.0 And k_1apermag3 > 9.5
And zxi Between -1.0 And +1.0 And yxi Between -1.0 And +1.0
And jxi Between -1.0 And +1.0 And hxi Between -1.0 And +1.0
And k_1xi Between -1.0 And +1.0
And zeta Between -1.0 And +1.0 And yeta Between -1.0 And +1.0
And jeta Between -1.0 And +1.0 And heta Between -1.0 And +1.0
And k_1eta Between -1.0 And +1.0
And zclass Between -2 And -1 And yclass Between -2 And -1
And jclass Between -2 And -1 And hclass Between -2 And -1
```

```
And k_1class Between -2 And -1
And (priorsec = 0 Or priorsec = g.framesetid)
And g.framesetid=I.framesetid And I.jmfid=mj.multiframeid
```

Chapter 4

Brown Dwarf Disks

The clear majority of low-mass stars lose their disk within less than 5 Myr (Haisch et al., 2001; Jayawardhana et al., 2006). As the oldest nearby star forming region with a substantial number of brown dwarfs, UpSco is perhaps the best testbed for the longevity of disks. UpSco is often assumed to have an age of 5 Myr (Preibisch et al., 2002) but recently Pecaut et al. (2012) have derived an older age of 10 Myr for this region. In UpSco, Carpenter et al. (2006) derived a disk frequency of $< 8\%$ for F and G stars and $19 \pm 4\%$ for K0-M5 stars (with $1\,\sigma$ binomial confidence intervals). The brown dwarfs in this region exhibit a disk fraction of $37 \pm 9\%$, based on an examination of 35 objects (Scholz et al., 2007). So, the Spitzer data tentatively shows that the disk fractions *in UpSco increase monotonically with decreasing object mass for early F- to late M-type objects.* This would imply a mass dependence in the disk evolution, resulting in long-lived disks in the substellar regime.

So far, the brown dwarf disk frequency in UpSco is affected by low number statistics. In this chapter I set out to test previous findings based on a much enlarged number of brown dwarfs in UpSco, identified from UKIDSS. To identify the objects in my sample that have a disk (Class II objects) and those that do not (Class III objects), data from the Wide-Field Infrared Survey Explorer (WISE) (Wright et al., 2010) is utilised. As will be shown, with improved statistics, I find a disk fraction for brown dwarfs that is consistent with the value published for low-mass stars in this region. The results presented in this chapter are based on work which originally appeared in Dawson et al. (2011, 2013).

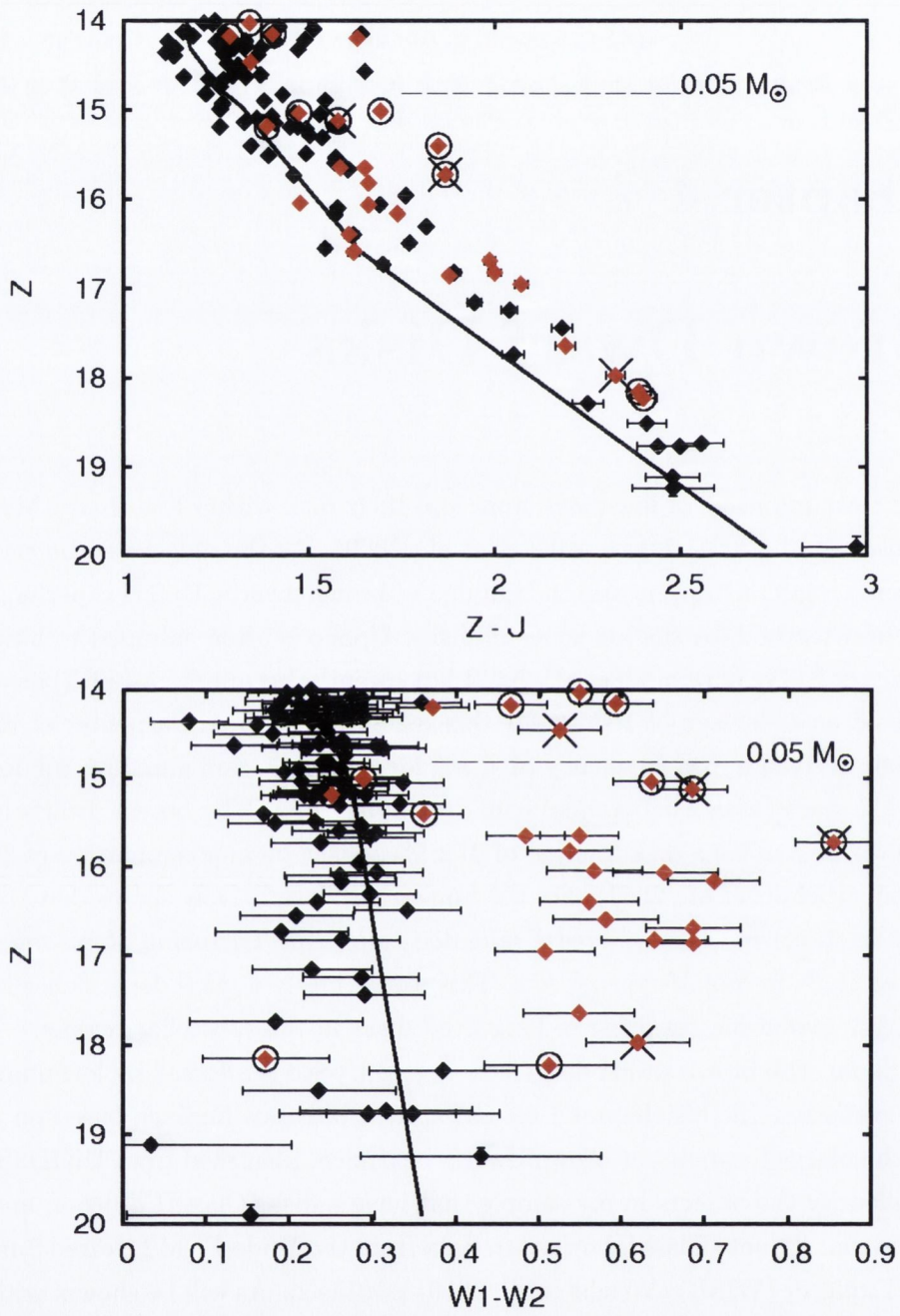

Figure 4.1 (Z-J,Z) and (W1-W2,Z) colour-magnitude diagrams for 116 Up-Sco brown dwarfs. Class II objects are marked in red. The 5 Myr DUSTY model (Chabrier et al., 2000) isochrones are shown with mass decreasing from 0.09 $M_\odot$ (top) to 0.01 $M_\odot$ (bottom), with the 0.05 $M_\odot$ position indicated. In the (Z-J,Z) diagram all the objects are grouped close to the isochrone. However, two distinct populations of objects are clearly visible in the (W1-W2,Z) diagram, one close to the isochrone and one showing an excess in W1-W2. The 11 objects ringed have bright signals in W4 (22 μm), diagnostic of the presence of a disk. The 4 objects marked with a cross have significant variations in their UKIRT and 2MASS J or H magnitudes.

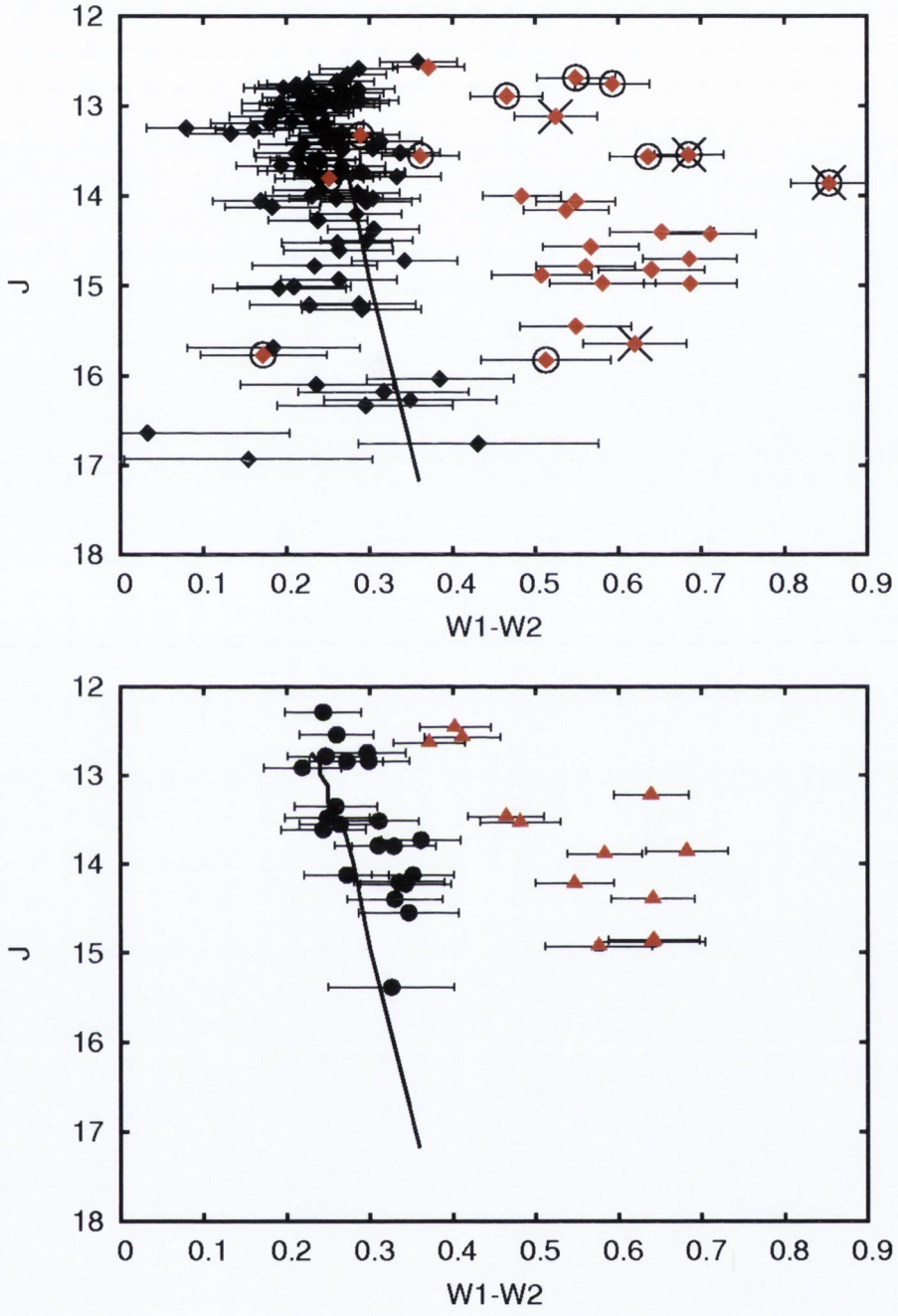

Figure 4.2 (W1-W2,J) colour-magnitude diagrams. The 116 brown dwarfs with available WISE data analysed in this work are shown in the upper panel with symbols and isochrone as in Fig. 4.1. The lower panel shows the same diagram for 35 objects in UpSco identified in Scholz et al. (2007). Objects confirmed as having disks in Scholz et al. (2007) are shown as closed triangles while those with no disk detected are shown as closed circles. As can be seen, the objects in the population with obvious colour excess all have disks. A few objects with disks exhibit a smaller, but still significant colour excess (i.e. they are more than $2\,\sigma$ away from the isochrone). Objects with no disk lie close to the isochrone.

4.1 Targets

In Chapter 3, and as first described in Dawson et al. (2011), I identified 19 new brown dwarf candidates in the south of UpSco via a photometric and proper motion analysis of the UKIDSS 8th Data Release. The level of contamination from background stars in the sample was shown to be negligible. Using the same method in the north of UpSco a further 49 objects previously identified by Lodieu et al. (2006, 2007) as brown dwarf candidates were recovered. Spectra have been taken of 26 of these 49 objects (Martín et al., 2004; Slesnick et al., 2006; Lodieu et al., 2006, 2008, 2011) and all 26 have been confirmed as brown dwarfs. This provides a sample of 68 very low mass stellar and substellar objects in UpSco. It was determined that the 68 objects ranged in mass from 0.01 $M_{\odot}$ to 0.09 $M_{\odot}$ by comparing their observed Z magnitudes with theoretical Z magnitudes from the DUSTY models for 5 Myr old objects. Subsequently, a further 51 objects in the same mass range were identified, from the UKIDSS 9th Data Release. The addition of these new objects increases the size of the homogeneous sample of objects uniformly selected via their colour and proper motion characteristics to 119. Although some objects in the sample may be slightly above the substellar threshold, I refer to the targets as "brown dwarfs" throughout this chapter, for simplicity.

All 119 objects lie close to the 5 Myr DUSTY model isochrones of Chabrier et al. (2000) in a (Z-J,Z) UKIDSS passbands colour-magnitude diagram, as shown in Fig. 4.1, i.e. none of them exhibit any substantial excess at these near-infrared wavelengths. The objects, as demonstrated in the previous chapter, are also generally free from reddening caused by extinction. Consequently it can be inferred that the (Z-J,Z) value for any of the objects is photospheric in origin with negligible contribution from any circumsubstellar disk. Thus, the method of selecting these 119 objects is unbiased with respect to the presence of circumsubstellar disks.

As pointed out above, the 26 objects in the sample with published spectra have been confirmed to be very low mass members of UpSco. In addition, I have recently obtained spectra for 24 further objects from this sample; and all of them are confirmed as very low mass members of UpSco as well (Dawson et al. (2014), and the final chapter of this thesis). The 100% success rate for almost half the sample indicates that my selection method, based

on photometry and proper motion, generates a clean, unbiased sample with negligible contamination by background objects.

4.2 WISE Data

For 116 of the 119 targets discussed above, WISE data were obtained. The remaining 3 were not listed in the WISE database. For the 116 the 2MASS identifier listed in the WISE database agrees with the one from UKIDSS. In addition, all objects were visually examined in the WISE images and in the UKIDSS images. It was found that for the 116 objects analysed here the identification of the UKIDSS source with the WISE source at the same position is unambiguous (for the three excluded targets this is not the case). Furthermore, since the target fields are sparsely populated and well above the Galactic Plane (latitude 10-30 deg), the likelihood of accidental contamination by other objects is very low.

WISE surveyed the whole sky in four mid-infrared wavebands simultaneously, using passbands with effective wavelengths of 3.4 μm (W1), 4.6 μm (W2), 12 μm (W3) and 22 μm (W4). I used the results of profile-fitting photometry from the All Sky Data Release, further details of which can be found in Cutri et al. (2011)[1]. Among the 116 objects are 2 that were previously examined by Scholz et al. (2007) and confirmed to have disks.

4.3 Colour Analysis

The five UKIRT passbands; Z, Y, J, H and K have respective wavelengths of 0.88 μm, 1.03 μm, 1.25 μm, 1.63 μm, and 2.20 μm. J, H and a passband similar to K are also used in 2MASS. As noted above, the four WISE passbands; W1, W2, W3, W4, have longer wavelengths of 3.4 μm, 4.6 μm, 12 μm and 22 μm respectively. Different colour-colour and colour-magnitude diagrams using combinations of all nine passbands were examined. The (Z-J,Z) and (W1-W2,Z) colour-magnitude diagrams are shown in Fig. 4.1. Theoretical isochrones for 5 Myr old substellar objects are also shown over-plotted on the diagrams. These isochrones are based on the DUSTY models derived by Chabrier et al. (2000) and obtained from both I. Baraffe and F. Allard

[1]For more details of the WISE All Sky Data Release also see http://wise2.ipac.caltech.edu/docs/release/allsky/expsup/

(private communications). The isochrones were computed using both the UKIDSS and WISE filter profiles. The (Z-J,Z) isochrone was used to assign masses to objects, as in Chapter 3. The uppermost point on the 5 Myr isochrone corresponds to a mass of $0.09\,M_{\odot}$ while the lowest point corresponds to a mass of $0.01\,M_{\odot}$.

4.3.1 WISE data for UpSco brown dwarfs

W1-W2 (3.4-4.6 μm)

In the (Z-J,Z) diagram all the objects are grouped close to the isochrone and none show any significant colour excess, as discussed above. However, two distinct populations of objects are clearly visible in the (W1-W2,Z) diagram, one close to the isochrone and one showing an excess in W1-W2 (3.4 μm-4.6 μm). The population with excess is best understood as objects harbouring dusty disks and therefore emitting thermal infrared radiation (Class II). These two populations do not show up in the diagrams that utilise only UKIRT passbands. Other diagrams that combine both UKIRT and WISE passbands do show the two populations. Colours that use a UKIRT and WISE W1 (3.4 μm) passband do show the two populations but not as clearly as colours incorporating W2 (4.6 μm). The K-W2 colour in particular discriminates between the two populations almost as well as the W1-W2 colour. The W1-W2 colour was chosen as the primary diagnostic for distinguishing between Class II and Class III objects in the work described in this chapter (see Figs. 4.1 and 4.2).

W1-W2: Comparison with Scholz (2007)

To test that the method outlined above was successfully discriminating between Class II and Class III objects it was also applied to the 35 objects in UpSco examined by Scholz et al. (2007). That study used a Spitzer survey combining spectroscopy from 8 to 12 μm and photometry at 24 μm. As 33 of the 35 objects lie outside the area covered by UKIDSS there is no Z or Y passband data available for them. However they are recorded in the J, H and K_S passbands of 2MASS. The 35 objects were plotted in a (W1-W2,J) colour-magnitude diagram (shown in the lower panel of Fig 4.2) using data from 2MASS. The 116 objects from this work were also plotted in a (W1-W2,J) colour-magnitude diagram (shown in the upper panel of Fig. 4.2) for

comparison, using data from the UKIDSS J passband. Two of the objects from Scholz et al. (2007) lie inside the area covered by UKIDSS and were recovered in the search detailed in the previous chapter. The differences in their UKIDSS and 2MASS J magnitudes are negligible (0.06mag in both cases).

As can be seen from the lower panel of Fig. 4.2, all the objects with circumsubstellar disks have sufficient excess in W1-W2 (3.4-4.6 μm) to stand clear of the objects with no disks clustered along the isochrone. A few of the objects with disks exhibit a lesser, but still significant colour excess in W1-W2 (i.e. they are more than $2\,\sigma$ away from the isochrone). The method successfully discriminated between the 13 Class II and 22 Class III objects in this sample.

W3 (12 μm)

Colours that utilise the longer wavelength W3 (12 μm) passband are of limited use as only 39 of the 116 objects have a S/N > 5.0 in W3. By contrast, all 116 objects have a S/N > 8.0 in W1 and W2. The 39 objects with a S/N > 5.0 in W3 were further examined in the (W1-W2,W3) colour-magnitude diagram shown in Fig. 4.3. They are all among the higher mass objects in the sample, as evidenced by the lack of objects around the lower part of the isochrone. The population with the W1-W2 (3.4-4.6 μm) colour excess is again distinct from the population close to the isochrone as in the previous diagrams. The ninth brightest object in W3 now stands clear from the population near the isochrone. While this object is not obviously part of the population with excess in W1-W2 seen in Figs. 4.1 and 4.2, it is more than $2\,\sigma$ away from the isochrone. On the combined basis of its excess in W1-W2 and its brightness in W3 it appears to have a disk and so is included in the group of Class II objects. This object is one of the 2 objects common to both this study and that of Scholz et al. (2007) who note that it has a binary companion at a separation of 12 au.

W4 (22 μm)

The objects also had their detection in the W4 (22 μm) WISE passband examined. Photospheric emission from brown dwarfs is negligible by comparison with emission from a disk at wavelengths longer than 20 μm (Scholz

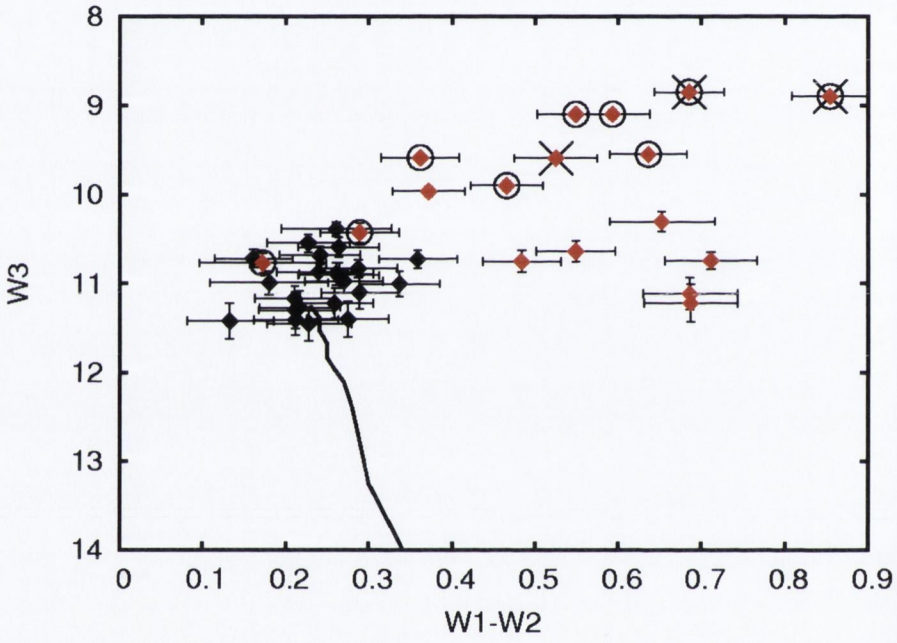

Figure 4.3 (W1-W2,W3) colour-magnitude diagram for 39 of the 116 objects with a S/N > 5.0 in W3 ($12\,\mu$m). Symbols and isochrone are as in Fig. 4.1. The 39 objects are all among the higher mass objects in the sample, as evidenced by the lack of objects around the lower part of the isochrone.

et al., 2007). Therefore any object with a bright unambiguous signal in W4 shows clear evidence of the presence of a dusty disk, even if it does not have an excess in W1-W2 (3.4-4.6 μm). 105 of the objects were not distinguishable from the background in W4, having S/N varying from 4.7 to zero. The remaining 11 were detected with S/N > 5.0 and have the brightest signals in W4. These 11 are marked with rings in Figs. 4.1, 4.2, 4.3 and 4.4. Of the 11, 7 are in the population of 22 with distinct W1-W2 (3.4-4.6 μm) colour excess.

(W1-W2, J-K)

The (W1-W2,J-K) colour-colour diagram in Fig. 4.4 was examined to see if Class II and Class III objects could be clearly separated. Apart from the 2 objects which are bright in W4 and have large differences in their UKIDSS and 2MASS J magnitudes, none of the objects show any significant excess in J-K. This serves to confirm previous findings (Natta & Testi, 2001; Natta et al., 2002) that the efficacy of using J-K excess as a diagnostic for the presence of disks around very low mass stars and brown dwarfs is very limited.

4.3.2 Variable Objects

A comparison was also made of the UKIDSS and 2MASS photometry for each object. UKIDSS and 2MASS data were gathered at different epochs several years apart - 2MASS between 1997 and 2001 (Skrutskie et al., 2006) and UKIDSS from 2005 onwards (Lawrence et al., 2007). Of the 116 objects, 112 showed a variation of less than 0.2 mag in J, H and K. The remaining 4, which are listed in Table 4.1 (and marked with crosses in Figs 4.1, 4.2, 4.3 and 4.4), showed variations of greater than 0.2 mag in J, H or K. Such variations in J have been interpreted by Scholz et al. (2009) as signatures of accretion. Scholz et al. (2009) further note that cool spots (comparable to sunspots) are expected to produce variations of < 0.15mag in J and < 0.1mag in K while large-scale photometric variability with amplitudes declining towards longer wavelengths - as displayed by the 3 most variable objects in Table 4.1 - is generally caused by hotspots or variable extinction due to a rotating disk. Hotspots in young stars and brown dwarfs are thought to be a direct consequence of accretion and so they are evidence of the existence of a disk. Likewise, variable extinction is also evidence of the existence of a

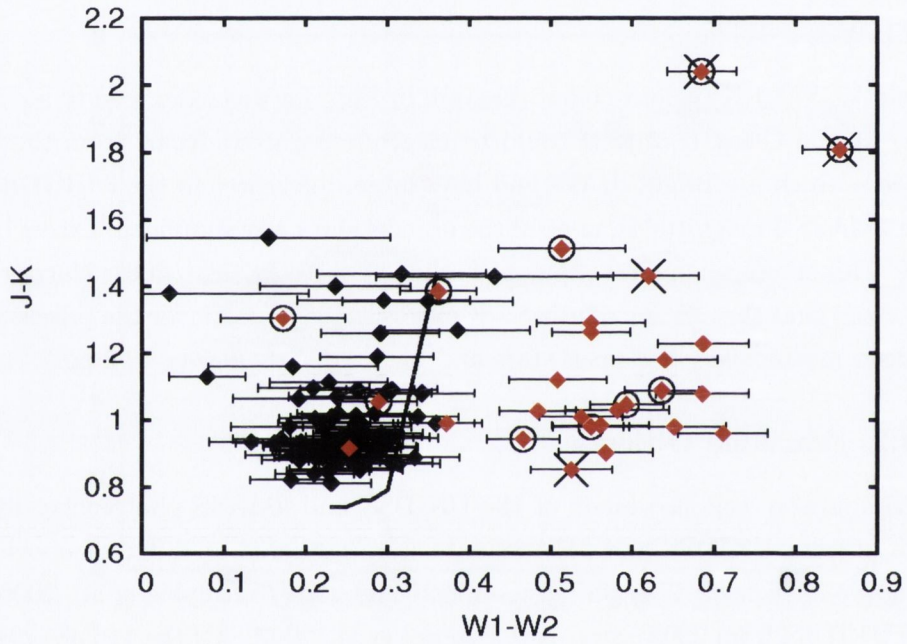

Figure 4.4 (W1-W2,J-K) colour-colour diagram with brown dwarfs and isochrones as in Figs 4.1 and 4.2. The two objects which are bright in W4 and which show signs of accretion have an excess in both W1-W2 and J-K. Apart from those two the rest of the population with excess in W1-W2 shows no obvious excess in J-K.

disk. All 4 objects are in the population with W1-W2 colour excess.

4.4 Discussion

In all, 22 objects were identified as Class II objects on the basis of their W1-W2 colour alone. 1 object with a small W1-W2 excess was also placed in the population of Class II objects because of its bright W3 signal. A further 4 other objects with no W1-W2 excess were also categorised as Class II because of their bright signals in the 22 μm W4 passband. All 27 objects are listed in Table 4.2. The remaining 89 objects, which are listed in Table 4.3, were deemed to be Class III i.e. they have no disks or disks with a large inner opacity hole of at least 5 - 20 au - see Scholz et al. (2007). The spectral energy distributions for 6 characteristic examples of the Class II objects are shown in Section 4.4.3.

4.4.1 Disk Fraction

The overall disk fraction is 27 out of 116 or 23±5% (the uncertainty corresponds to a 1 σ confidence interval based on binomial statistics). As noted in Section 4.1 above, contamination in the sample appears to be negligible. Conservatively assuming that 10% of the objects are contaminants which do not exhibit mid-infrared excess would only increase the disk fraction to 27/104, i.e. 26%. This contrasts with the previous results for UpSco of $37 \pm 9\%$ (Scholz et al., 2007) obtained with a smaller sample of 35 objects. The sample of 35 objects in Scholz et al. (2007) was selected from the surveys of Ardila et al. (2000) (12 objects) and Martín et al. (2004) (23 objects). The higher disk fraction reported in Scholz et al. (2007) may be the result of using a smaller sample of objects or of a possible bias.

The results of Scholz et al. (2007) were also in contrast to the disk fraction of 19% for K0 to M5 stars in the same region obtained by Carpenter et al. (2006) using a sample of 127 K0 to M5 stars. This new result, of 23±5%, from a similarly sized sample of 116 objects, is statistically indistinguishable from the result of Carpenter et al. (2006), suggesting that disk lifetimes in UpSco for objects later than K0 show no dependency on the mass of the central object. I note that from my sample of 27 disks, 22 (from 72, 31%) are found to be in the mass range 0.01-0.05 $M_{\odot}$, while only 5 (from 44, 11%) are in the mass range 0.05-0.09 $M_{\odot}$. This may indicate a trend

towards higher disk fractions for very low mass brown dwarfs, but it is not sufficiently robust to warrant further discussion.

Disk Fractions In Other Clusters

This result for UpSco can be compared with those for Cha I (Damjanov et al., 2007; Luhman et al., 2005), IC348 (Luhman et al., 2005; Lada et al., 2006) and σ Ori (Hernandez et al., 2007), 3 other associations for which similar information is available. Damjanov et al. (2007) reports a disk fraction of 52±6% from a sample of 81 K3 to M8 objects in Cha I, while Luhman et al. (2005) finds a disk fraction of 50±17% from a much smaller sample of 18 objects later than M6. Luhman et al. (2005) also finds a disk fraction of 42±13% for 24 objects later than M6 in IC348, where Lada et al. (2006) reports a disk fraction of 47±12% in the range of K6 to M2 stars. In an analysis of disks in σ Ori, Hernandez et al. (2007) finds a disk fraction of 36±4% for stars in the mass range of 0.1 to 1.0 $M_{\odot}$ and 33±10% for brown dwarfs (defined as objects $< 0.1\,M_{\odot}$). The spectral type of the most massive stars in this range defined by Hernandez et al. (2007) are a little earlier than K (up to G8). However, the vast bulk of their sample is in the mass range of K and M stars, so their result is noted here as being valid for K and M stars in σ Ori. Fig. 4.5 shows that in the wake of this revision of the results for UpSco, all 4 associations now show similar disk fractions for K/M stars and brown dwarfs. Thus, average disk lifetime does not appear to be dependent on the mass of the central object in any of these regions.

The Ages Of The Associations

All the associations listed above are young, i.e. < 10 Myr old. As stated before, Preibisch et al. (2002) determined an age of about 5 Myr for UpSco, while a revised age of 10 Myr has been proposed by Pecaut et al. (2012). Cha I, IC348 and σ Ori have each had various ages of between 2 and 5 Myr reported for each of them (Luhman, 2004, 2007; Luhman et al., 2003; Mayne et al., 2007; Zapatero Osorio et al., 2002; Oliveira et al., 2002; Sherry et al., 2004). So while UpSco appears to be the oldest of the 4 associations, Cha I, IC348 and σ Ori cannot yet be readily distinguished in terms of their ages. Ergo, apart from stating that the oldest association has the smallest disk fraction, no robust correlation can be safely determined in respect of the

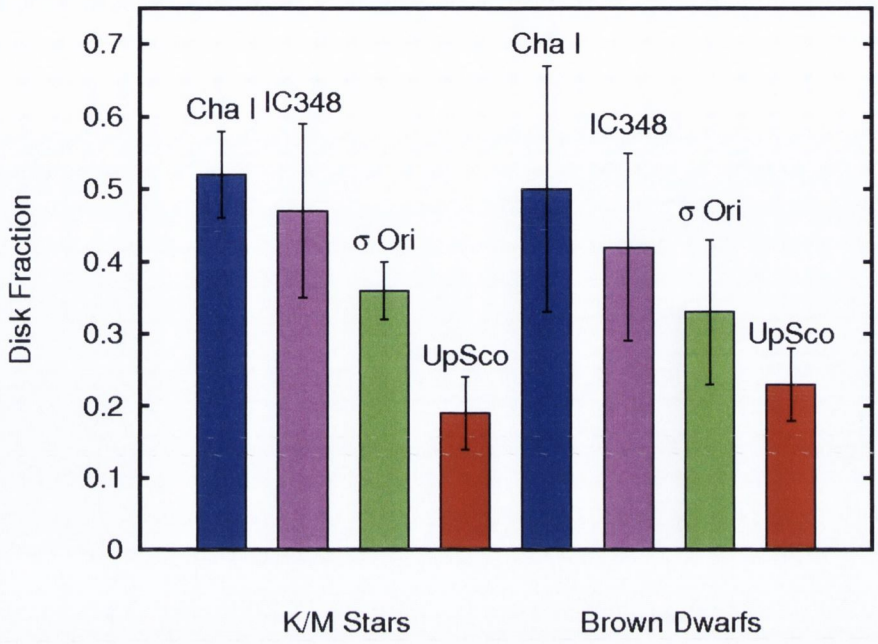

Figure 4.5 Disk fractions for K/M stars compared to disk fractions for brown dwarfs in Cha 1, IC348, σ Ori and UpSco. In each case the disk fraction for the K/M stars is statistically indistinguishable from the disk fraction for the brown dwarfs (see text; Section 4.4.1).

disk fractions and ages of the 4 associations.

4.4.2 Transition disks

Objects with very little or no excess at near- to mid-infrared wavelengths but exhibiting excess at longer wavelengths are best understood by assuming an opacity hole in the inner disk (see sections 3.4.3 and 3.4.4). They may be in the process of clearing dust from their inner disks (Calvet et al., 2002; Muzerolle et al., 2006). Such objects are often termed "transition disks", but the criteria used to define transition disks differ in the literature (see Luhman & Mamajek (2012); Merin et al. (2010) for a discussion of the various criteria). Here, the term is used to identify objects with little or no excess in W1-W2, i.e. shortwards of 10 μm, but bright W3 and/or W4 signals (see Section 4.3.1). The five objects that satisfy this criterion are included in the Class II group and may be in the process of a transition from Class II to Class III.

I do not find any object that might be called a "pre-transitional disk" (Espaillat et al., 2008, 2012), showing evidence for an opacity gap (as opposed to an inner hole) in the disk, i.e. with exess at $< 10\,\mu$m, no excess at $12\,\mu$m, and excess again at $22\,\mu$m.

Based on my adopted definition, the fraction of transition disks around Class II brown dwarfs in the sample is 5/27 or 19%. Due to the small sample size, the uncertainty in this number is in the range of $\pm 10\%$. Taking this into account, the value is consistent with most previous estimates for the transition disk fraction for low-mass stars which are, for criteria similar to the one adopted here, in the range of 0-20% e.g., Ercolano et al. (2009); Muzerolle et al. (2010). Thus, based on the estimate derived above for the brown dwarf regime, there is no evidence for a mass-dependence in the transition disk frequency.

The small number of transition disks in the sample indicates that the transition phase lasts only a short time compared with the total lifetime of the disks. Assuming the upper limit for the age spread of 2 Myr (Preibisch & Zinnecker, 1999), I obtain an upper limit of 0.4 Myr for the transition timescale, i.e. about one order of magnitude shorter than the disk lifetime. Thus a two timescale model for the evolution of the disks, as often adopted for low-mass stars (Muzerolle et al., 2010), is required for brown dwarfs as well.

4.4.3 Selected Spectral Energy Distributions

The objects in the sample have been designated as Class II or Class III based on their mid-infrared colours and magnitudes. As described in the Introduction (Section 1.3), objects were originally denoted as Class II or Class III based on the form of their spectral energy distributions, as shown in Fig. 1.4. Here, I show the spectral energy distributions of 12 objects from the sample, 6 Class II and 6 Class III objects for comparison. The Class III objects used have the closest magnitude in the J passband to the Class II objects with which they are compared. Shown in the Fig. 4.6 are 2 of the typical examples that were deemed Class II on the basis of their W1-W2 (3.4-4.6 μm) colour alone. The difference in slopes between the W1 and W2 points on the Class II and Class III spectral energy distributions are apparent, as are the higher W3 (12 μm) and W4 (22 μm) values of the Class II objects. The 2 Class II objects that stand out in Fig. 4.4 because of their large J-K excess are shown in Fig. 4.7. Of all the 27 Class II objects, the spectral energy distributions for these 2 show the greatest divergence from those of their corresponding Class III objects. Fig. 4.8 shows 2 of the 5 Class II objects that could not be distinguished on the basis of their W1-W2 colour alone. The lower panel is the most extreme example of all the 5 objects with little or no W1-W2 excess and deemed Class II based on their bright W3 and/or W4 signals (the transition disks). It exhibits no W1-W2 excess and has a weak W3 signal. Apart from its strong W4 signal it resembles a Class III object.

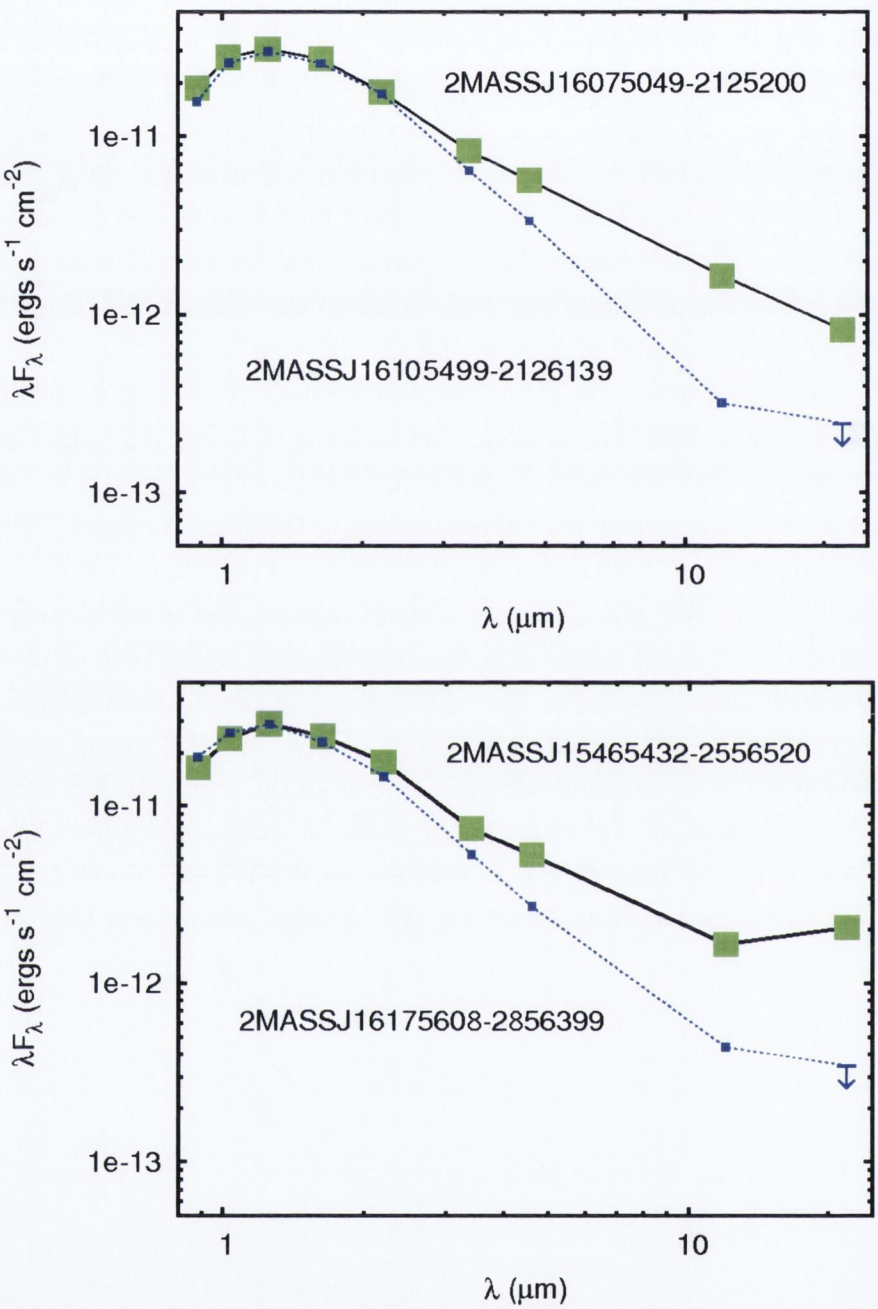

Figure 4.6 Spectral energy distributions for 2 of the 27 Class II objects (solid lines with large squares) shown alongside 2 of the 89 Class III objects (dotted lines with small squares). Detections with a S/N of < 5.0 are marked as upper limits. Errors on other data points are, at most, of the order of the size of the small squares. These Class II objects are among the 22 distinguished using their W1-W2 (3.4-4.6 μm) colour alone.

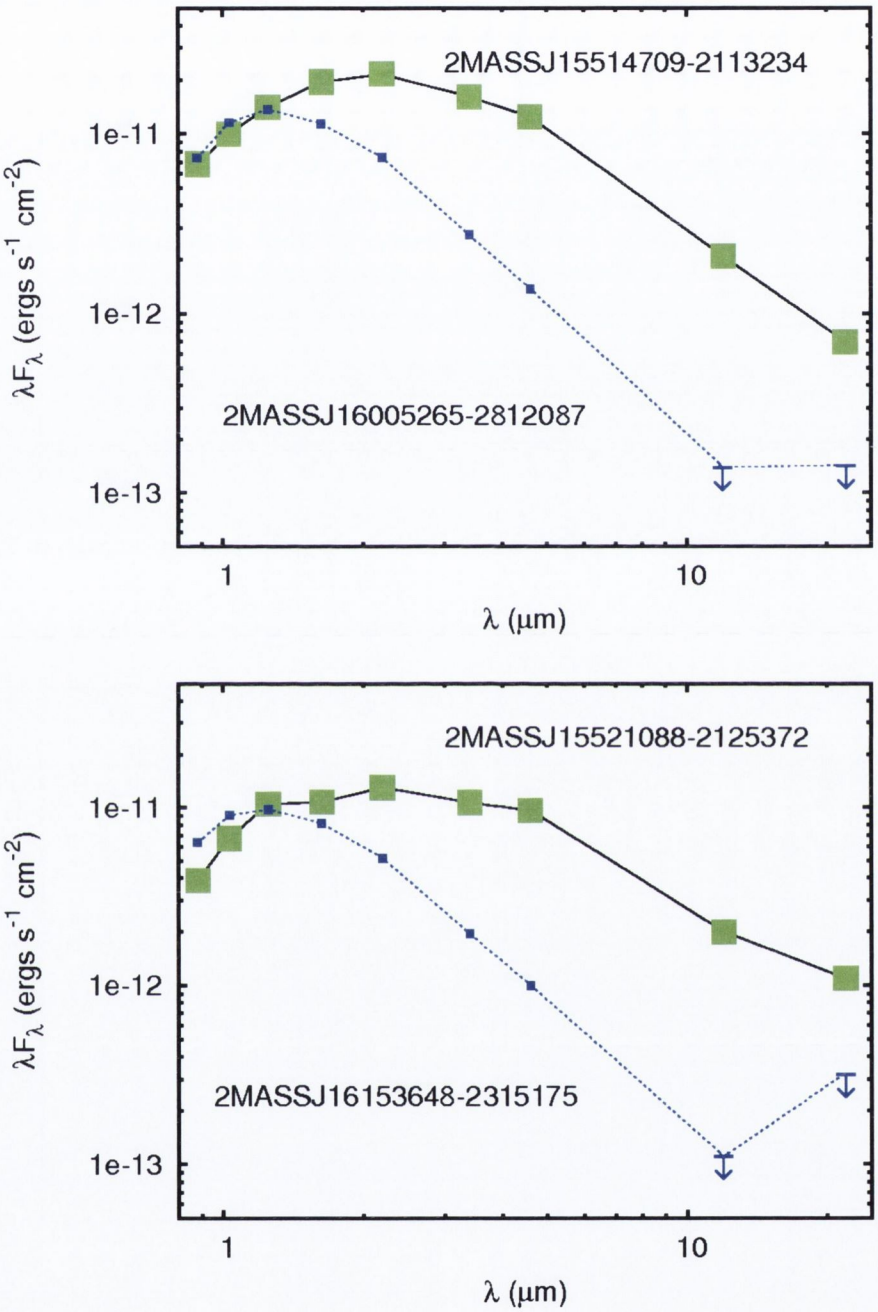

Figure 4.7 Spectral energy distributions for 2 of the 27 Class II objects (solid lines with large squares) shown alongside 2 of the 89 Class III objects (dotted lines with small squares). Detections with a S/N of < 5.0 are marked as upper limits. Errors on other data points are, at most, of the order of the size of the small squares. The Class II objects are the 2 objects that also have the large J-K excess, as well as having the brightest W3 signals, bright W4 signals and significant photometric variability (see Fig. 4.4 and Table 4.1).

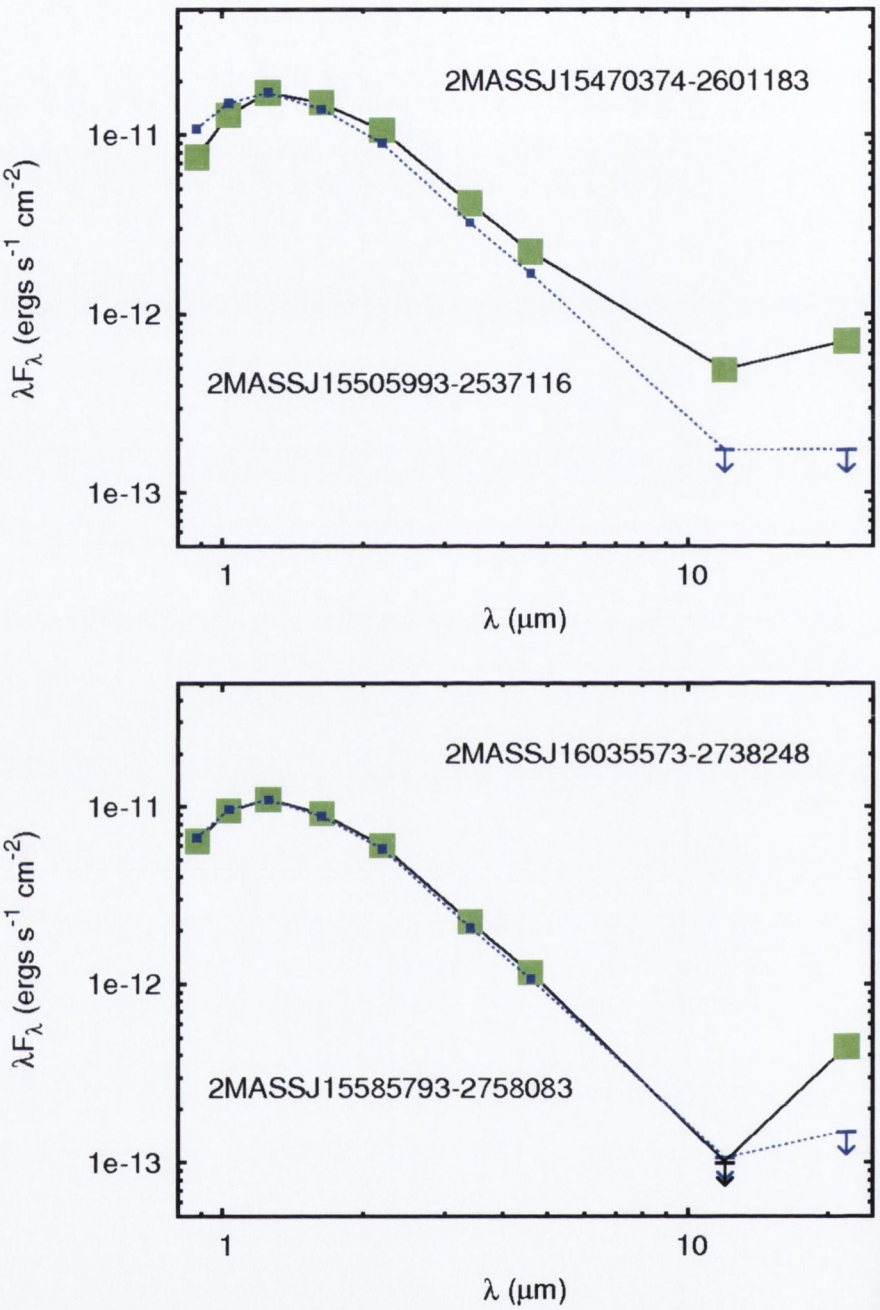

Figure 4.8 Spectral energy distributions for 2 of the 27 Class II objects (solid lines with large squares) shown alongside 2 of the 89 Class III objects (dotted lines with small squares). Detections with a S/N of < 5.0 are marked as upper limits. Errors on other data points are, at most, of the order of the size of the small squares. The Class II objects shown are 2 of the 5 with little or no W1-W2 excess that are included in the Class II group on the basis of their bright W3 and/or W4 signals.

4.4.4 Radiative Transfer Models

Scholz et al. (2007) produced model spectral energy distributions based on Monte Carlo radiative transfer simulations for the 13 Class II objects that they found in UpSco. I requested new models, from one of the original authors (K. Wood, private communication), for the 2 of those 13 objects that are recovered in this work, which would also incorporate the new WISE data. Fig. 4.9 shows the resulting spectral energy distributions, which have been recreated using the original model parameters. Data shown for the J, H, K, 9, 10, 11 and 24 μm wavelengths is taken from that of Scholz et al. (2007). The new data for the W1, W2 and W3 passbands is also shown overplotted on the two spectral energy distribution diagrams. It is clear from Fig. 4.9 that the data for W1 (3.4 μm), W2 (4.6 μm) and W3 (12 μm) agree very well with both original models, lying on or very close to the modelled flux for a combined photosphere and disk (solid lines in Fig. 4.9).

Models of the inner part of a disk rely on observational data in the mid-infrared to refine their accuracy. Scholz et al. (2007) noted that the gap in their data coverage in the 3-8 μm region restricted their ability to constrain the size of any inner disk holes in sources that exhibited excesses at 9 μm and beyond. The addition of the W1 and W2 datapoints for the two objects in Fig. 4.9 now allows the accuracy of the models in this region to be probed.

The data for the object in the upper panel was originally fitted with a model which included an excess in the mid-infrared which necessitated the presence of an optically thick inner disk. The newly overplotted W1 (3.4 μm) and W2 (4.6 μm) values observed by WISE conform with that part of the model, further indication that a significant W1-W2 excess is evidence for the presence of a disk. The W1-W2 excess for this object places it more than 4σ away from the isochrone in the (W1-W2,Z) colour-magnitude diagram in Fig. 4.1.

The diagram in the lower panel of Fig. 4.9 is for the object noted in Sections 4.3.1 and 4.4.2 above, that may be in the process of transition from Class II to Class III. Its lesser excess at W1 and W2 is clear, as is its relatively greater excess at W3. Again, the accuracy of the original model at these wavelengths is confirmed by the newly observed WISE values. While the model shown does preclude the existence of an optically thick inner disk, it does not require the presence of an evacuated hole in the inner disk. Instead, a reduced scale height, i.e. a flatter inner disk is sufficient. This evolution

to a flatter disk could be caused by grain growth and dust settling along the lines proposed by Dullemond & Dominik (2004). Ergo, in this model, the process of transition from Class II to Class III that may be occurring around this object's disk does not require the presence of mechanisms (e.g. planet formation) that would completely clear the inner disk.

4.4.5 Comparison with Riaz (2012)

In a recent paper, Riaz et al. (2012) analyse a sample of 43 spectroscopically confirmed very low mass members (spectral types M4-M8.5) in UpSco using WISE data. They find 6 new Class II objects and recover 4 others previously recorded by Scholz et al. (2007) and a further 2 that were found by Slesnick et al. (2008). These 12 objects are listed in their Table 1. I have been kindly provided with a table which includes the 31 other brown dwarfs that they investigated and categorised as Class III by B. Riaz (private communication). From the 12 Class II and 31 Class III objects that they list, there are 12 in common to both that study and this one. Both studies categorise the same 5 objects as Class II and the same 7 objects as Class III.

Also included in the table supplied by B. Riaz are 6 other objects with S/N < 3.0 in the W3 passband. Riaz et al. (2012) rely on the use of the W3 signal and require that a source have a W3 S/N of ≥ 3.0. As a result they do not categorise these 6 brown dwarfs. However, using the W1-W2 colour as a primary diagnostic instead of W3 allows a larger range of objects to be successfully examined. All 116 objects investigated in my work have a S/N > 8 in the W1 and W2 passbands, while only 64 of them have a S/N of ≥ 3.0 in the W3 passband. The 6 objects which cannot be categorised in Riaz et al. (2012) because they have a weak W3 signal have been determined in this work to be Class III objects using their W1 and W2 signals alone.

Requiring that a source have a W3 S/N of ≥ 3.0 not only restricts the number of objects in any sample from UpSco, it also produces a sample that is biased with respect to the presence of disks. Class III objects in UpSco are less likely than Class II objects to have a strong W3 signal. Of the 116 objects examined in this work, 78% of the Class II objects, but only 48% of the Class III objects have a W3 S/N of ≥ 3.0. Restricting the analysis to those 64 objects only would have yielded an artificially high disk fraction of 33%, rather than the 23% found from the larger unbiased sample of 116 objects, while also increasing the statistical errors. For these reasons, my

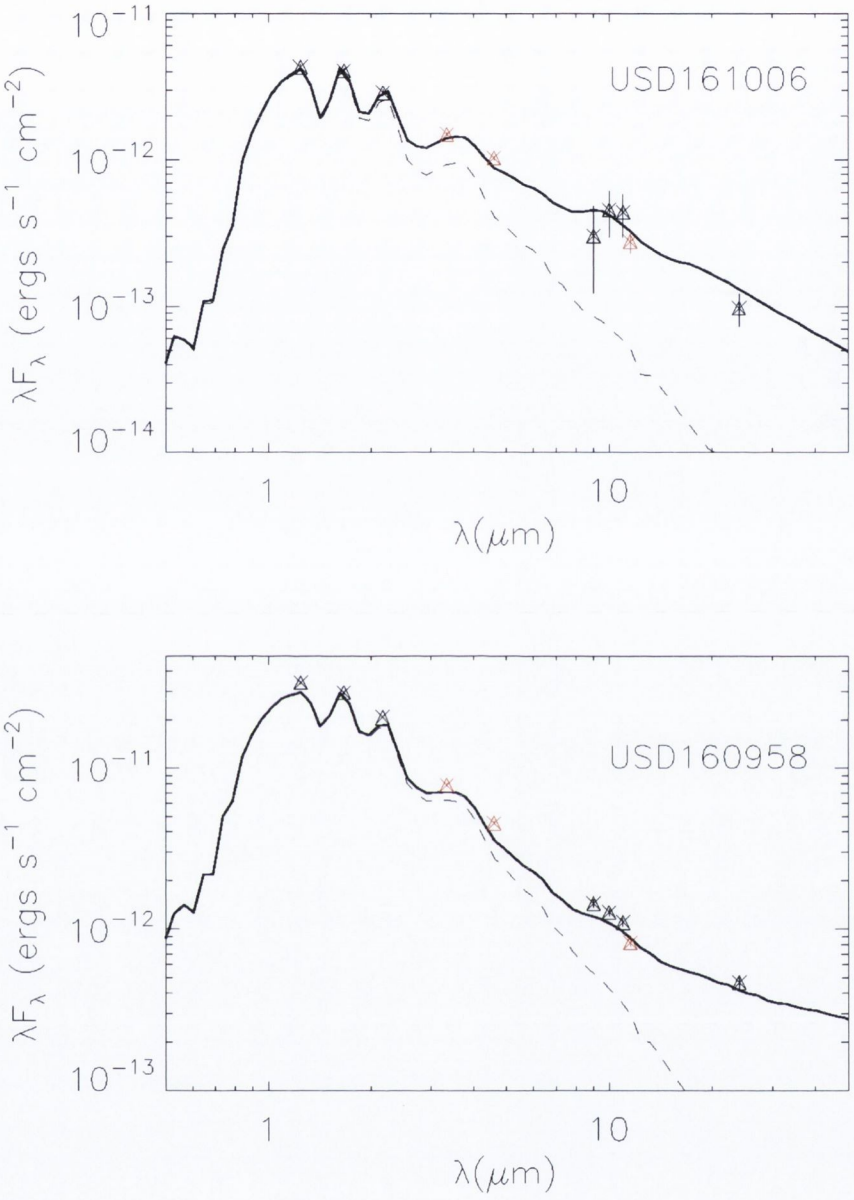

Figure 4.9 Spectral energy distribution for the two Class II objects originally identified in Scholz et al. (2007) and recovered in this work. Data shown is taken from that of Scholz et al. (2007) for the J, H, K, 9, 10, 11 and 24 μm wavelengths, along with the newly acquired W1, W2 and W3 values. The Monte Carlo radiative transfer simulations shown for comparison use the same parameters as were given in Scholz et al. (2007). The dotted lines depict calculated photospheric flux while the solid lines represent combined photospheric and disk flux.

disk fraction is a more representative value for the brown dwarf population in UpSco.

4.4.6 Comparison with Luhman & Mamajek (2012)

Another recent paper focused on the disks of UpSco members has been published by Luhman & Mamajek (2012). Similar to Riaz et al. (2012) they look at a sample of spectroscopically confirmed members. Their list of targets includes 387 objects with spectral types M4-M8 and another 23 with M8-L2 and is thus substantially larger than the Riaz et al. sample. They analyse the available Spitzer and WISE photometry for these objects. To identify the objects with disks, they use the spectral regime from 4.5 to 24 μm, similar to this chapter.

48 of their targets also appear in my total sample of 119, among them 13 classified as Class II in this work. In most cases, my Class II/III distinction agrees with the one in Luhman & Mamajek (2012). The only exception is the M9-L1 object 2MASSJ16082847-2315103, which clearly fulfills my Class II criterion based on its W1-W2 colour, whereas Luhman & Mamajek (2012) conclude that it has no disk based on its K-W2 colour. At these late spectral types, however, the intrinsic colours of young brown dwarfs increase significantly with spectral type and cover a broad range, i.e. it is challenging to unambiguously distinguish between Class II and Class III. Whether this source does or does not have infrared excess emission remains to be determined, but this does not affect my results in any way.

The remainder of my own sample (71 in total, among them 14 with disks) is new and not covered by Luhman & Mamajek (2012), i.e. my work increases the sample of brown dwarfs analysed with mid-infrared data significantly.

The disk fraction derived by Luhman & Mamajek (2012) for very low mass and substellar members of UpSco is $\sim 25\%$, and thus agrees very well with my own result. They also find that disk fractions increase from very small values for B-G stars ($\leq 10\%$) to 25% for $\geq$ M5 objects. This seems at odds with my own statement of spectral type-independent disk fractions, but a more detailed examination shows that the two studies actually give consistent results for K and M stars.

Luhman & Mamajek (2012) report disk fractions of 6/67 for K0-M0, 35/231 for M0-M4, 97/387 for M4-M8 and 4/23 for M8-L2. To compare with

my own values, the binomial confidence intervals for their disk fractions were calculated and found to be $14 \pm 3\%$ for K0-M4 and $25 \pm 3\%$ for M4 to L2. This is consistent with the numbers quoted in Section 4.4.1. (19% for K0-M5 and 23% for my sample of brown dwarfs). Note that the uncertainties quoted above only give the statistical confidence interval and do not take into account possible biases (e.g., age spread across the region, uncertainties in spectral types). Thus, based on the current samples, the evidence for a mass dependence of the disk fraction for objects later than K0 is marginal at best.

4.5 Summary

I have carried out a survey for disks around a homogeneous sample of 119 brown dwarfs, the majority of which have not been previously discussed in the literature (Dawson et al., 2013), in the 5 Myr old UpSco star forming region using photometry from WISE. Contamination in the sample appears to be negligible and the method of selection is unbiased with respect to the presence of disks.

Examining all the UKIDSS, 2MASS and WISE colour-magnitude and colour-colour combinations shows that the WISE W1-W2 colour is the best primary diagnostic for the presence of a disk around the objects.

27 Class II objects are identified from the sample. 22 were classified via their W1-W2 colour excess alone. 5 other objects were also categorised as Class II from their W3 and/or W4 signals. These 5 objects (19% of all disks) appear to be in the transition phase between Class II and Class III, leading to the conclusion that this phase is short lived, lasting less than 0.4 Myr, an estimate that is consistent with findings for low-mass stars.

The disk fraction is found to be $23\% \pm 5\%$. This fraction is statistically indistinguishable from results for K/M stars in UpSco. Results from the literature for Cha I, IC348 and σ Ori show that their brown dwarf disk fractions are also indistinguishable from their K/M star disk fractions. Therefore the average lifetime of the disks in each of these regions shows no obvious dependency on the mass of the central object. Combined with the short transitional phase from Class II to Class III, this suggests that the evolution of brown dwarf disks follows what is generally referred to as a "two timescale model" (see Section 4.4.2), similar to low mass stars.

Table 4.1. Objects with photometric variability >0.2mag in J,H or K.

Name	ΔJ	ΔH	ΔK
2MASSJ15514709-2113234	0.84	0.59	0.25
2MASSJ15521088-2125372	0.24	0.11	0.03
2MASSJ15472282-2139141	0.38	0.25	0.21
2MASSJ16030235-2626163	0.17	0.30	0.11

Table 4.2. Positions, UKIDSS Z and J photometry, WISE W1, W2, W3 and W4 photometry of the 27 Class II objects. Objects are listed in order of decreasing Z magnitude. Coordinates are J2000, and are taken from the UKIDSS GCS 9th Data Release (2011).

Name	R.A.	Dec.	Z Mag.	J Mag.	W1 Mag.	W2 Mag.	W3 Mag.	W4 Mag.
2MASSJ16075049-2125200	16:07:50.49	-21:25:20.2	14.03	12.69	11.27	10.73	9.10	7.22
2MASSJ15465432-2556520	15:46:54.32	-25:56:52.1	14.16	12.75	11.40	10.81	9.10	6.23
2MASSJ16052875-2655496	16:05:28.75	-26:55:49.7	14.18	12.89	11.67	11.21	9.90	8.03
2MASSJ16095852-2345186	16:09:58.52	-23:45:18.7	14.20	12.57	11.34	10.97	9.96	8.73*
2MASSJ16030235-2626163	16:03:02.36	-26:26:16.4	14.46	13.12	11.44	10.92	9.59	8.04*
2MASSJ15470374-2601183	15:47:03.74	-26:01:18.4	15.02	13.32	12.03	11.74	10.42	7.39
2MASSJ16134880-2509006	16:13:48.81	-25:09:00.7	15.04	13.56	11.96	11.32	9.55	7.58
2MASSJ15514709-2113234	15:51:47.09	-21:13:23.5	15.12	13.54	10.56	9.88	8.85	7.41
2MASSJ16035573-2738248	16:03:55.73	-27:38:25.1	15.19	13.80	12.70	12.45	12.13*	7.89
2MASSJ15472572-2609185	15:47:25.73	-26:09:18.5	15.40	13.55	11.87	11.51	9.58	7.37
2MASSJ16145253-2718557	16:14:52.53	-27:18:55.7	15.65	14.06	12.34	11.79	10.63	8.70*
2MASSJ15412655-2613253	15:41:26.55	-26:13:25.4	15.65	14.00	12.59	12.10	10.75	8.24*
2MASSJ15521088-2125372	15:52:10.88	-21:25:37.4	15.72	13.86	11.01	10.15	8.90	6.92
2MASSJ16143287-2242133	16:14:32.87	-22:42:13.5	15.82	14.16	12.88	12.34	11.74*	8.38*
2MASSJ15501958-2805237	15:50:19.58	-28:05:23.9	16.04	14.56	13.28	12.72	12.03*	8.98*
2MASSJ16080745-2345055	16:08:07.45	-23:45:05.6	16.06	14.40	12.86	12.21	10.30	8.43*
2MASSJ15524513-2705560	15:52:45.13	-27:05:56.1	16.16	14.42	13.06	12.35	10.74	8.66*
2MASSJ15571880-2711567	15:57:18.81	-27:11:56.8	16.39	14.78	13.42	12.86	11.90*	9.05*
2MASSJ16142144-2339146	16:14:21.44	-23:39:14.8	16.59	14.97	13.57	12.99	11.95*	8.25*
2MASSJ16012238-2708194	16:01:22.39	-27:08:19.5	16.68	14.70	13.24	12.55	11.11	8.43*
2MASSJ16100608-2127440	16:10:06.08	-21:27:44.1	16.82	14.82	13.29	12.65	11.90*	8.72*
2MASSJ15541998-2135428	15:54:19.99	-21:35:43.0	16.85	14.98	13.26	12.57	11.22	8.39*
2MASSJ16083048-2335109	16:08:30.49	-23:35:11.0	16.95	14.88	13.37	12.86	11.69*	8.63*
2MASSJ16082847-2315103	16:08:28.47	-23:15:10.4	17.64	15.45	13.77	13.22	12.21*	8.34*

Table 4.2 (cont'd)

Name	R.A.	Dec.	Z Mag.	J Mag.	W1 Mag.	W2 Mag.	W3 Mag.	W4 Mag.
2MASSJ15472282-2139141	15:47:22.82	-21:39:14.3	17.97	15.65	13.69	13.07	11.63*	8.67*
2MASSJ15433947-2535549	15:43:39.47	-25:35:54.9	18.15	15.77	13.91	13.73	10.77	7.78
2MASSJ15553614-2546591	15:55:36.15	-25:46:59.2	18.23	15.83	13.63	13.12	11.10*	7.92

*S/N < 5.

Table 4.3. Positions, UKIDSS Z and J photometry, WISE W1, W2, W3 and W4 photometry of the 89 Class III objects. Objects are listed in order of decreasing Z magnitude. Coordinates are J2000, and taken from the UKIDSS GCS 9th Data Release (2011).

Name	R.A.	Dec.	Z Mag.	J Mag.	W1 Mag.	W2 Mag.	W3 Mag.	W4 Mag.
2MASSJ16175608-2856399	16:17:56.09	-28:56:40.0	14.01	12.76	11.76	11.53	10.54	8.17*
2MASSJ16034797-2801319	16:03:47.97	-28:01:31.9	14.03	12.81	11.83	11.62	11.17	9.02*
2MASSJ16105728-2359540	16:10:57.28	-23:59:54.1	14.04	12.80	11.68	11.48	11.72*	8.72*
2MASSJ15554229-2546477	15:55:42.29	-25:46:47.8	14.07	12.65	11.52	11.24	10.93*	8.18*
2MASSJ16055898-2556228	16:05:58.99	-25:56:22.9	14.10	12.59	11.50	11.22	10.83	9.08*
2MASSJ16105429-2309108	16:10:54.29	-23:09:11.1	14.13	12.97	11.88	11.68	11.60*	8.27*
2MASSJ15591513-2840411	15:59:15.12	-28:40:41.3	14.14	12.96	12.00	11.77	12.39*	8.75*
2MASSJ16095217-2136277	16:09:52.17	-21:36:27.8	14.15	12.51	11.33	10.97	10.72	9.14*
2MASSJ16063691-2720548	16:06:36.91	-27:20:54.9	14.16	12.88	11.85	11.60	11.91*	8.73*
2MASSJ15411513-2539447	15:41:15.14	-25:39:44.8	14.16	12.76	11.59	11.37	11.30	8.71*
2MASSJ16033799-2611544	16:03:37.99	-26:11:54.4	14.17	12.98	11.96	11.70	11.22	8.63*
2MASSJ16105499-2126139	16:10:54.99	-21:26:14.0	14.22	12.73	11.56	11.30	10.89	8.53*
2MASSJ16154869-2710546	16:15:48.69	-27:10:54.7	14.22	12.82	11.69	11.40	11.65*	8.86*
2MASSJ15450519-2559047	15:45:05.20	-25:59:04.7	14.23	12.90	11.76	11.54	12.00*	8.53*
2MASSJ16072196-2358452	16:07:21.96	-23:58:45.3	14.24	12.99	11.86	11.64	11.27	8.79*
2MASSJ16152819-2315439	16:15:28.19	-23:15:44.1	14.24	13.12	12.08	11.90	11.78*	8.18*
2MASSJ16370523-2625439	16:37:05.24	-26:25:44.0	14.27	12.96	11.96	11.69	11.40	8.91*
2MASSJ15492909-2815384	15:49:29.08	-28:15:38.6	14.29	12.96	11.85	11.63	12.05*	8.91*
2MASSJ15491602-2547146	15:49:16.02	-25:47:14.6	14.31	13.01	11.87	11.60	10.90	8.20*
2MASSJ16082229-2217029	16:08:22.29	-22:17:03.0	14.31	12.94	11.85	11.56	11.10	8.81*
2MASSJ16061595-2218279	16:06:15.95	-22:18:28.0	14.31	13.17	12.11	11.91	11.92*	9.02*
2MASSJ15544260-2626270	15:54:42.61	-26:26:27.0	14.32	13.05	11.91	11.72	11.61*	8.23*
2MASSJ16090168-2740521	16:09:01.68	-27:40:52.3	14.33	12.86	11.71	11.44	10.97	8.72*
2MASSJ15582376-2721435	15:58:23.76	-27:21:43.7	14.35	13.07	12.02	11.79	11.37*	8.78*

Table 4.3 (cont'd)

Name	R.A.	Dec.	Z Mag.	J Mag.	W1 Mag.	W2 Mag.	W3 Mag.	W4 Mag.
2MASSJ16132180-2731219	16:13:21.80	-27:31:22.0	14.36	13.25	11.93	11.85	11.60*	8.77*
2MASSJ15415562-2538465	15:41:55.63	-25:38:46.5	14.37	13.10	12.02	11.79	12.14*	8.93*
2MASSJ16002535-2644060	16:00:25.35	-26:44:06.1	14.38	13.02	11.90	11.66	11.67*	8.50*
2MASSJ15545410-2114526	15:54:54.11	-21:14:52.7	14.40	13.26	12.10	11.94	10.71	8.31*
2MASSJ16062637-2306113	16:06:26.37	-23:06:11.4	14.48	13.20	12.12	11.87	11.68*	8.90*
2MASSJ16121609-2344248	16:12:16.09	-23:44:25.0	14.50	13.19	11.96	11.78	10.99	8.21*
2MASSJ16090451-2224523	16:09:04.51	-22:24:52.5	14.57	12.92	11.66	11.40	10.59	8.23*
2MASSJ16113470-2219442	16:11:34.70	-22:19:44.3	14.61	13.24	12.11	11.87	12.25*	8.77*
2MASSJ15505993-2537116	15:50:59.94	-25:37:11.7	14.62	13.33	12.30	12.05	11.55*	8.90*
2MASSJ15524857-2621453	15:52:48.57	-26:21:45.4	14.62	13.30	12.27	12.00	12.51*	9.14*
2MASSJ16372782-2641406	16:37:27.83	-26:41:40.7	14.63	13.30	12.14	12.00	11.42	8.95*
2MASSJ15522943-2721003	15:52:29.44	-27:21:00.4	14.64	13.47	12.45	12.14	12.36*	9.06*
2MASSJ15530374-2600306	15:53:03.75	-26:00:30.7	14.66	13.43	12.36	12.14	12.03*	8.62*
2MASSJ15493660-2815141	15:49:36.59	-28:15:14.3	14.66	13.39	12.36	12.05	11.63*	8.79*
2MASSJ16133476-2328156	16:13:34.76	-23:28:15.7	14.74	13.48	12.39	12.12	11.77*	8.81*
2MASSJ15490803-2839550	15:49:08.02	-28:39:55.2	14.82	13.60	12.45	12.21	10.68	8.15*
2MASSJ16112630-2340059	16:11:26.30	-23:40:06.1	14.83	13.40	12.16	11.92	12.04*	8.55*
2MASSJ15495733-2201256	15:49:57.33	-22:01:25.7	14.89	13.35	12.15	11.89	11.56*	8.64*
2MASSJ16062870-2856580	16:06:28.70	-28:56:58.2	14.90	13.52	12.39	12.18	11.41	9.06*
2MASSJ15572692-2715094	15:57:26.93	-27:15:09.5	14.93	13.66	12.59	12.39	12.00*	9.10*
2MASSJ16164539-2333413	16:16:45.39	-23:33:41.6	14.99	13.73	12.62	12.33	11.61*	8.44*
2MASSJ16005265-2812087	16:00:52.66	-28:12:09.0	15.04	13.57	12.48	12.27	11.79*	9.13*
2MASSJ16132665-2230348	16:13:26.66	-22:30:35.0	15.05	13.52	12.33	11.99	11.00	8.82*
2MASSJ16115737-2215066	16:11:57.37	-22:15:06.8	15.07	13.67	12.51	12.24	11.76*	8.84*

Table 4.3 (cont'd)

Name	R.A.	Dec.	Z Mag.	J Mag.	W1 Mag.	W2 Mag.	W3 Mag.	W4 Mag.
2MASSJ16064910-2216382	16:06:49.10	-22:16:38.4	15.09	13.73	12.63	12.37	11.90*	8.79*
2MASSJ15585793-2758083	15:58:57.93	-27:58:08.5	15.13	13.81	12.78	12.54	12.08*	9.06*
2MASSJ15420830-2621138	15:42:08.31	-26:21:13.8	15.15	13.74	12.59	12.32	12.10*	9.07*
2MASSJ16090197-2151225	16:09:01.98	-21:51:22.7	15.16	13.59	12.32	12.08	10.87	8.45*
2MASSJ16124692-2338408	16:12:46.92	-23:38:40.9	15.18	13.60	12.42	12.19	12.20*	8.25*
2MASSJ16153648-2315175	16:15:36.48	-23:15:17.6	15.19	13.93	12.85	12.61	12.03*	8.23*
2MASSJ16134264-2301279	16:13:42.64	-23:01:28.0	15.19	13.72	12.47	12.25	12.20*	8.38*
2MASSJ16113837-2307072	16:11:38.37	-23:07:07.5	15.19	13.74	12.60	12.31	11.97*	8.59*
2MASSJ15583403-2803243	15:58:34.03	-28:03:24.5	15.21	13.72	12.53	12.30	11.45	9.03*
2MASSJ16192399-2818374	16:19:23.99	-28:18:37.5	15.29	13.79	12.73	12.40	11.51*	8.57*
2MASSJ15490414-2120150	15:49:04.14	-21:20:15.2	15.31	13.77	12.64	12.37	11.50*	8.92*
2MASSJ16051243-2624513	16:05:12.43	-26:24:51.4	15.40	14.06	12.93	12.76	12.29*	9.08*
2MASSJ15533067-2617307	15:53:30.68	-26:17:30.7	15.49	13.99	12.83	12.60	12.06*	8.64*
2MASSJ15544486-2843078	15:54:44.85	-28:43:07.9	15.51	14.12	12.99	12.81	12.60*	8.90*
2MASSJ15531698-2756369	15:53:16.98	-27:56:37.2	15.53	13.96	12.84	12.55	12.50*	8.58*
2MASSJ15551960-2751207	15:55:19.59	-27:51:21.0	15.60	14.03	12.93	12.67	12.30*	9.10*
2MASSJ15564227-2646467	15:56:42.28	-26:46:46.8	15.62	14.03	12.85	12.54	11.65*	8.51*
2MASSJ16101316-2856308	16:10:13.15	-28:56:31.0	15.67	14.06	12.89	12.59	12.16*	9.09*
2MASSJ16115439-2236491	16:11:54.39	-22:36:49.3	15.73	14.27	13.04	12.80	11.86*	8.32*
2MASSJ16092938-2343121	16:09:29.39	-23:43:12.2	15.96	14.20	12.94	12.65	12.30*	8.98*
2MASSJ16103014-2315167	16:10:30.14	-23:15:16.8	16.06	14.37	13.05	12.75	11.97*	8.35*
2MASSJ15561721-2638171	15:56:17.21	-26:38:17.2	16.10	14.52	13.26	13.00	10.38	8.23*
2MASSJ16072641-2144169	16:07:26.41	-21:44:17.1	16.17	14.60	13.43	13.17	12.26*	8.55*
2MASSJ16142061-2745497	16:14:20.61	-27:45:49.8	16.31	14.49	13.22	12.93	12.26*	8.69*

Table 4.3 (cont'd)

Name	R.A.	Dec.	Z Mag.	J Mag.	W1 Mag.	W2 Mag.	W3 Mag.	W4 Mag.
2MASSJ15572820-2708430	15:57:28.21	-27:08:43.0	16.40	14.78	13.71	13.47	12.21*	8.77*
2MASSJ16134079-2219459	16:13:40.79	-22:19:46.1	16.49	14.72	13.42	13.08	12.05*	8.99*
2MASSJ15442275-2136092	15:44:22.75	-21:36:09.3	16.55	15.01	13.69	13.48	11.68*	8.55*
2MASSJ15543065-2536054	15:54:30.65	-25:36:05.5	16.73	15.03	13.80	13.61	11.58*	8.17*
2MASSJ16064818-2230400	16:06:48.18	-22:30:40.1	16.82	14.93	13.63	13.37	12.04*	8.68*
2MASSJ15444172-2619052	15:44:41.72	-26:19:05.3	17.16	15.21	13.86	13.63	12.26*	8.86*
2MASSJ16072382-2211018	16:07:23.82	-22:11:02.0	17.24	15.20	13.70	13.41	12.20*	8.87*
2MASSJ16104714-2239492	16:10:47.13	-22:39:49.4	17.44	15.26	13.80	13.51	12.02*	8.57*
2MASSJ16084744-2235477	16:08:47.44	-22:35:47.9	17.74	15.69	14.30	14.11	12.28*	8.79*
2MASSJ15491331-2614075	15:49:13.32	-26:14:07.5	18.29	16.04	14.50	14.12	12.16*	8.88*
2MASSJ16081843-2232248	16:08:18.43	-22:32:25.0	18.51	16.10	14.28	14.05	11.56*	8.72*
2MASSJ16195827-2832276	16:19:58.26	-28:32:27.8	18.74	16.18	14.42	14.10	12.47*	8.77*
2MASSJ15451990-2616529	15:45:19.91	-26:16:53.0	18.77	16.27	14.41	14.06	11.85*	8.20*
2MASSJ16362646-2720024	16:36:26.47	-27:20:02.5	18.77	16.33	14.52	14.22	11.44*	8.79*
2MASSJ16360175-2703305	16:36:01.75	-27:03:30.5	19.12	16.64	14.95	14.91	12.07*	8.86*
2MASSJ16073799-2242468	16:07:37.99	-22:42:47.0	19.24	16.76	15.16	14.73	12.51*	8.25*
2MASSJ15504498-2554213	15:50:44.99	-25:54:21.4	19.90	16.93	14.86	14.70	11.84*	8.33*

*S/N < 5.

Chapter 5

Near-Infrared Spectroscopy

The first step for all observational studies of young brown dwarfs is deep survey work in nearby star forming regions, with the goal of identifying and characterising large samples. These samples can then be used to constrain the mass function, the disk properties, and other diagnostics for the star formation process. This is the process described in the previous chapters where I have detailed the identification of a list of brown dwarf candidates in UpSco based on the Galactic Cluster Survey that was carried out as part of the UKIRT Infrared Deep Sky Survey (Dawson et al., 2011, 2013). This survey work covered the southern part of the association and so it is complementary to previous work by other groups (Lodieu et al., 2006, 2007, 2008, 2011, 2013; Slesnick et al., 2006, 2008).

In this chapter, I present spectroscopic follow-up for a large number of these candidates. The aims are twofold: to verify the nature of the sources and to examine the spectroscopic properties of the substellar objects in this region. An advantage of conducting such a study in UpSco is that it has a disk fraction of only 23% (Dawson et al., 2013), as derived in Chapter 4. This means that the flux received comes mostly from photospheres with little contamination from disks. The results presented in this chapter are based on work which originally appeared in Dawson et al. (2014).

5.1 Sample

A total of 30 objects from the survey were chosen for follow-up spectroscopy. They were chosen from a list of 96 candidate brown dwarfs identified from the

UKIDSS Ninth Data Release. The magnitudes of the 30 are representative of those of the 96 from which they are taken. Their locations in UpSco are shown in Fig. 5.1. 24 of these objects have the photometric and proper motion characteristics of very low mass members of UpSco, as described in Chapter 3. As shown in the vector point diagram in Fig. 5.2, they form part of a population of objects that lie inside a $2\,\sigma$ selection circle which is centred on the known proper motion of UpSco (-11, -25 mas/yr) (de Bruijne et al., 1997; Preibisch et al., 2002) and hereinafter are referred to as "the $2\,\sigma$ sample". Of these 24 objects, 2 were first identified by Lodieu et al. (2006), 13 by Dawson et al. (2011), and the remaining 9 by Dawson et al. (2013). The other 6 objects were shown, in Chapter 3, to have the photometric characteristics of very low mass members of UpSco. However, as shown in Fig. 5.2, they form part of a smaller population of objects that lie just outside the selection circle.

Based on mid-infrared photometry from the WISE satellite, 18 of the objects from the $2\,\sigma$ sample are Class III objects while 6 of them are Class II objects, as shown in Chapter 4. The 6 objects that lie outside the selection circle have been examined in the same manner. They exhibit the 3.4-4.6 μm mid-infrared colours and weak 12 and 22 μm signals typical of Class III objects in UpSco. None of the 30 objects had been spectroscopically investigated before. The 2MASS name and the position of each object are listed in Table 5.1. For the sake of simplicity and clarity, the objects are also numbered from 1 to 30 and are identified by these numbers throughout this chapter.

5.2 Observations

Spectra of the above targets were obtained during the nights of the 8th, 9th and 10th of June 2012 using the SpeX spectrograph (Rayner et al., 2003) at the IRTF on Mauna Kea. During the observing run, the IRTF was operated remotely from the offices of the Dublin Institute for Advanced Studies. Targets were observed with SpeX in single-prism mode covering a wavelength range of 0.8 - 2.5 μm. Slits used were either $0.''5$ or $0.''8$ x $15''$, depending on the seeing. Airmass varied from 1.35 to 1.93 across the objects observed. Single exposure times used were either 60, 90 or 120 s. Spectra were also obtained of several A0 V stars in the vicinity of the 30 targets.

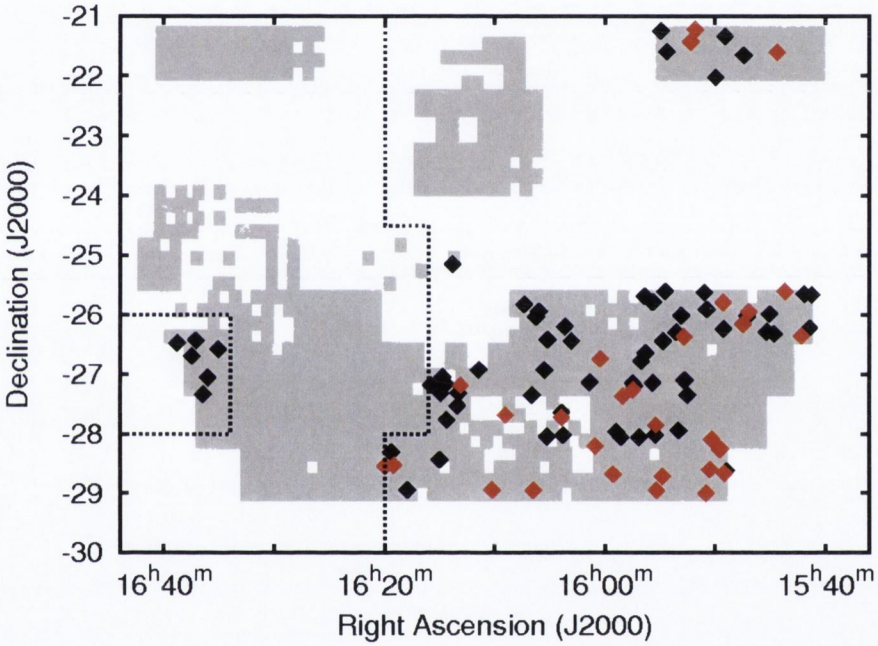

Figure 5.1 Coverage in Z, Y, J, H and K filters of 57 $\deg^2$ in Upper Scorpius from the UKIDSS GCS. The diamonds mark the position of 96 candidate brown dwarfs as identified from the UKIDSS Ninth Data Release. The 30 objects investigated in this work are shown in red.

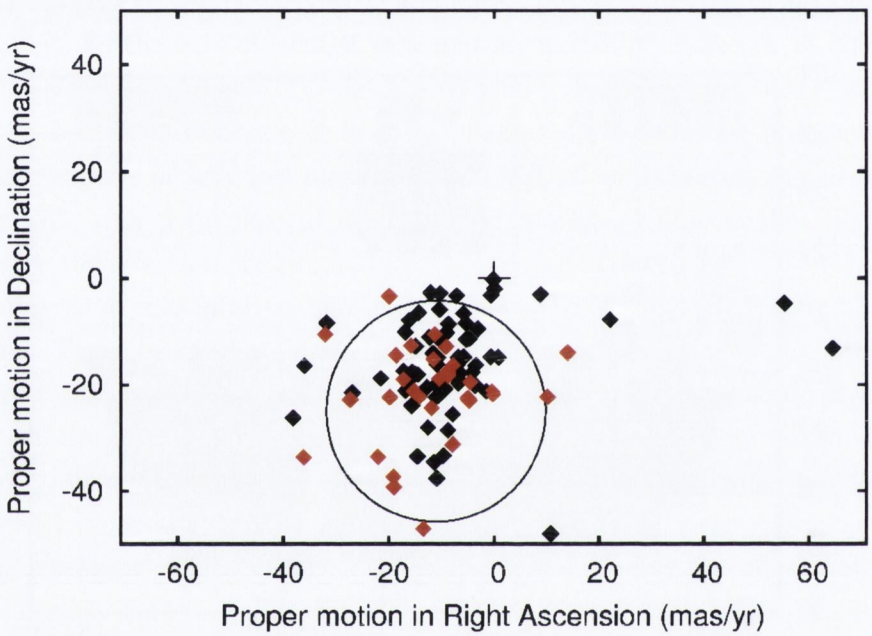

Figure 5.2 Vector point diagram for 96 candidate brown dwarfs in Upper Scorpius as identified from the UKIDSS Ninth Data Release. There is an obvious and identifiable cluster around (-11,-25), while there is no significant clustering around the origin, indicating that there is very little contamination from background objects in the photometrically selected sample. The 20 candidates lying outside the 2σ selection circle were classified as non-members by Dawson et al. (2013), as described in Chapter 3. The 30 objects investigated in this work are shown in red.

These spectra of standard stars were used to correct for telluric absorption in the target spectra. As detailed in Cushing et al. (2004), SpeX has an external calibration unit containing the lamps needed for flat-fielding and wavelength calibration. Exposures of these lamps were taken 3 times during each observing night. Table 5.1 details the slit width used, the airmass, single exposure time and associated standard star for all 30 objects.

5.3 Data Reduction

The raw spectra were reduced with Spextool, an IDL-based spectral reduction package designed specifically for use with data obtained from SpeX (Cushing et al., 2004). Flat-field and wavelength calibration exposure frames were made using the Spextool package. The target object spectra and the standard star spectra were then extracted. Telluric absorption features in the target object spectra were subsequently removed using the standard star spectra and the *xtellcor* IDL widget within the Spextool package, using the method of Vacca et al. (2003). The spectra were then normalised at the 1.25 μm J band to facilitate comparison with each other. The spectra are shown in Figs. 5.3, 5.4 and 5.6 to 5.9.

5.4 Spectral Analysis

The primary aim of the spectral analysis was to determine the spectral type of each object in order to confirm its nature as a young very low mass object in UpSco. For brown dwarfs with $0.013 < M < 0.08\,\mathrm{M}_{\odot}$ the spectral type is expected to range from about M6 to L0 at the age of this region (5-10 Myr). For this range of spectral types, the near-infrared spectra are expected to show a peak in the H band at 1.68 μm and another in the K band at 2.25 μm. These peaks are caused by H_2O absorption features at 1.3-1.5 μm and another at 1.75-2.05 μm and can be used as a diagnostic for objects of M-type and later. The definition of the H band peak is gravity sensitive, being sharp in young objects and much less so in evolved objects, exhibiting a plateau in the region on the blue side of 1.68 μm (Kirkpatrick et al., 2006; Peterson et al., 2008). In addition, late-type objects exhibit a steep edge at 1.35 μm, again caused by H_2O absorption, and CO absorption bands at 2.3 μm. For a more detailed discussion of infrared spectra of M-L

type objects, see Cushing et al. (2005); Scholz et al. (2009).

5.4.1 Spectral Sequence

Inspection of the spectra showed that each object in the sample exhibited a peak in the H band at 1.68 μm. Its presence in each spectrum indicates that all the objects examined are M or L type objects. Later objects within this range are expected to have deeper troughs, and hence steeper slopes, on both the J and K side of the peak in the H band. The consequent prominence of the H band peak becomes correspondingly less in earlier type objects that have shallower troughs and slopes on either side of the peak. The spectra were plotted and then arranged by eye in a sequence, from earliest to latest, based on a comparison of the shape of each spectrum in the vicinity of the peak in the H band (Figs. 5.3 and 5.4).

It is clear from Fig. 5.4 that object 30, in the left panel, has a more rounded H band peak than the others, indicating that it is an old field object rather than a young substellar member of UpSco. It is one of the 6 objects shown in Fig. 5.2 which lie outside the selection circle.

I compared the sequence with templates of young late type objects that had been given spectral types based on their optical spectrum. This comparison was carried out to calibrate the visually arranged spectral sequence. The templates were taken from the SpeX library on www.browndwarfs.org[1]. The selected templates are; MHO4 (M7), KPNO5 (M7.5), J1207 (M8) and J1245 (M9.5), taken from Muench et al. (2007) and Looper et al. (2007). Judged by their near-infrared colours, these four show little extinction ($A_V < 1$ mag), see Scholz et al. (2012a), and so are comparable with the UpSco sample. The conclusion from this visual comparison was that about a third of the objects were within half a subtype of M7 (right panel in Fig. 5.3), while about a third were earlier (left panel in Fig. 5.3), and the remaining third were later than M7.5 (left panel in Fig. 5.4).

The ordering of the spectra and their visual comparison with the template objects had established that most of the objects appear to be young and of late M type, apart from object 30 which was determined to be an evolved field object with a type of M8.

[1]See http://pono.ucsd.edu/~adam/browndwarfs/spexprism/

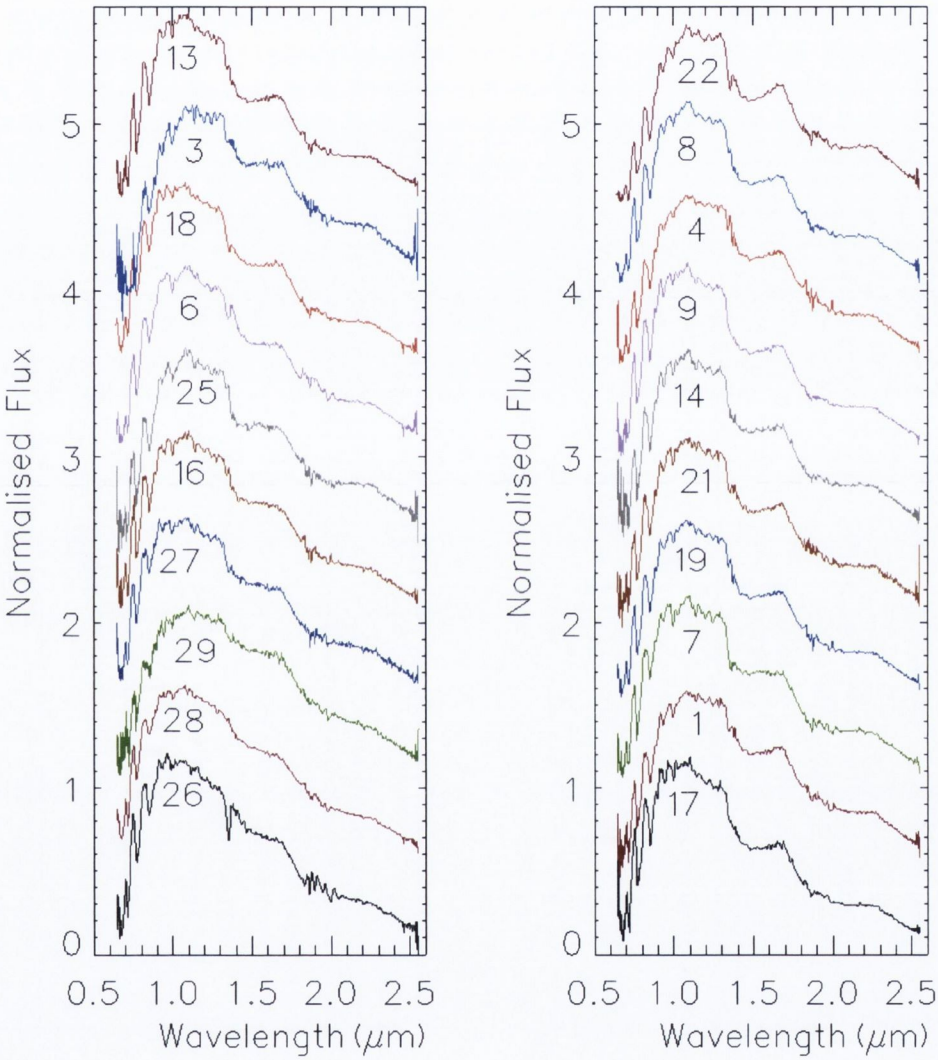

Figure 5.3 Two of four panels (see also Fig. 5.4) showing the spectra of the earliest 20 of the 30 targets, arranged in order of the prominence of the peak in the H band at 1.68 μm. Spectra are normalised at 1.25 μm (J) and offset by 0.5.

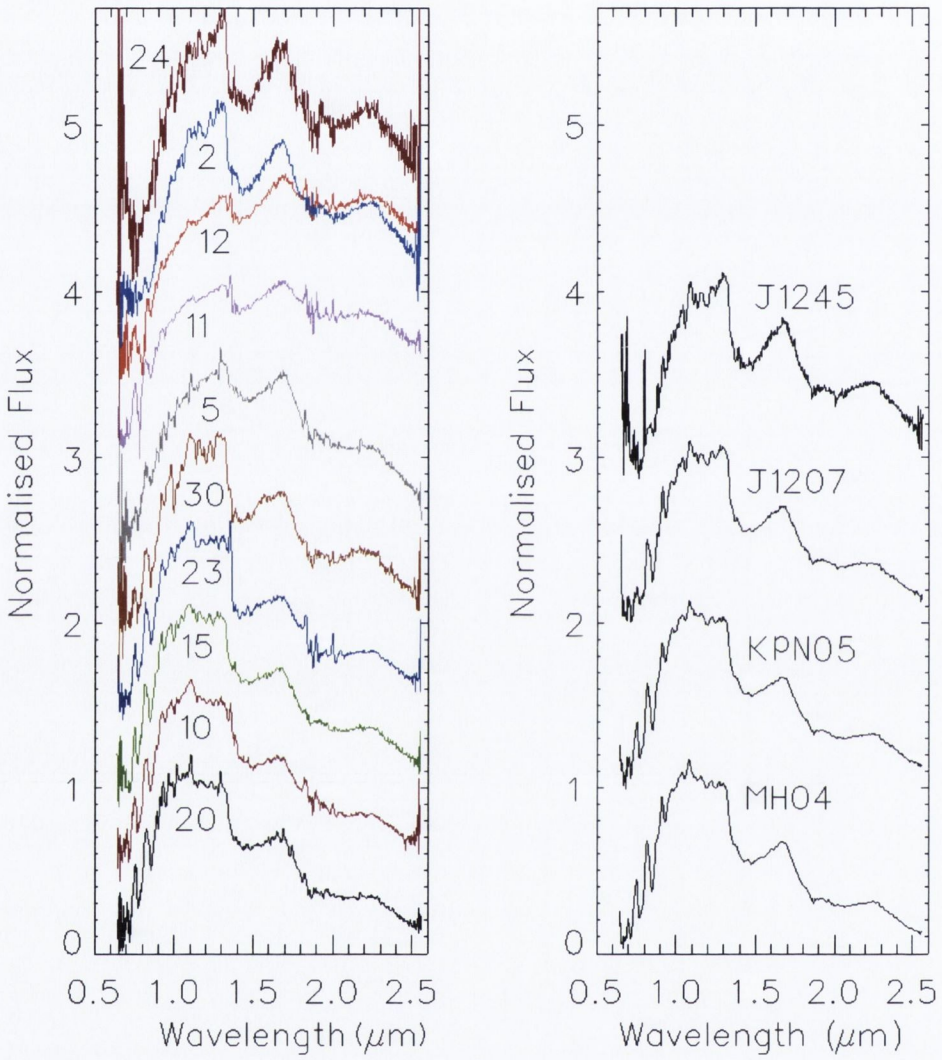

Figure 5.4 The left panel shows the spectra of the latest 10 of the 30 targets arranged in order of the prominence of the peak in the H band at 1.68 μm. Also shown, in the right panel, are the spectra of 4 templates with known spectral types for comparison (from bottom to top: M7, M7.5, M8 and M9.5). Spectra are normalised at 1.25 μm (J) and offset by 0.5. The different profiles of the spectra of the Class II objects (5, 11 and 12) in the left panel are quite distinct.

5.4.2 Spectral Indices

In order to derive spectral types I use and compare 3 spectral definitions that have been used in the recent literature. The analysis of each spectrum and calculation of each index was performed using IDL routines.

The H-peak Index

Described in Scholz et al. (2012a), the H-peak index (HPI) is defined as the ratio of the fluxes measured in the intervals between 1.675-1.685 μm and 1.495-1.505 μm. The first interval in this ratio is at the position of the peak in the H band (Figs. 5.3 and 5.4). The second interval is located near the flux minimum on the blue side of the peak. The HPI therefore utilises the maximum flux range available between the bottom of the H_2O absorption band at 1.3-1.5 μm and the peak in flux at 1.68 μm. Scholz et al. (2012a) determined an empirical relationship between the HPI and spectral types for the range from M7 to M9.5, noting that this relationship may also hold for spectral types later than M9.5, but does not apply for spectral types earlier than M7. The correlation between the HPI and spectral type (SpT) is given by Scholz et al. (2012a) as

$$\mathrm{SpT} = -0.84 + 7.66 \times \mathrm{HPI} \tag{5.1}$$

From the sample, 20 of the objects are classified as M7 or later via the HPI, with L0.3 as the latest type (Table 5.2 and Fig. 5.5). The remaining 10 are all given spectral types of between M6.1 and M6.9. Notably, 5 of the 6 objects from outside the selection circle in Fig. 5.2 are among those with spectral types earlier than M7. The 6th object from outside the selection circle is object 30 with a spectral type of M8.4, but - as noted above - this is the object with the plateau near the H band peak suggesting it is a field object too old to be a member of UpSco.

In summary, of the 24 objects from the 2σ sample, the HPI categorises 18 of them as young very low mass objects, with spectral types of M7.0-L0.3, placing them all within the brown dwarf mass regime.

The H_2O Index

The H_2O index devised by Allers et al. (2007) uses the ratio of the fluxes in the intervals between 1.550-1.560 μm and 1.492-1.502 μm to characterise spectra. Compared to the HPI it utilises a shorter part of the same slope on the blue side of the H band peak. The correlation between the H_2O index and spectral type given by Allers et al. (2007) is

$$H_2O = 0.75 + 0.044 \times \mathrm{SpT} \tag{5.2}$$

Allers et al. (2007) state that the relationship is independent of gravity and can be used to determine spectral types for field dwarfs, giants and young brown dwarfs over the spectral type range of M5 to L0.

Using the H_2O index, all 30 objects in the sample are classified as M5 or later with 16 of the objects classified as M6 or later, and with L1.1 as the latest spectral type (Table 5.2). These spectral types tend to be 1 subtype earlier than those given by the HPI (see Fig. 5.5), as already noted by Mužić et al. (2012). 4 of the 5 objects from outside the selection circle in Fig. 5.2, which are classified among the earliest spectral types via the HPI, are also assigned the earliest spectral types (M5.2 to M5.4) via the H_2O index. The other (object 25) is classified as an M6.4 object, while the field dwarf (object 30) is given a spectral type of M8.7.

The 24 objects from the 2σ sample are all given spectral types of M5.5 and later. Therefore the H_2O index classifies all of these 24 objects as very low mass members of UpSco ranging from the lowest stellar masses to the lower end of the mass range of brown dwarfs.

The H_2O-K2 Index

The H_2O-K2 index was devised by Rojas-Ayala et al. (2012) to represent the change in the overall shape of the spectra of M dwarfs due to water absorption in the K band from 2.07 to 2.38 μm. It uses the ratio of two ratios i.e. the ratio of the fluxes between 2.070-2.090 μm and 2.235-2.255 μm to the ratio of the fluxes between 2.235-2.255 μm and 2.360-2.380 μm. For objects between spectral type M0 and M9 Rojas-Ayala et al. (2012) gives the relationship between spectral type and H_2O-K2 index as

$$\mathrm{SpT} = 24.699 - 23.788 \times H_2O - \mathrm{K2} \tag{5.3}$$

As can be seen in Table 5.2 and Fig. 5.5, the H_2O-K2 index spectral types agree with the H_2O index to within 1 subtype for most (23/30) of the objects. However, the H_2O-K2 index returns 2 markedly earlier spectral types; M3.3 and M3.7, for objects 11 and 12 respectively. They have HPI spectral types of M7.8 and M8.5 and H_2O index spectral types of M6.6 and M7.2. These are 2 of the Class II objects which can be seen in Fig. 5.3 and 5.4 to have distinctly different spectral profiles to most of the other objects. They were shown, in the preceeding chapter, to exhibit an obvious excess in their near-infrared J-K colours, the result of excess emission in the K band from circumsubstellar disks. So the H_2O-K2 index is measuring that part of their near-infrared spectral profiles which, as already shown, is mostly non photospheric in origin. Apart from these 2 objects all the objects from the 2σ sample are classified with spectral types ranging from M4.7 to L0.8.

Of the objects that are not in the 2σ sample, objects 26, 27, 28 and 29 are given spectral types varying from M2.6 to M3.7, about 2 or more subclasses earlier than their H_2O index spectral types. The field dwarf, object 30, is given a spectral type of M7.5, earlier than its H_2O index classification of M8.7, while object 25 is assigned spectral type M6.9, similar to its H_2O index derived type of M6.4.

With the exception of objects 11 and 12, the H_2O-K2 index yields spectral types of M4.7 and later for the objects in the 2σ sample, which again classifies them as very low mass members of UpSco ranging from the lowest stellar masses down into the mass range of brown dwarfs.

5.4.3 Summary Of Spectral Classifications

Spectral types were determined from comparisons with templates and with 3 different spectral indices in the H and K bands. The types are listed in Table 5.2 and shown in Fig. 5.5. The overall results are summarised as follows.

1. The 24 objects from the 2σ sample have spectral types ranging from M5 to L1, with about 20 being of type M6 or later and they all exhibit evidence for youth. This classifies them as likely brown dwarfs and young members of UpSco.

2. Of the 6 other objects, 1 of them is a field M8-M9 dwarf (and is most probably in the foreground) while the remaining 5 are early to mid-type (M3-M6) young M dwarfs. These five could still be members of UpSco, but

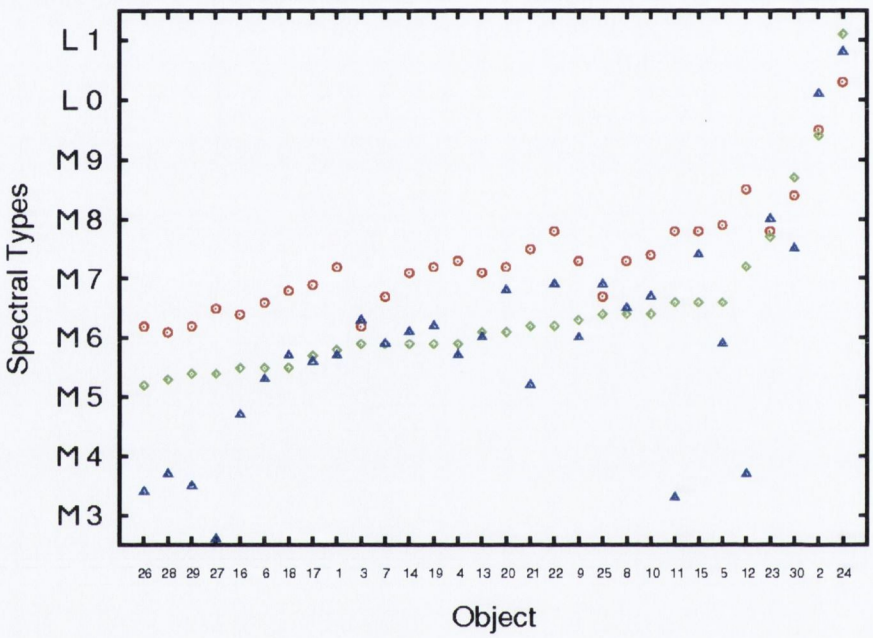

Figure 5.5 Spectral types of all 30 objects as derived via the H-peak (circles), H_2O (diamonds) and H_2O-K2 (triangles) indices. Objects are ordered in terms of their H_2O index spectral type. The H_2O and H-peak indices give similar spectral types for each object, the H_2O index results tending to be 1 subtype earlier. 24 of the H_2O-K2 index spectral types agree to within 1 subtype with at least one of the other indices, while the remaining 6 have anomalously earlier types.

with slightly different kinematical characteristics.

5.4.4 Contamination

In Chapter 3, and Dawson et al. (2013), I demonstrated that there was minimal contamination of the sample of 76 brown dwarf members of UpSco identified from the UKIDSS Ninth Data Release, based on the distribution of the proper motion vectors.

The spectral types of the 24 objects in the $2\,\sigma$ sample obtained via the methods outlined above confirm that each one is a young object with a spectral type between M5 and L1, classifying them as either brown dwarfs or very low mass stars. Ergo, there is no measurable contamination in this sample ($< 1/24$, i.e. $< 4\%$). This confirms the efficacy of using photometric and proper motion data from both the UKIDSS Galactic Cluster Survey and 2MASS as outlined in Lodieu et al. (2006, 2007, 2013) and Dawson et al. (2011, 2013), and Chapter 3 of this thesis, to reliably identify brown dwarf members of UpSco.

5.5 Discussion Of Spectral Types

Each object in the sample had spectral types assigned to it using different indices that measured specific parts of each spectrum. Spectra of objects with similar types were compared to each other to see how closely their overall profiles matched.

5.5.1 Divergence Of Class II And Class III Spectra

The spectra shown in Figs. 5.3 and 5.4 include 3 that display radically different profiles from all the others. These objects (5, 11 and 12) were shown in Chapter 4, to be Class II objects, based on their WISE photometry in the W1 ($3.4\,\mu$m) and W2 ($4.6\,\mu$m) bands. Objects 11 and 12 were also the only 2 of 27 Class II objects analysed in Chapter 4 to exhibit an obvious excess in their near-infrared J-K colours. The differences in profile can be seen more clearly in Fig. 5.6 which compares these spectra with the spectra of 3 of the Class III objects (15, 22 and 23). All 6 objects have similar HPI spectral types, the Class III objects all being of type M7.8, while objects 5, 11 and 12 are of type M7.9, M7.8 and M8.5 respectively. The Class III objects have

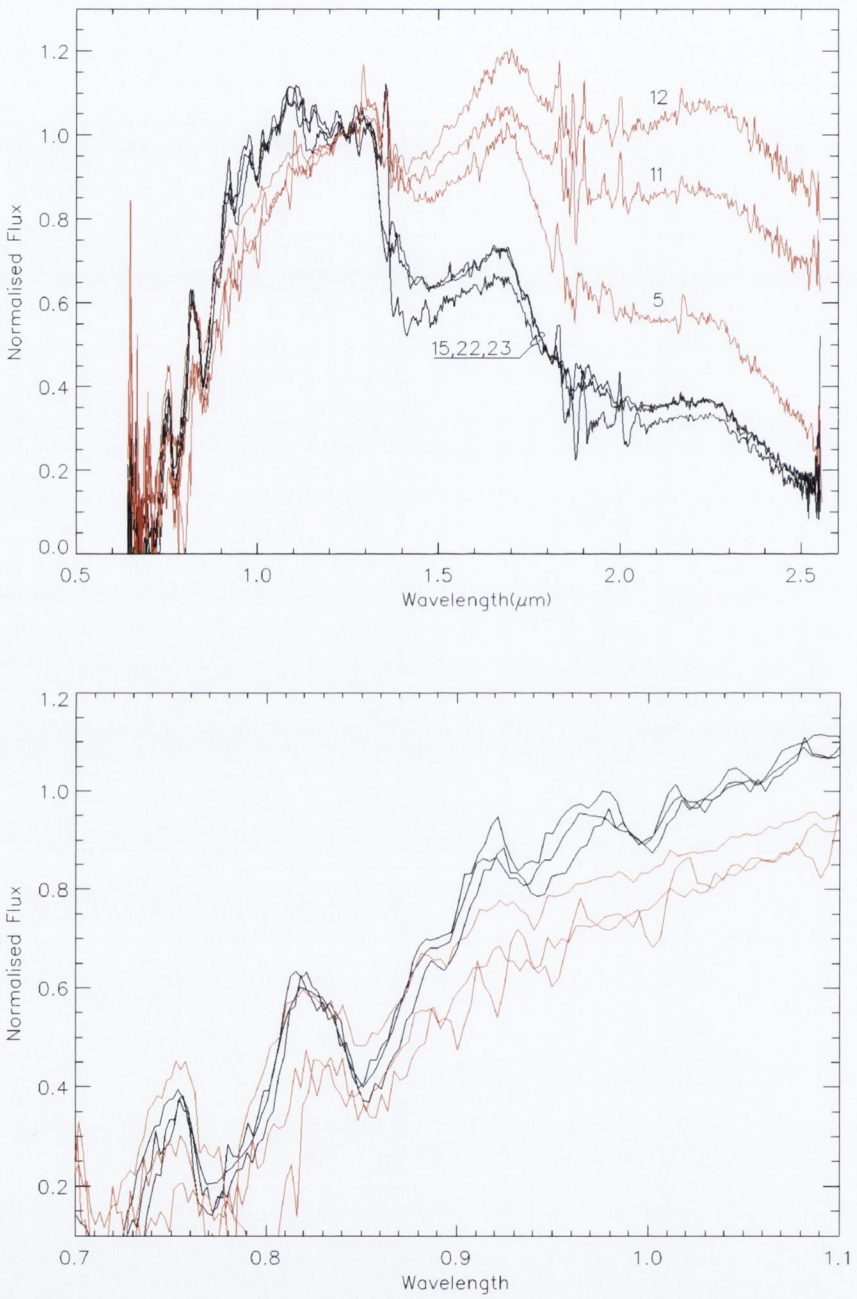

Figure 5.6 Spectra for 3 Class III objects classified as spectral type M7.8 via the H-peak index are shown in black. Overplotted in red are the spectra of 3 Class II objects with H-peak index spectral types (reading from bottom to top) of M7.9, M7.8 and M8.5. All spectra are normalised at 1.25 μm and are not offset. The radically different shapes of the Class II spectra are readily apparent in the upper panel. The lower panel shows the shorter wavelength part of the spectra in more detail. In this region, the Class II spectra are mostly deficient in normalised flux and their features are weak by comparison with the Class III spectra.

very similar spectra. The Class II objects, on the other hand, have quite different spectra from the Class III objects, and each other. However there are several features common to the Class II spectra: (i) the most obvious feature is the higher normalised flux levels at the H and K band peaks relative to the J band, (ii) the profiles of the Class II spectra in the region on the blue side of the J band share a distinctive rounded shape, generally being deficient in normalised flux in this wavelength range by comparison with the Class III objects, (iii) features in this part of the Class II spectra also tend to be attenuated. In particular, the TiO feature at 0.85 μm tends to be much weaker among the Class II objects. Taken together, the presence of these characteristics in a spectrum appear to be diagnostic of a Class II object. An examination of the other Class II objects in the sample (2, 4 and 10) showed that they exhibit these same characteristics when compared to Class III objects of similar spectral type.

The most likely origin of these spectral features is excess emission from a circumsubstellar disk. In these objects, warm dust from the inner disk absorbs photospheric light and emits it at longer wavelengths. This causes the observed excess in the near-infrared bands. As seen in Fig. 5.6, the excess becomes stronger from the J to the K band. At the blue end of these spectra, the attenuation of the photospheric features is similar to the veiling observed in T-Tauri stars, a phenomenon which has been attributed, at least in part, to accretion processes (Hartigan et al., 1991; Folha & Emerson, 1999).

The presence of these characteristics raises questions about the reliability of the spectral typing of Class II objects using near-infrared spectra. If the flux at wavelengths longer than J contains significant contributions from a dusty disk, the shape of the H band or K band peak cannot be relied upon to represent the shape of the underlying photospheric spectrum. Fig. 5.6 shows that contributions from the disks of the Class II objects seem to be altering the shape of the spectra in the region of the K band by filling in the H_2O absorption band at 1.75-2.05 μm. This appears to be the reason that the H_2O-K2 index yielded much earlier spectral types for objects 11 and 12 than the other indices. Moreover, it is also clear from Fig. 5.6 that the spectra of the Class II objects also have significant contributions from their disks in the region of the H band. Without a clear understanding of how that part of the spectral profile is affected by contributions from the

disk it is impossible to be confident that the spectral types derived from the H-peak and H_2O indices are any more reliable than the H_2O-K2 index spectral types for these 3 objects.

Fig. 5.6 indicates that to obtain a reliable spectral type of a Class II brown dwarf using near-infrared spectroscopy, the overall shape of the spectrum from 0.8 - 2.5 μm needs to be taken into account. If it resembles that of the Class II objects in Fig. 5.6 any spectral type derived using only a small part of this wavelength range should be regarded as provisional. For such objects, the most reliable spectral types might still only be obtained from optical data. As a result, I caution against relying on near-infrared spectra for spectral typing of objects with known excess emission from a disk.

5.5.2 Diversity Of Class III Spectra

The Class III spectra show a lesser, but still significant diversity between objects of the same spectral type. In the following, I illustrate this by comparing spectra of Class III objects with similar spectral types.

Fig. 5.7 shows the spectra of Class III objects 1, 9, 13 and 19, all of which are classified between M7.1 and M7.3 using the HPI. The spectra have similar shapes on the blue side of the H band peak. However, in the H and K band, object 1 has higher normalised flux levels (by $\sim 10\%$) than the other objects and its features are a little shallower at the shorter wavelengths. The characteristics seen in the spectrum of object 1 are qualitatively similar to the appearance of the Class II spectra (Section 5.6.1).

The same pattern of diversity can be seen between the spectra of the Class III objects 7, 14 and 19 and the Class II object 4 in Fig. 5.8. All have spectral types of M5.9 as determined via the H_2O index. Object 4 exhibits slight traces of the Class II characteristics seen in Fig. 5.6. It has higher normalised flux levels in the H band, while at the shorter wavelengths it exhibits a deficiency in normalized flux and attenuated features.

The spectrum of object 1 is very similar to that of object 4 in Fig. 5.9, where they are shown along with the Class III objects 17 and 18. All are classified as type M5.6 or M5.7 via the H_2O-K2 index. The similarity of objects 1 and 4 is such that it appears that the spectrum of object 1 is not completely photospheric in origin but also contains small contributions from a dusty disk. This tallies with its position relative to the other spectra in Fig 5.7. Objects 17 and 18 have lower normalised flux levels on the red side

of J and display higher levels on the blue side of J, indicating that their spectra are more photospheric in origin.

In summary, the differences between the spectra shown in Figs. 5.7, 5.8 and 5.9 are of a similar pattern to the differences between the Class II and Class III objects shown in Fig. 5.6, albeit on a lesser scale. Compared with the cases shown in Fig. 5.6, the observed spectral diversity is minute and does not affect the spectral type significantly (i.e. by more than 1 subtype).

The Class II like characteristics are present in 7 of the 18 ($\sim$ 40%) Class III objects in the $2\,\sigma$ sample.

The nature of the mild excess in the H and K bands observed in some Class III objects remains unclear. It is conceivable that the spectral diversity in the Class III objects is related to the presence of traces of dust and gas surrounding these objects. One possibility is that these objects represent an intermediate stage - a Class II.5 as it were - between the objects with bona fide disks and the "clean and clear" Class III sources without any evidence for excess emission.

Alternately, the diversity among the Class III spectra may be due to reddening. To test this, I artificially reddened the spectra of objects 13, 17, 18, 19 and 23, and compared them with those of the other objects. To redden the spectra, I used the near-infrared extinction law:

$$\left(\frac{\mathrm{A}_\lambda}{\mathrm{A}_\mathrm{J}}\right) = \left(\frac{\lambda}{1.25\mu\mathrm{m}}\right)^{-\alpha} \tag{5.4}$$

with a value of 1.7 for α, as given by Mathis (1990), and took $A_J = 0.282 A_\mathrm{V}$ (Rieke & Lebofsky, 1985). I then adapted the method used by Rayner et al. (2009), to correct for reddening in spectra obtained with SpeX, and reddened each spectrum using a range of values for A_V between 1 and 10. In each case, the least reddened spectra differed from the original spectrum in a manner that closely resembled the pattern of differences shown in Figs. 5.7, 5.8 and 5.9.

The differences that were observed are typified by the example shown in Fig. 5.10. Reddened spectra of object 19 are plotted alongside its real spectrum and compared to the spectrum of object 1. Both objects (which also feature in Figs. 5.7, 5.8 and 5.9) are classified as M7.2 using the HPI. The spectrum of object 1 most closely resembles the spectrum of object 19 that has been reddened using an $A_V = 1$. An $A_V = 1$ is within the limits

of the little extinction that exists in the region of UpSco where the objects are located (Ardila et al., 2000). On this basis, a plausible amount of interstellar reddening could account for the diversity among the spectra of the class III objects.

Reddening alone is not a plausible cause of the different shape of the spectra of the class II objects shown in Fig. 5.6. Objects 5 and 11 have similar spectral types (M7.8 and M7.9 via the HPI), and yet their spectra are very different *to each other*, as well as to the spectra of the class III objects in the same diagram. No single reddening law could produce a match for both spectra. A comparison with the reddened spectra of object 23, (which has a similar HPI spectral type of M7.8), also shows that none of its reddened spectra are a match for the spectra of objects 5 or 11. Therefore, while reddening may be present in these cases, it cannot be the predominant cause of the diversity among these class II spectra. Nor, if present, can it be readily distinguished from the overwhelming contributions of the circumsubstellar discs.

All the class II objects in this survey were shown, in the previous chapter, to have excess flux in the mid-infrared. The objects with the largest mid-infrared excess were also shown to have a corresponding contiguous excess in the near-infrared, as shown in Figs. 4.4 and 4.7. All of the class II objects exhibit these characteristics, although they may be present to a much lesser extent, while they are present in only $\sim$ 40% of the class III objects, in the $2\,\sigma$ sample. Among the class III spectra that exhibit these characteristics, disentangling the relative contributions of small amounts of excess emission, veiling and reddening involved is not possible. Therefore, although near-infrared spectroscopy may be more sensitive to residual disc emission than mid-infrared photometry, it does not, in these cases, provide the robust certainty required for identifying circumsubstellar discs that is provided by mid-infrared photometry. In each case, whatever the exact cause of these effects, the underlying photospheric spectrum is being obscured and distorted.

5.5.3 Templates For Spectral Typing

There is a need for a catalogue of spectral templates of young brown dwarfs that are clean and clear of the effects of veiling, excess emission and reddening, in order to establish benchmarks that can be used to correct for

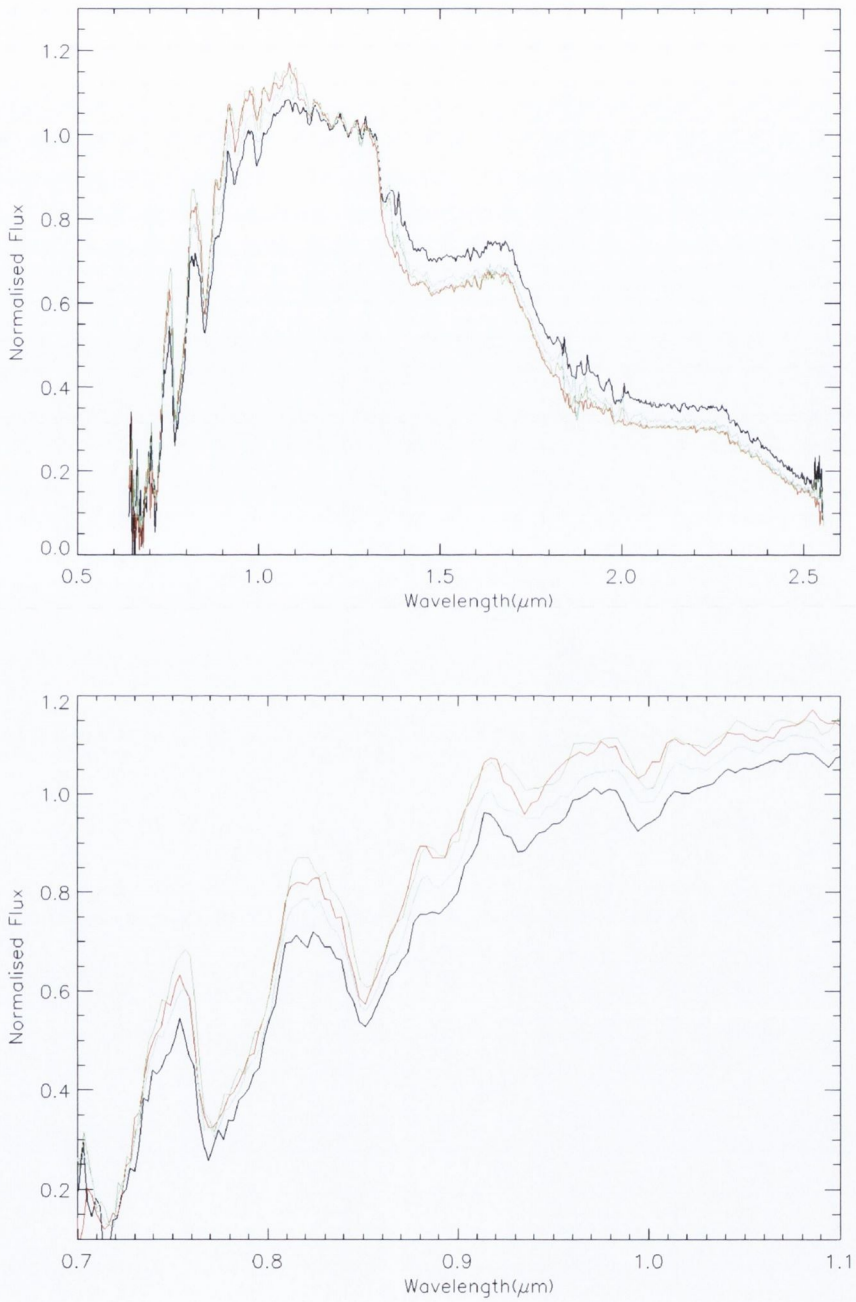

Figure 5.7 Spectra for objects 1 (black), 9 (red), 13 (green) and 19 (blue), all classified via the H-peak index as having spectral types between M7.1 and M7.3. In the upper panel the similar profiles of the spectra in the region blue of the H band peak are obvious. However, object 1 displays noticeably higher normalised flux levels in the H and K bands, and in the region blue of J most of its features are shallower than those of the other objects. The lower panel shows the latter region in more detail. Object 1 has the shallowest TiO feature at 0.85 μm.

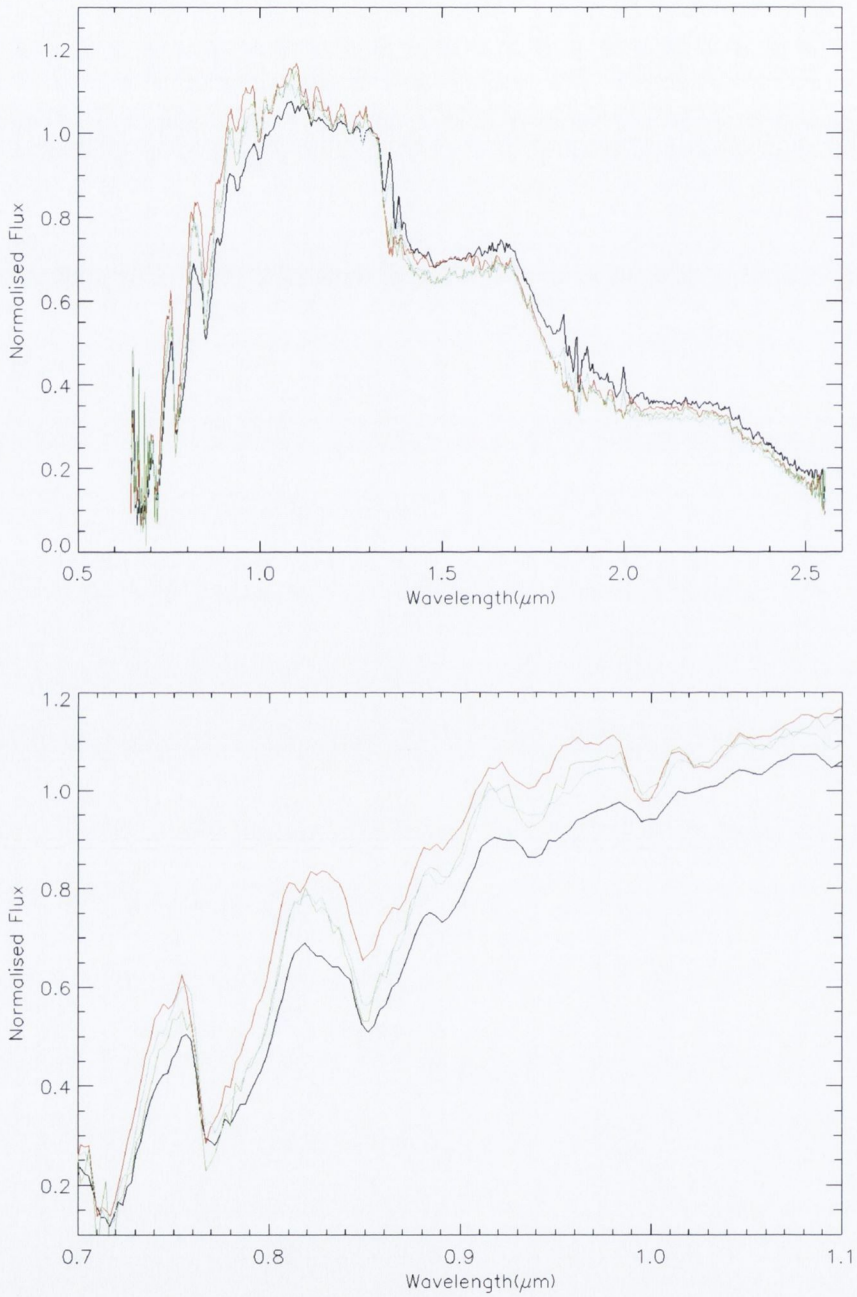

Figure 5.8 Spectra for objects 4 (black), 7 (red), 14 (green) and 19 (blue), all classified as spectral type M5.9 via the H_2O index. Object 4 is a Class II object and it has the highest normalised flux levels in the region red of J (upper panel) along with the lowest levels in the region blue of J (shown in detail in the lower panel) where its features are also visibly weaker by comparison with objects 14 and 19. These are the same traits exhibited by the Class II objects shown in Fig. 5.6, albeit on a lesser scale.

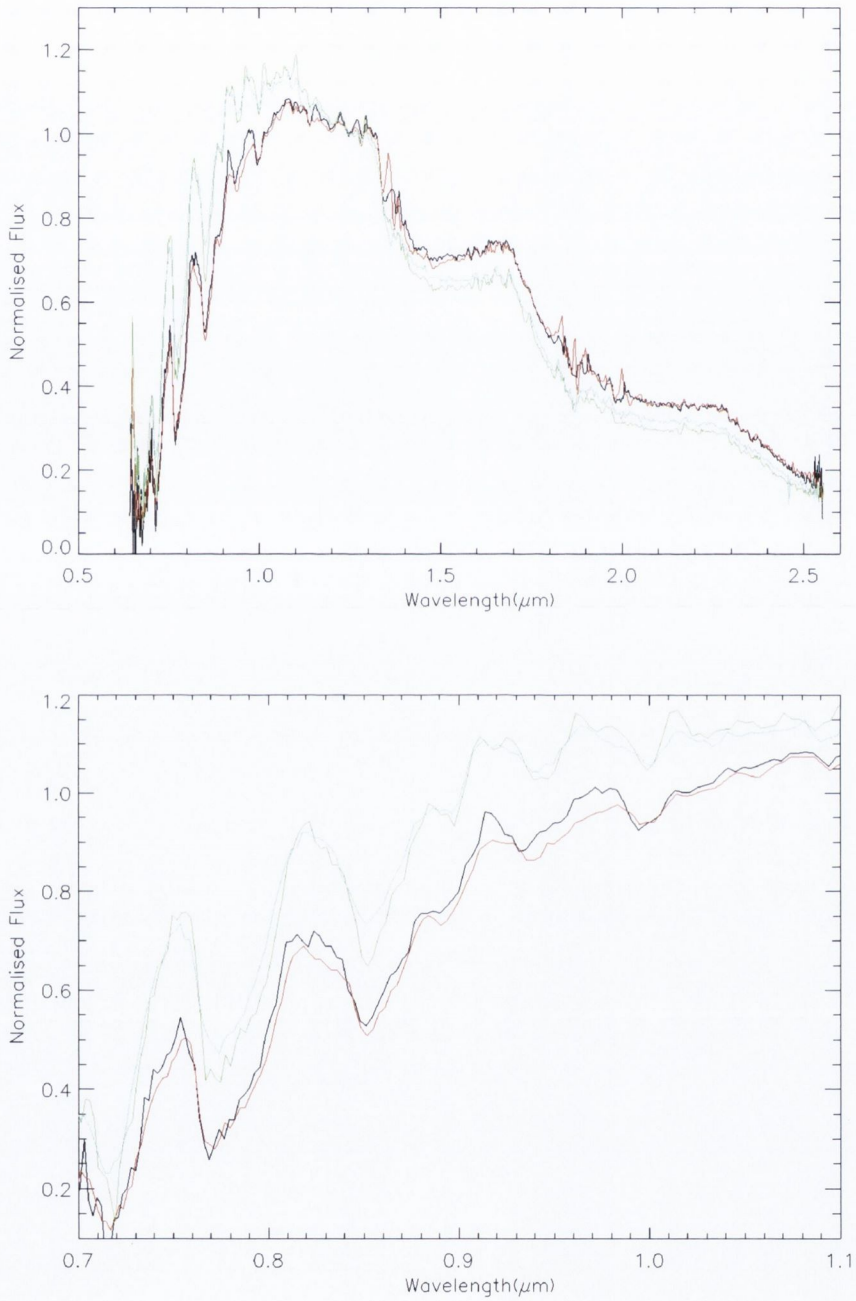

Figure 5.9 Spectra for objects 1 (black), 4 (red), 17 (green) and 18 (blue) classified as spectral types M5.6 and M5.7 via the H_2O-K2 index. In these graphs, the spectra of the Class III objects 17 and 18 can be seen to be very similar to each other, and distinct from those of objects 1 and 4. The spectrum of the Class III object 1 has a shape very similar to that of the Class II object 4.

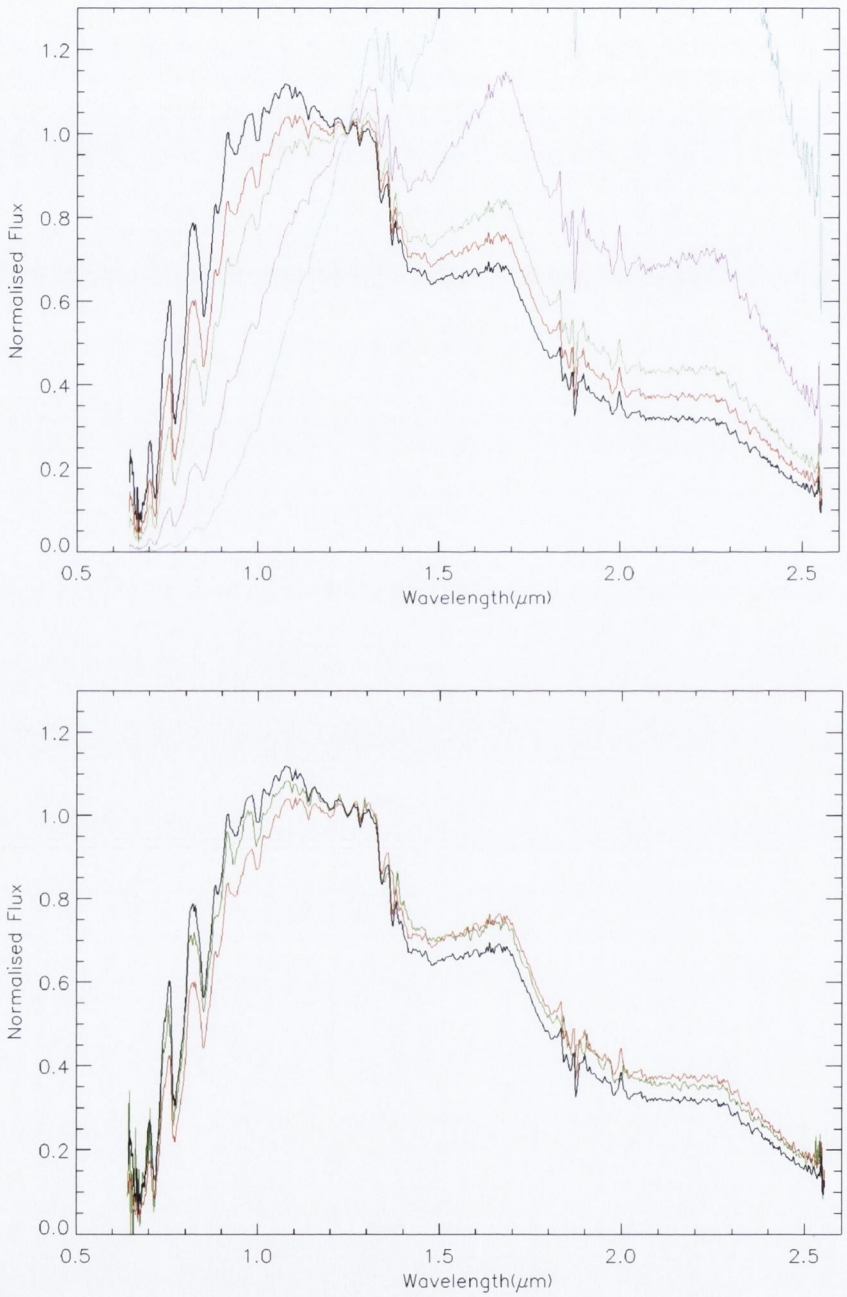

Figure 5.10 Spectrum of object 19, with artificially reddened spectra overplotted (upper panel). The original spectrum (black) is the one with the lowest normalised flux in the vicinity of the H band peak. The 4 reddened spectra represent A_V of 1 (red), 2 (green), 5 (pink) and 10 (blue). The lower panel shows the spectrum of object 1 (dark green), overlaid on the unreddened, and slightly reddened ($A_V = 1$) spectra of object 19 (black and red respectively). The spectrum of object 1 is similar to the least reddened spectrum of object 19.

these effects. The spectra of the 24 objects in the 2σ sample were examined with the intent of producing a sequence of template spectra of young brown dwarfs that are free of contributions from any source other than their photospheres. This spectroscopic survey is ideal for producing such a catalogue for two reasons: 1) UpSco is not significantly affected by extinction, 2) the disk fraction in UpSco (23%) is low by comparison with other young star forming regions (Dawson et al., 2013), which maximises the chances of obtaining spectra that are purely photospheric in origin.

In a first step, objects 5, 11 and 12 - the Class II objects from Fig. 5.6 - were summarily disregarded. Object 4 - the Class II object which features in Figs. 5.8 and 5.9 - was also disregarded, along with the Class II objects 2 and 10. Each Class III object had its spectrum compared with others of a similar spectral type from each index, as in Figs. 5.6 to 5.9. The spectra of objects 1, 3, 6, 7, 15, 16 and 22 were found to exhibit excess emission and veiling. Each spectrum was also compared to every other member of the 2σ sample to check if any other pattern of diversity or anomaly among the spectra could be discerned. No other pattern of diversity or anomaly was found.

The spectra of the remaining Class III objects (Table 5.3) are those that, by comparison, show no evidence of excess emission, veiling or reddening. I present them as a catalogue of spectra of young brown dwarfs which, to the greatest extent discernible, are clear of contributions from sources other than their photospheres. The spectral types of the chosen objects, as determined from their near-infrared spectra, range from M5.5 to L1.1. Table 5.3 also includes a rough estimate of the effective temperature (T_{eff}) of each object. The T_{eff} of each object was estimated using the Spectral Type-T_{eff} relationship given in Mužić et al. (2014) for objects of spectral types later than M1. The different spectral types of each object, derived via the 3 different spectral indices, yielded a range of values of T_{eff} for each object. The T_{eff} listed in Table 5.3 is the median of these values, rounded to the nearest 50K. The typical uncertainty in each estimated T_{eff} is 150-200K. The catalogue of these spectra can be accessed at: http://browndwarfs.org/sonyc.

5.6 Summary

I have carried out a near-infrared spectroscopic analysis of 30 objects in the UpSco star forming region, 24 of which had been previously identified as brown dwarf candidates based on their photometry and proper motion alone. The resulting spectra confirm that all 24 are young very low mass objects with spectral types that range from M5.5 to L1.1. This reinforces the results described in Chapter 3 and strengthens the contention that the objects identified by photometric analysis are brown dwarfs. It further bolsters the results detailed in Chapter 4 and lends weight to the assertion that the Class II and Class III objects analysed are all substellar objects.

I have observed a diversity in form among the spectra that can impact on spectral type determination. Class II objects display excess emission and veiling in their spectra. The same form of excess emission and veiling is also present in the spectra of 7 out of 18 ($\sim 40\%$) Class III objects. This is evidence that these Class III objects are still accreting from an inner disk of dust and gas which is too faint to be detected via mid-infrared photometry, or that they may be more affected by reddening than the other Class III objects.

I present a catalogue of near-infrared spectra for young brown dwarfs that are clear from discernible contributions from anything other than their photospheres. I recommend the use of these objects as spectroscopic templates for identifying young brown dwarfs, and make them available at: http://browndwarfs.org/sonyc.

Table 5.1. Summary of SpeX observations. The first 24 objects are those in the 2σ sample. The last 6 objects have proper motions that caused them to be classified as non-members of UpSco. The names and positions of the objects are listed, followed by details from the observation records for each; slit width used, airmass, single exposure time and associated standard star.

Object Number	2MASS Name	R.A. J2000	Dec. J2000	Slit Width (arcsec)	Airmass	Single Exposure Time (s)	Standard Star
1	2MASSJ15420830-2621138	15:42:08.31	-26:21:13.8	0.5	1.73	60	HD 143747
2	2MASSJ15433947-2535549	15:43:39.47	-25:35:54.9	0.5	1.53	120	HD 143747
3	2MASSJ15442275-2136092	15:44:22.75	-21:36:09.3	0.5	1.50	90	HD 143747
4	2MASSJ15465432-2556520	15:46:54.32	-25:56:52.1	0.5	1.56	60	HD 143747
5	2MASSJ15472572-2609185	15:47:25.73	-26:09:18.5	0.5	1.82	60	HD 138813
6	2MASSJ15490803-2839550	15:49:08.02	-28:39:55.2	0.8	1.55	90	HD 143822
7	2MASSJ15491602-2547146	15:49:16.02	-25:47:14.6	0.5	1.67	60	HD 138813
8	2MASSJ15492909-2815384	15:49:29.08	-28:15:38.6	0.8	1.93	90	HD 138813
9	2MASSJ15493660-2815141	15:49:36.59	-28:15:14.3	0.5	1.92	90	HD 138813
10	2MASSJ15501958-2805237	15:50:19.58	-28:05:23.9	0.8	1.63	120	HD 143822
11	2MASSJ15514709-2113234	15:51:47.09	-21:13:23.5	0.5	1.37	60	HD 136602
12	2MASSJ15521088-2125372	15:52:10.88	-21:25:37.4	0.5	1.35	60	HD 136602
13	2MASSJ15524857-2621453	15:52:48.57	-26:21:45.4	0.5	1.49	60	HD 143747
14	2MASSJ15544486-2843078	15:54:44.85	-28:43:07.9	0.5	1.63	90	HD 138813
15	2MASSJ15551960-2751207	15:55:19.59	-27:51:21.0	0.5	1.56	90	HD 143822
16	2MASSJ15572692-2715094	15:57:26.93	-27:15:09.5	0.5	1.48	60	HD 143747
17	2MASSJ15582376-2721435	15:58:23.76	-27:21:43.7	0.5	1.50	90	HD 146606
18	2MASSJ15591513-2840411	15:59:15.12	-28:40:41.3	0.8	1.87	90	HD 143882
19	2MASSJ16002535-2644060	16:00:25.35	-26:44:06.1	0.5	1.58	60	HD 143747
20	2MASSJ16005265-2812087	16:00:52.66	-28:12:09.0	0.5	1.84	90	HD 138813
21	2MASSJ16062870-2856580	16:06:28.70	-28:56:58.2	0.5	1.68	90	HD 143747
22	2MASSJ16090168-2740521	16:09:01.68	-27:40:52.3	0.8	1.74	90	HD 143822
23	2MASSJ16101316-2856308	16:10:13.15	-28:56:31.0	0.8	1.56	90	HD 143747

Table 5.1 (cont'd)

Object Number	2MASS Name	R.A. J2000	Dec. J2000	Slit Width (arcsec)	Airmass	Single Exposure Time (s)	Standard Star
24	2MASSJ16195827-2832276	16:19:58.26	-28:32:27.8	0.5	1.57	120	HD 143822
25	2MASSJ15502934-2835535	15:50:29.32	-28:35:53.9	0.8	1.53	120	HD 143747
26	2MASSJ15504920-2900030	15:50:49.19	-29:00:03.1	0.8	1.53	90	HD 146606
27	2MASSJ15551768-2856579	15:55:17.70	-28:56:58.1	0.5	1.52	60	HD 143822
28	2MASSJ16035601-2743335	16:03:56.00	-27:43:33.6	0.8	1.48	90	HD 143747
29	2MASSJ16130482-2711214	16:13:04.84	-27:11:21.8	0.5	1.50	90	HD 146606
30	2MASSJ16190983-2831390	16:19:09.82	-28:31:39.5	0.5	1.53	90	HD 143822

Table 5.2. UKIDSS Z photometry, Class, H peak index & Spectral Type, H_2O index & Spectral Type, H_2O-K2 index & Spectral Type of the 30 objects observed with SpeX. Objects are listed in the same order as in Table 5.1.

Object Number	2MASS Name	Z Mag.	Object Class	H peak index	Spectral Type	H_2O index	Spectral Type	H_2O-K2 index	Spectral Type
1	2MASSJ15420830-2621138	15.15	III	1.05	M7.2	1.01	M5.8	0.80	M5.7
2	2MASSJ15433947-2535549	18.15	II	1.36	M9.5	1.16	M9.4	0.61	L0.1
3	2MASSJ15442275-2136092	16.55	III	0.92	M6.2	1.01	M5.9	0.77	M6.3
4	2MASSJ15465432-2556520	14.16	II	1.06	M7.3	1.01	M5.9	0.80	M5.7
5	2MASSJ15472572-2609185	15.40	II	1.14	M7.9	1.04	M6.6	0.79	M5.9
6	2MASSJ15490803-2839550	14.82	III	0.97	M6.6	0.99	M5.5	0.81	M5.3
7	2MASSJ15491602-2547146	14.31	III	0.99	M6.7	1.01	M5.9	0.79	M5.9
8	2MASSJ15492909-2815384	14.29	III	1.07	M7.3	1.03	M6.4	0.77	M6.5
9	2MASSJ15493660-2815141	14.66	III	1.06	M7.3	1.03	M6.3	0.79	M6.0
10	2MASSJ15501958-2805237	16.04	II	1.07	M7.4	1.03	M6.4	0.76	M6.7
11	2MASSJ15514709-2113234	15.12	II	1.13	M7.8	1.04	M6.6	0.90	M3.3
12	2MASSJ15521088-2125372	15.72	II	1.21	M8.5	1.07	M7.2	0.88	M3.7
13	2MASSJ15524857-2621453	14.62	III	1.04	M7.1	1.02	M6.1	0.79	M6.0
14	2MASSJ15544486-2843078	15.51	III	1.04	M7.1	1.01	M5.9	0.78	M6.1
15	2MASSJ15551960-2751207	15.60	III	1.13	M7.8	1.04	M6.6	0.73	M7.4
16	2MASSJ15572692-2715094	14.93	III	0.94	M6.4	1.00	M5.5	0.84	M4.7
17	2MASSJ15582376-2721435	14.35	III	1.00	M6.9	1.00	M5.7	0.80	M5.6
18	2MASSJ15591513-2840411	14.14	III	1.00	M6.8	0.99	M5.5	0.80	M5.7
19	2MASSJ16002535-2644060	14.38	III	1.05	M7.2	1.01	M5.9	0.78	M6.2
20	2MASSJ16005265-2812087	15.04	III	1.05	M7.2	1.02	M6.1	0.75	M6.8
21	2MASSJ16062870-2856580	14.90	III	1.09	M7.5	1.02	M6.2	0.82	M5.2
22	2MASSJ16090168-2740521	14.33	III	1.13	M7.8	1.03	M6.2	0.75	M6.9
23	2MASSJ16101316-2856308	15.67	III	1.12	M7.8	1.09	M7.7	0.70	M8.0

Table 5.2 (cont'd)

Object Number	2MASS Name	Z Mag.	Object Class	H peak index	Spectral Type	H_2O index	Spectral Type	H_2O-K2 index	Spectral Type
24	2MASSJ16195827-2832276	18.74	III	1.45	L0.3	1.24	L1.1	0.59	L0.8
25	2MASSJ15502934-2835535	16.05	III	0.99	M6.7	1.03	M6.4	0.75	M6.9
26	2MASSJ15504920-2900030	14.35	III	0.91	M6.2	0.98	M5.2	0.90	M3.4
27	2MASSJ15551768-2856579	14.32	III	0.96	M6.5	0.99	M5.4	0.93	M2.6
28	2MASSJ16035601-2743335	14.41	III	0.91	M6.1	0.98	M5.3	0.88	M3.7
29	2MASSJ16130482-2711214	15.56	III	0.92	M6.2	0.99	M5.4	0.89	M3.5
30	2MASSJ16190983-2831390	16.63	III	1.20	M8.4	1.13	M8.7	0.72	M7.5

Table 5.3. UKIDSS Z photometry, HPI Spectral Type, H_2O Spectral Type, H_2O-K2 Spectral Type and T_{eff} of the 11 objects selected as near-infrared spectral templates for young low mass stars and brown dwarfs between M5 and L1.

Object Number	2MASS Name	Z Mag.	HPI Spectral Type	H_2O Spectral Type	H_2O-K2 Spectral Type	T_{eff}
18	2MASSJ15591513-2840411	14.14	M6.8	M5.5	M5.7	3,050
17	2MASSJ15582376-2721435	14.35	M6.9	M5.7	M5.6	3,050
14	2MASSJ15544486-2843078	15.51	M7.1	M5.9	M6.1	3,000
19	2MASSJ16002535-2644060	14.38	M7.2	M5.9	M6.2	3,000
13	2MASSJ15524857-2621453	14.62	M7.1	M6.1	M6.0	3,000
20	2MASSJ16005265-2812087	15.04	M7.2	M6.1	M6.8	2,950
21	2MASSJ16062870-2856580	14.90	M7.5	M6.2	M5.2	3,050
9	2MASSJ15493660-2815141	14.66	M7.3	M6.3	M6.0	2,950
8	2MASSJ15492909-2815384	14.29	M7.3	M6.4	M6.5	2,950
23	2MASSJ16101316-2856308	15.67	M7.8	M7.7	M8.0	2,750
24	2MASSJ16195827-2832276	18.74	L0.3	L1.1	L0.8	2,300

Chapter 6

Conclusions & Future Work

6.1 Conclusions

A significant number (65) of new brown dwarfs were identified from wide-field photometric surveys. Criteria that enabled the distinction of young brown dwarf candidates from other objects in colour-magnitude diagrams were established. Initially, a survey for brown dwarfs in the UpSco star forming region, based on photometry and proper motions from a combination of the UKIDSS Galactic Cluster Survey and 2MASS, was carried out. This resulted in the identification of 19 new substellar objects with estimated masses between 0.01 and 0.09 $M_{\odot}$. These objects are located in the southern part of the association, which had not been covered by previous brown dwarf surveys. A further 8 objects, with slightly higher proper motion were also identified. These may be UpSco members with slightly higher dispersion velocities than the stellar members. Although spectroscopic confirmation had not been obtained at this stage, it was demonstrated that the level of contamination appeared to be negligible. The same method was employed again on a search of an extended area of UpSco that had been added to the UKIDSS GCS in a subsequent data release. A further 46 new objects, with the same substellar mass range as the 19 already discovered, were identified.

A follow-up near-infrared spectroscopic analysis of 24 of the 65 newly identified brown dwarfs confirmed that they are all young, very low mass objects, with spectral types that range from M5 to L1. The lack of contamination in this sample affirms the reliability of using photometry and proper motion studies as a means of identifying populations of brown dwarfs in

UpSco.

The number of new brown dwarfs discovered showed that there are 3 substellar members of UpSco for every 10 stellar members. This is further evidence that their formation is a common and frequent consequence of star formation events.

The ratio of stars to brown dwarfs in the South of UpSco was determined to be $3.5^{+2.0}_{-1.3}$, in the same range as elsewhere in UpSco. A comparison of this with literature findings showed that young clusters with OB associations tend to have lower ratios than clusters without OB stars. This might indicate that brown dwarf formation is a function of environment.

An analysis of disks around brown dwarfs demonstrated that their occurrence is as frequent as in low mass stars and that they evolve on similar timescales. This suggests that brown dwarfs and low mass stars may follow a very similar path to planet formation, at least in the initial phase. In total, a homogeneous sample of 116 brown dwarfs in UpSco, the majority of which had not been previously discussed in the literature, was analysed for disks, using photometry from WISE. Contamination in the sample appeared to be negligible and the method of selection was unbiased with respect to the presence of disks.

An examination of all the UKIDSS, 2MASS and WISE colour-magnitude and colour-colour combinations showed that the WISE W1-W2 colour is the best primary diagnostic for the presence of a disk around such objects.

From the sample, 27 Class II objects were identified. Of these, 22 were classified via their W1-W2 colour excess alone. Another 5 objects were also categorised as Class II, based on their W3 and/or W4 signals. These 5 objects (19% of all disks) appear to be in the transition phase between Class II and Class III, leading to the conclusion that this phase is short lived, lasting less than 0.4 Myr, an estimate that is consistent with findings for low-mass stars.

The disk fraction was found to be 23±5%. This fraction is statistically indistinguishable from results for K/M stars in UpSco. Results from the literature for Cha I, IC348 and σ Ori show that their brown dwarf disk fractions are also indistinguishable from their K/M star disk fractions. Therefore the average lifetime of the disks in each of these regions shows no obvious

dependency on the mass of the central object. Combined with the short transitional phase from Class II to Class III, this suggests that the evolution of brown dwarf disks follows a so-called "two timescale model", similar to low mass stars. Hence, the conditions which accompany planet formation in disks around K/M stars also appear to be the prevalent conditions in the disks around brown dwarfs. This indicates that the process of planet formation in brown dwarf disks may be as robust as it is in disks around low mass stars.

The need for a new catalogue of spectral templates of young brown dwarfs was demonstrated. This resulted from the observation that there is a diversity in form among the spectra that can impact on spectral type determination. Class II objects display excess emission and veiling in their spectra. The same form of excess emission and veiling is also present in the spectra of 7 out of 18 ($\sim 40\%$) Class III objects. This is evidence that these Class III objects are still surrounded by, and possibly accreting from, an inner disk of dust and gas which is too faint to be detected via mid-infrared photometry, or that they may be more affected by reddening than the other Class III objects.

In order to address this challenge, a catalogue of near-infrared spectra of those young brown dwarfs that are clean and clear of discernible contributions from anything other than their photospheres, has been assembled. It has been made available at: http://browndwarfs.org/sonyc. The spectra within it can be used as benchmarks to correct for the effects of veiling, excess emission and reddening on spectral typing. I recommend the use of the spectra in this new catalogue, as templates for improving the categorisation of young brown dwarfs in the future.

6.2 Future Work - Where do we go from here?

Our understanding of brown dwarfs has progressed from the first theoretical works of the 1960's, e.g. Kumar (1963); Hayashi & Nakano (1963), through to the first observations in the 1990's (Nakajima et al., 1995; Oppenheimer et al., 2000). Since then, theoretical studies, e.g. Chabrier et al. (2000), have concentrated on modelling the appearance of their atmospheres, while

observational works have focussed on identifying more and more of them, across a greater range of spectral types (Briceño et al., 2007; Luhman, 2012). In the years since the start of the millenium, we have also begun to grapple with the theoretical and observational challenges posed by the formation of brown dwarfs. Research and analysis on this topic, such as that outlined in this thesis, has concentrated on identifying young brown dwarfs, establishing their characteristics, and investigating the factors that govern their formation and evolution.

The next advances in our understanding are likely to be made by exploring two different aspects of the formation of substellar objects. The first is a more rigorous assessment of the *major influences* on the formation of brown dwarfs. The second is an exploration of the *details* of the formation process itself. Investigating each will require the use of different observational techniques and strategies. Both types of investigation should be able to take advantage of new and imminent developments.

6.2.1 The Next Generation Of Surveys

Testing the major influences responsible for brown dwarf formation will rely on the completion of wider and deeper surveys of young clusters and associations. The evidence presented and discussed in Chapter 3 indicates that the formation of brown dwarfs in young clusters may be influenced by the presence of OB stars. In a recent study, Scholz et al. (2013) has found that the brown dwarf formation rate may also be influenced by the number density of stars in a cluster. In both cases, the conclusions are tentative, and subject to substantial uncertainty, due to the small number of clusters on which these results are based. The only way to improve upon these results is to take a census of young brown dwarfs in a greater number of clusters. The clusters and associations surveyed should ideally contain the widest possible range of ages, environments and conditions. This will enhance our chances of obtaining more statistically meaningful results, which may reveal the strength of the influence of the environment within a cluster on its brown dwarf formation rate. Such results should provide insight into both the validity, and relative importance, of any theory of brown dwarf formation. A larger census of young brown dwarfs, in more associations, will also refine and further constrain the shape of the substellar IMF and

test its universality.

In the short term, extensions of surveys by UKIRT will continue to provide new data, particularly for nearby clusters. The European Southern Observatory (ESO) Visible and Infrared Survey Telescope for Astronomy (VISTA) survey, currently being conducted, will probe deeper into some nearby clusters already covered by the UKIDSS GCS. It will also enable the identification of brown dwarfs in a greater number of both nearby and more distant clusters, as it is both more sensitive than the GCS, and covers a wider area of sky. The recently launched Gaia satellite should be able to detect young brown dwarfs in associations covered by both the GCS and the VISTA survey and provide proper motion and astrometric data for them. As well as providing a valuable addition to our knowledge of the structure of nearby associations such as UpSco, it should also provide an extra discriminant between members and non-members of clusters and associations. This will be particularly useful for exploring those clusters where proper motions are not as reliable a diagnostic of cluster membership. By resolving uncertainties in distance, such data will allow for a more accurate appraisal of the photometric signature of more distant brown dwarf candidates, as well as allowing for more accurate assessments of the density of members in distant clusters. In the longer term, the advent of the James Webb Space Telescope (JWST), with its greater sensitivity at both near- and mid-infrared wavelengths, will enable surveys of young brown dwarf populations at even greater distances to be carried out.

The conclusions presented in this thesis indicate that the environment of a cluster may have a significant influence on the number of brown dwarfs formed within it. This also implies that the substellar IMF may vary substantially from cluster to cluster. Over the coming decade, VISTA, Gaia and the JWST, should provide researchers with the data neccessary to reliably verify, refine, or completely alter these conclusions.

6.2.2 Advances In Angular Resolution

Gaining a deeper understanding of the details of the formation and evolution process will depend on making observations with greater angular resolution, to discern features at smaller spatial scales. Progress in this area will also depend on the use of sub-mm and mm wavelength studies, to study the

colder, outer parts of disks. Another addition to our understanding should come from spectroscopic observations that can investigate the details of the *chemical* processes that accompany the physical processes of evolution.

The angular and spectroscopic resolution of the ESO Very Large Telescope (VLT) has greatly extended our ability to observe nearby brown dwarfs at smaller scales in recent years. It will continue to provide researchers with new insight into the local environment of nearby brown dwarfs for many years to come. The 2 objects that stand out in Fig. 4.4, that have bright, hot inner disks are currently the subject of a spectroscopic study by the VLT. In the medium to long term, the instruments that hold the greatest promise of providing major advances in observations are the Atacama Large Millimeter/submillimeter Array (ALMA) and the JWST. Both instruments can achieve an angular resolution that should be capable of probing the structure of inner disks. The wavelength range of ALMA is also perfectly suited to studies designed to determine the extents of the outer parts of brown dwarf disks. Spectroscopic instruments on both ALMA and the JWST will also be capable of detecting chemical changes in disks to a significantly greater degree than current instruments. ALMA is now in the earliest stages of operation, while the JWST is scheduled for launch in 2018. Together, they should collect data that will allow substantial progress to be made in this field over the next two decades.

The conclusions presented in this thesis indicate that the evolution of disks around brown dwarfs mirrors that of disks around low mass stars. This strongly suggests that the formation of planets around both brown dwarfs and stars could follow a similar pattern. The capabilities of ALMA and the JWST should allow researchers to examine the extent of this similarity. Because of their proximity, and stages of evolution, the brown dwarfs identified in UpSco represent some of the most promising targets for studies of this nature.

At this point, we stand on the verge of gaining a deeper and wider understanding of the formation of brown dwarfs, stars and planets. Future developments hold out the promise of providing many new answers. If we are lucky, they will also provide many new questions.

Bibliography

Akeson R.L., Chen X., Ciardi D., Crane M., Good J., Harbut M., Jackson E., Kane S.R., Laity A.C., Leifer S., Lynn M., McElroy D.L., Papin M., Plavchan P., Ramirez S.V., Rey R., von Braun K., Wittman M., Abajian M., Ali B., Beichman C., Beekley A., Berriman G.B., Berukoff S., Bryden G., Chan B., Groom S., Lau C., Payne A.N., Regelson M., Saucedo M., Schmitz M., Stauffer J., Wyatt P., Zhang A., 2013, PASP, 125, 989A.

Allers K.N., Jaffe D.T., Luhman K.L., 2007, ApJ, 657, 511.

AMI Consortium: Ainsworth R.E. et al, 2012, MNRAS, 423, 1089.

Ambartsumian V.A., 1947, in Stellar Evolution and Astrophysics, Erevan Acad. Sci. Armenian SSR.

Andersen M., Meyer M. R., Greissl J., Aversa A., 2008, ApJ, 683, L183.

André P., Ward-Thompson D., Barsony M., 1993, ApJ, 406, 122.

André P., Ward-Thompson D., Greaves J., 2012, Science, 337, 69.

Ardila D., Martín E., Basri G., 2000, AJ, 120, 479.

Ballesteros-Paredes J., Klessen R.S., MacLow M.M., Vazquez-Semadeni E., 2007, in Protostars and Planets V, ed. B. Reipurth, D. Jewitt, K. Keil (Tucson: Univ. Arizona Press), 63.

Bally J., Reipurth B., Davis C.J., 2007, in Protostars and Planets V, ed. B. Reipurth, D. Jewitt, K. Keil (Tucson: Univ. Arizona Press), 215.

Barnard E.E., 1907, ApJ, 25, 218.

Barrado y Navascués D., Bouvier J., Stauffer J.R., Lodieu N., McCaughrean M.J., 2002, A& A, 395, 813B.

Bate M.R., Bonnell I.A., Bromm V., 2002, MNRAS, 332, L65.

Bate M.R., Bonnell I.A., Bromm V., 2003, MNRAS, 339, 577.

Bate M.R., 2009, MNRAS, 392, 590B.

Béjar V.J.S., Martín E.L., Zapatero Osorio M.R., Rebolo R., Barrado y Navascués D., Bailer-Jones C.A.L., Mundt R., Baraffe I., Chabrier G., Allard F., 2001, ApJ, 556, 830.

Bergin E.A., Tafalla M., 2007, ARA&A, 45, 339.

Bertout C., 1989, ARA&A, 27, 351.

Bethe H.A., 1939, PhRv, 55, 434.

Blum J., Wurm G., 2008, ARA&A, 46, 21.

Bonnell I.A., Larson R.B., Zinnecker H., 2007, in Protostars and Planets V, ed. B. Reipurth, D. Jewitt, K. Keil (Tucson: Univ. Arizona Press), 149.

Bonnell I.A., Clark P., Bate M.R., 2008, MNRAS, 389, 1556.

Bok B.A., Reilly E.F., 1947, ApJ, 105, 255.

Boss A., 2011, ApJ, 731, 74B.

Bouy H., Martín E.L., 2009, A&A, 504, 981

Briceño C., Preibisch T., Sherry W.H., Mamajek E.A., Mathieu R.D., Walter F.M., Zinnecker H., 2007, in Protostars and Planets V, ed. B. Reipurth, D. Jewitt, K. Keil (Tucson: Univ. Arizona Press), 345.

Burrows, A., Marley M., Hubbard W.B., Lunine J.I., Guillot T., 1997, ApJ, 491, 856.

Burrows, A., Hubbard W.B., Lunine J.I., Liebert J., 2001, Rev. Mod. Phys., 73, 719.

Calvet N., D'Alessio P., Hartmann L., Wilner D., Walsh A., Sitko M., 2002, ApJ, 568, 1008C.

Cambrésy L., 1999, A&A, 345, 965.

Carpenter J.M., Mamajek E.E., Hillenbrand L.A., Meyer M.R., 2006, ApJ, 651, L49.

Casali M., Adamson A., Alves de Oliveira C., Almaini O., Burch K., Chuter T., Elliot J., Folger M., Foucaud S., Hambly N., Hastie M., Henry D., Hirst P., Irwin M., Ives D., Lawrence A., Laidlaw K., Lee D., Lewis J., Lunney D., McLay S., Montgomery D., Pickup A., Read M., Rees N., Robson I., Sekiguchi K., Vick A., Warren S., Woodward B., 2007, A& A, 467, 777.

Casewell S.L., Baker D.E.A., Jameson R.F., Hodgkin S.T., Dobbie P.D., Moraux E., 2012, MNRAS, 425, 3112C.

Chabrier G., Baraffe I., 1997, A&A, 327, 1039.

Chabrier G., Baraffe I., 2000, ARA&A, 38, 337C.

Chabrier G., Baraffe I., Allard F., Hauschildt P., 2000, ApJ, 542, 464.

Chabrier G., 2003, PASP, 115, 763C.

Chabrier G., 2005, in The Initial Mass Function 50 Years Later, eds. E. Corbelli, F. Palla, H. Zinnecker, Astrophys. Space Sci. Lib., 327, 41.

Chabrier G., Baraffe I., Selsis F., Barman T.S., Hennebelle P., Alibert Y., 2007, in Protostars and Planets V, ed. B. Reipurth, D. Jewitt, K. Keil (Tucson: Univ. Arizona Press), 623.

Chauvin G., Lagrange A.M., Dumas C., Zuckerman B., Mouillet D., Song I., Beuzit J.L., Lowrance P., 2004, A&A, 425, L29.

Cushing M.C., Vacca W.D., Rayner J.T., 2004, PASP, 116, 362C.

Cushing M.C., Rayner J.T., Vacca W.D., 2005, ApJ, 623, 1115.

Cutri R.M., Wright E.L., Conrow T., Bauer J., Benford D., Brandenburg H., Dailey J., Eisenhardt P.R.M., Evans T., Fajardo-Acosta S., Fowler J., Gelino C., Grillmair C., Harbut M., Hoffman D., Jarrett T., Kirkpatrick J.D., Leisawitz D., Liu W., Mainzer A., Marsh K., Masci F., McCallon H., Padgett D., Ressler M.E., Royer D., Shrutskie M.F., Stanford S.A., Wyatt P.L., Tholen D., Tsai C.W., Wachter S., Wheelock S.L., Yan L., Alles R., Beck R., Grav T., Masiero J., McCollum B., McGehee P., Papin

M., Wittman M., 2012, Explanatory Supplement to the WISE All Sky Data Release.

Damjanov I., Jayawardhana R., Scholz A., Ahmic M., Nguyen D.C., Brandeker A., van Kerkwijk M.H., 2007, ApJ, 670, 1337D.

D'Antona F., Mazzitelli I., 1985 , ApJ, 296, 502D.

Dawson P., Scholz A., Ray T.P., 2011, MNRAS, 418, 1231D.

Dawson P., Scholz A., Ray T.P., Marsh K.A., Wood K., Natta A., Padgett D., Ressler M.E., 2013, MNRAS, 429, 903.

Dawson P., Scholz A., Ray T.P., Peterson D.E., Rodgers-Lee D., Geers V., 2014, MNRAS in press, arXiv:1405.3842.

de Bruijne J.H.J., Hoogerwerf R., Brown A.G.A., Aguilar L.A., de Zeeuw P.T., 1997, in Perryman M.A.C., Bernacca P.L., Battrick B., eds, in ESA SP-402: Hipparcos - Venice '97 Improved Methods for Identifying Moving Groups. p. 575.

de Bruijne J.H.J., 1999, MNRAS, 310, 585.

de Zeeuw P.T., Hoogerwerf R., de Bruijne J.H.J., Brown A.G.A., Blaauw A., 1999, AJ, 117, 354.

Dobashi K., Uehara H., Kandori R., Sakurai T., Kaiden M., Umemoto T., Sato F., 2005, PASJ, 57, 1.

Dullemond C.P., Dominik C., 2004, A&A, 421, 1075D.

Dullemond C.P., Natta A., Testi L., 2006, ApJ, 645L, 69D.

Dullemond C.P., Hollenbach D., Kamp I., D'Alessio P., 2007, in Protostars and Planets V, ed. B. Reipurth, D. Jewitt, K. Keil (Tucson: Univ. Arizona Press), 555.

Dullemond C.P., 2013, AN, 334, 589D.

Durisen R.H., Boss A.P., Mayer L., Nelson A.F., Quinn T., Rice W.K.M., 2007, in Protostars and Planets V, ed. B. Reipurth, D. Jewitt, K. Keil (Tucson: Univ. Arizona Press), 607.

Dye S., Warren S.J., Hambly N.C., Cross N.J.G., Hodgkin S.T., Irwin M.J., Lawrence A., Adamson A.J., Almaini O., Edge A.C., Hirst P., Jameson R.F., Lucas P.W., van Breukelen C., Bryant J., Casali M., Collins R.S., Dalton G.B., Davies J.I., Davis C.J., Emerson J.P., Evans D.W., Foucaud S., Gonzales-Solares E.A., Hewett P.C., Kendall T.R., Kerr T.H., Leggett S.K., Lodieu N., Loveday J., Lewis J.R., Mann R.G., McMahon R.G., Mortlock D.J., Nakajima Y., Pinfield D.J., Rawlings M.G., Read M.A., Riello M., Sekiguchi K., Smith A.J., Sutorius E.T.W., Varricatt W., Walton N.A., Weatherley S.J., 2006, MNRAS, 372, 1227.

Eddington A.S., 1919, Obs, 42, 371.

Edgeworth K.E., 1949, MNRAS, 109, 600E.

Elmegreen B.G., 2011, ApJ, 731, 61.

Ercolano B., Clarke C.J., Robitaille T.P., 2009, MNRAS, 394L, 141E.

Espaillat C., Calvet N., Luhman K.L., Muzerolle J., D'Alessio P., 2008, ApJ, 682L, 125E.

Espaillat C., Ingleby L., Hernandez J., Furlan E., D'Alessio P., Calvet N., Andrews S., Muzerolle J., Qi C., Wilner D., 2012, ApJ, 747, 103E.

Folha D.F.M., Emerson J.P., 1999, A&A, 352, 517.

Geers V., Scholz A., Jayawardhana R., Lee E., Lafreniere D., Tamura M., 2011, ApJ, 726, 23.

Goodwin S.P., Whitworth A., 2007, A&A, 466, 943G.

Haisch K.E.jr., Lada E.A., Lada C.J., 2001, ApJ, 553, L153.

Hartigan P., Kenyon S.J., Hartmann L., Strom S.E., Edwards S., Welty A.D., Stauffer J., 1991, ApJ, 382, 617.

Hayashi C., 1961, PASJ, 13, 450.

Hayashi C., Nakano T., 1963, PThPh, 30, 460.

Hayashi C. 1970, MSRSL, 19, 127.

Hambly N.C., Collins R.S., Cross N.J.G., Mann R.G., Read M.A., Sutorius E.T.W., Bond I., Bryant J., Emerson J.P., Lawrence A., Rimoldini L., Stewart J.M., Williams P.M., Adamson A., Hirst P., Dye S., Warren S.J., 2008, MNRAS, 384, 637.

Hennebelle P., Chabrier G., 2008, ApJ, 684, 395.

Hernandez J., Hartmann L., Megeath T., Gutermuth R., Muzerolle J., Calvet N., Vivas A.K., Briceño C., Allen L., Stauffer J., 2007, ApJ, 662, 1067H.

Herschel W., 1785, Philos. Trans. Ser. I., 75, 213.

Hertzsprung E., 1905, Zeitschrift fur wissenschaftliche Photographie, 3, 429.

Hertzsprung E., 1911, Publikationen des Astrophysikalischen Observatoriums zu Potsdam, 22, 1.

Hester J.J., Scowen P.A., Sankrit R., Lauer T.R., Ajhar E.A., Baum W.A., Code A., Currie D.G., Danielson G.E., Ewald S.P., Faber S.M., Grillmair C.J., Groth E.J., Holtzman J.A., Hunter D.A., Kristian J., Light R.M., Lynds C.R., Monet D.G., O'Neil E.J., Shaya E.J., Seidelmann K.P., Westphal J.A., 1996, AJ, 111, 2349.

Hodgkin S.T., Irwin M.J., Hewett P.C., Warren S.J., 2009, MNRAS, 394, 675.

Iben I., 1965 ApJ, 141, 993I.

Irwin M.J. et al., in preparation.

Jayawardhana R., Coffey J., Scholz A., Brandeker A., van Kerkwijk M.H., 2006, ApJ, 648, 1206J.

Jeans J., 1929, in Astronomy And Cosmogony, Cambridge Univ. Press.

Jeffries R.D., 2012, in EAS Publ. Ser., 57, 45.

Joy A.H., 1945, ApJ, 102, 168.

Kirkpatrick J.D., Barman T.S., Burgasser A.J., 2006, ApJ, 639, 1120.

Kroupa P., 2001, MNRAS, 322, 231.

Kroupa P., 2002, Science, 295, 82.

Kumar S.S., 1963, ApJ, 137, 1121.

Lada C.J., 1987, in IAUS, 115, 1, Star Forming Regions, eds. Peimbert M., Jugaku J., (Dordrecht: Kluwer).

Lada C.J., Alves J., Lada E.A., 1999, ApJ, 512, 250.

Lada C.J., Muench A.A., Luhman K.L., Allen L., Hartmann L., Megeath T., Myers P., Fazio G., Wood K., Muzerolle J., Rieke G., Siegler N., Young E., 2006, AJ, 131, 1574.

Larson R.B., 1969, MNRAS, 145, 271.

Lawrence A., Warren S.J., Almaini O., Edge A.C., Hambly N.C., Jameson R.F., Lucas P., Casali M., Adamson A., Dye S., Emerson J.P., Foucaud S., Hewett P., Hirst P., Hodgkin S.T., Irwin M.J., Lodieu N., McMahon R.G., Simpson C., Smail I., Mortlock D., Folger M., 2007, MNRAS, 379, 1599.

Lissauer J.J., Stevenson D.J., 2007, in Protostars and Planets V, ed. B. Reipurth, D. Jewitt, K. Keil (Tucson: Univ. Arizona Press), 591.

Lissauer J.J., Slartibartfast., 2008, in ASP Conf. Ser. 398, Extreme Solar Systems, ed. D. Fischer et al.(San Francisco, CA: ASP), 491.

Lodieu N., Hambly N.C., Jameson R.F., 2006, MNRAS, 373, 95.

Lodieu N., Hambly N.C., Jameson R.F., Hodgkin S.T., Carraro G., Kendall T.R., 2007, MNRAS, 374, 372.

Lodieu N., Hambly N.C., Jameson R.F., Hodgkin S.T., 2008, MNRAS, 383, 1385.

Lodieu N., Dobbie P.D., Hambly N.C., 2011, A&A, 527A, 24L.

Lodieu N., 2013, MNRAS, 431, 3222.

Lombardi M., Alves J., 2001, A&A, 377, 1023.

Looper D.L., Burgasser A.J., Kirkpatrick J.D., Swift B.J., 2007, ApJ, 669L, 97L.

Lucas P. W., Roche P. F., 2000, MNRAS, 314, 858L.

Luhman K.L., Briceño C., Rieke G.H., Hartmann L., 1998, ApJ, 493, 909L.

Luhman K.L., Stauffer J.R., Muench A.A., Rieke G.H., Lada E.A., Bouvier J., Lada C.J., 2003, ApJ, 593, 1093L.

Luhman K.L., 2004, ApJ, 602, 816L.

Luhman K.L., Lada C.J., Hartmann L., Muench A.A., Megeath S.T., Allen L.E., Myers P.C., Muzerolle J., Young E., Fazio G.G., 2005, ApJ, 631L, 69L.

Luhman K.L., 2007, ApJS, 173, 104L.

Luhman K. L., Joergens V., Lada C., Muzerolle J., Pascucci I., White R., 2007, in Protostars and Planets V, ed. B. Reipurth, D. Jewitt, K. Keil (Tucson: Univ. Arizona Press), 443.

Luhman K.L., Mamajek E.E., Allen P.R., Muench A.A., Finkbeiner D.P., 2009, ApJ, 691, 1265L.

Luhman K.L., 2012, ARA&A, 50, 65L.

Luhman K.L., Mamajek E.E., 2012, ApJ, 758, 31L.

Marois C., Zuckerman B., Konopacky Q.M., Macintosh B., Barman T., 2010, Nature, 468, 1080.

Martín E.L., Rebolo R., Zapatero-Osorio M.R., 1996, ApJ, 469, 706M.

Martín E.L., Delfosse X., Guieu S., 2004, AJ, 127, 449.

Mathis J.S., 1990, ARA&A, 28, 37M.

Mayne N.J., Naylor T., Littlefair S.P., Saunders E.S., Jeffries R.D., 2007, MNRAS, 375, 1220M.

Mayor M., Queloz D., 1995, Nature, 378, 355.

Merin, B., Brown J.M., Oliveira I., Herczeg G.J., van Dishoeck E.W., Bottinelli S., Evans N.J.II., Cieza L., Spezzi L., Alcala J.N., Harvey P.M., Blake G.A., Bayo A., Geers V.G., Lahuis F., Prusti T., Augereau J-C., Olofsson J., Walter F.M., Kuenley C., 2010, ApJ, 718, 1200M.

Mohanty S., Burgasser A., Chabrier G., Padoan P., Hennebelle P., Pascucci I., Kraus A., Baraffe I., Stassun K., Greaves J., Reiners A., Dunham M., Scholz A., Oppenheimer B., Ray T., Apai D., Goodman A., Cruz K., Rebull L., Moraux E., 2009, White Paper for the Astro 2010 Decadal Survey, 2009astro2010S.212M.

Muench A.A., Lada C.J., Luhman K.L., Muzerolle J., Young E., 2007, AJ, 134, 411M.

Muzerolle J., Adame L., D'Alessio P., Calvet N., Luhman K.L., Muench A.A., Lada C.J., Rieke G.H., Siegler N., Trilling D.E., Young E.T., Allen L., Hartmann L., Megeath S.T., 2006, ApJ, 643, 1003M.

Muzerolle J., Allen L., Megeath S.T., Hernandez J., Gutermuth R.A., 2010, ApJ, 708, 1107M.

Mužić K., Scholz A., Geers V.C., Fissel L., Jayawardhana R., 2011, ApJ, 732, 86.

Mužić K., Scholz A., Geers V.C., Jayawardhana R., Tamura M., 2012, ApJ, 744, 134.

Mužić K., Scholz A., Geers V.C., Jayawardhana R., Tamura M., Dawson P., Ray T.P., 2013, MmSAI 84, 931M.

Mužić K., Scholz A., Geers V., Jayawardhana R., López Martí B., 2014, ApJ, 785, 159M.

Nakajima T., Oppenheimer B.R., Kulkarni S.R., Golimowski D.A., Matthews K., Durrance S.T., 1995, Nature, 378, 463.

Natta A., Testi L., 2001, A&A, 376L, 22N.

Natta A., Testi L., Comerón F., Oliva E., D'Antona F., Baffa C., Comoretto G., Gennari S., 2002, A&A, 393, 597.

Natta A., Testi L., Randich S., 2006, A&A, 452, 245.

Oliveira J.M., Jeffries R.D., Kenyon M.J., Thompson S.A., Naylor T., 2002, A&A, 382L, 22O.

Oliveira J.M., Jeffries R.D., van Loon J. Th., 2009, MNRAS, 392, 10340.

Oppenheimer B.R., Kulkarni S.R., Stauffer J. R., 2000, in Protostars and Planets IV, ed. Mannings V., Boss A., Russell S. (Tucson: Univ. Arizona Press), 1313.

Padoan P., Nordlund A., 2002, ApJ, 576, 870.

Padoan P., Nordlund A., 2004, ApJ, 617, 559.

Pecaut M.J., Mamajek E.E., Bubar E.J., 2012, ApJ, 746, 154P.

Peterson D.E., Megeath S.T., Luhman K.L., Pipher J.L., Stauffer J.R., Barrado y Navascués D., Wilson J.C., Skrutskie M.F., Nelson M.J., Smith J.D., 2008, ApJ, 685, 313.

Pollack J.B., Hubickyj O., Bodenheimer P., Lissauer J.J., Podolak M., Greenzweig Y., 1996, Icarus, 124, 62.

Preibisch T., Guenther E., Zinnecker H., Sterzik M., Frink S., Roser S., 1998, A&A, 333, 619.

Preibisch T., Zinnecker H., 1999, AJ, 117, 2381P.

Preibisch T., Brown A.G.A., Bridges T., Guenther E., Zinnecker H., 2002, AJ, 124, 404.

Preibisch T., Mamajek E., 2008, in Handbook of Star Forming Regions, Vol, II, ed B. Reipurth (San Francisco, CA: ASP), 235.

Ray T.P., 2007, in Jets from Young Stars, Ferreira J., Dougados C., Whelan E., eds, LNP, 723, 3R.

Rayner J.T., Toomey D.W., Onaka P.M., Denault A.J., Stahlberger W.E., Vacca W.D., Cushing M.C., Wang S., 2003, PASP, 115, 362R.

Rayner J.T., Cushing M.C., Vacca W.D., 2009, ApJS, 185, 289R.

Reipurth B., Clarke C., 2000, AJ, 122, 432.

Riaz B., Lodieu N., Goodwin S., Stamatellos D., Thompson M., 2012, MNRAS, 420, 2497R.

Ricci L., Testi L., Natta A., Scholz A., de Gregorio-Monsalvo I., 2012, ApJ, 761L, 20R.

Rieke G.H., Lebofsky M.J., 1985, AJ, 288, 618.

Rojas-Ayala B., Covey K.R., Muirhead P.S., Lloyd J.P., 2012, ApJ, 748, 93.

Russell H.N., 1913, Obs, 36, 324.

Russell H.N., 1914, PA, 22, 275.

Safronov V.S., 1969, Evoliutsiia do planetnogo oblaka.

Salpeter E.E., 1955, ApJ, 121, 161.

Schneider J., Dedieu C., Le Sidaner P., Savalle R., Zolotukhin I., 2011, A&A, 532, A79.

Scholz A., Jayawardhana R., Wood K., Meeus G., Stelzer B., Walker C., O'Sullivan M., 2007, ApJ, 660, 1517.

Scholz A., Geers V., Jayawardhana R., Fissel L., Lee E., Lafreniere D., Tamura M., 2009, ApJ, 702, 805S.

Scholz A., Xu X., Jayawardhana R., Wood K., Eislöffel J., Quinn C., 2009, MNRAS, 398, 873S.

Scholz A., Mužić K., Geers V., Bonavita M., Jayawardhana R., Tamura M., 2012, ApJ, 744, 6.

Scholz A., Jayawardhana R., Mužić K., Geers V., Tamura M., Tanaka I., 2012, ApJ, 756, 24.

Scholz A., Geers V., Clark P., Jayawardhana R., Mužić K., 2013, ApJ, 775, 138.

Sherry W.H., Walter F.M., Wolk S.J., 2004, AJ, 128, 2316S.

Shu F.H., Adams F.C., Lizano S., 1987, ARA&A, 25, 23.

Siess L., Dufour E., Forestini M., 2000, A&A, 358, 593.

Skrutskie M.F., Cutri R.M., Stiening R., Weinberg M.D., Schneider S., Carpenter J.M., Beichman C., Capps R., Chester T., Elias J., Huchra J., Liebert J., Lonsdale C., Monet D.G., Price S., Seitzer P., Jarrett T., Kirkpatrick J.D., Gizis J., Howard E., Evans T., Fowler J., Fullmer L., Hurt R., Light R., Kopan E.L., Marsh K.A., McCallon H.L., Tam R., Van Dyck S., Wheelock S., 2006, AJ, 131, 1163.

Slesnick C.L., Carpenter J.M., Hillenbrand L.A., 2006, AJ, 131, 3016.

Slesnick C.L., Hillenbrand L.A., Carpenter J.M., 2008, ApJ, 688, 377S.

Stamatellos D., Hubber D.A., Whitworth A.P., 2007, MNRAS, 382, L30.

Stamatellos D., Whitworth A.P., Maury A., André P., 2011, MNRAS, 413, 1787.

Strand K.A., 1977, IAUS, 80, 55.

Tarter J., 1975, Ph.D. thesis, Univ. California, Berkeley.

Tej A., Sahu K.C., Chandrasekhar T., Ashok N.M., 2002, ApJ, 578, 523.

Thommes E.W., Duncan M.J., Levison H.F., 2003, Icarus, 161, 431.

Todorov K., Luhman K.L., McLeod K.K., 2010, ApJ, 714, L84.

Vacca W.D., Cushing M.C., Rayner J.T., 2004, PASP, 115, 389V.

Vorobyov E.I., Basu S., 2010, ApJ, 714L, 133V.

Vorobyov E.I., 2013, A&A, 552, A129.

von Weizsacker C.F., 1938, Physikalische Zeitschrift, 39, 633.

Warren S.J., Hambly N.C., Dye S., Almaini O., Cross N.J.G., Edge A.C., Foucaud S., Hewett P.C., Hodgkin S.T., Irwin M.J., Jameson R.F., Lawrence A., Lucas P.W., Adamson A.J., Bandyopadhyay R.M., Bryant J., Collins R.S., Davis C.J., Dunlop J.S., Emerson J.P., Evans D.W., Gonzales-Solares E.A., Hirst P., Jarvis M.J., Kendall T.R., Kerr T.H., Leggett S.K., Lewis J.R., Mann R.G., McLure R.J., McMahon R.G., Mortlock D.J., Rawlings M.G., Read M.A., Riello M., Simpson C., Smith D.J.B., Sutorius E.T.W., Targett T.A., Varicatt W.P., 2007, MNRAS, 375, 213.

Weidenschilling S.J., 1977, MNRAS, 180, 57.

Whitworth A., Zinnecker H., 2004, A&A, 427, 299.

Whitworth A., Bate M.R., Nordlund A., Reipurth B., Zinnecker H., 2007, in Protostars and Planets V, ed. B. Reipurth, D. Jewitt, K. Keil (Tucson: Univ. Arizona Press), 459.

Williams J.P., Blitz L., McKee C.F., 2000, in Protostars and Planets IV, ed. Mannings V., Boss A., Russell S. (Tucson: Univ. Arizona Press), 97.

Wright E.L., Eisenhardt P.R.M., Mainzer A.K., Ressler M.E., Cutri R.M., Jarrett T., Kirkpatrick J.D., Padgett D., McMillan R.S., Skrutskie M., Stanford S.A., Cohen M., Walker R.G., Mather J.C., Leisawitz D., Gautier T.N.III., McLean I., Benford D., Lonsdale C.J., Blain A., Mendez B., Irace W.R., Duval V., Liu F., Royer D., Heinrichsen I., Howard J., Shannon M., Kendall M., Walsh A.L., Larsen M., Cardon J.G., Schick S., Schwalm M., Abid M., Fabinsky B., Naes L., Tsai C.-W., 2010, AJ, 140, 1868W.

Wright J.T., Fakhouri O., Marcy G.W., Han E., Feng Y., Johnson J.A., Howard A.W., Fischer D.A., Valenti J.A., Anderson J., Piskunov N., 2011, PASP, 123, 412.

Zapatero Osorio M. R., Béjar V.J.S., Martín E.L., Rebolo R., Barrado y Navascués D., Bailer-Jones, C.A.L., Mundt R., 2000, Science, 290, 103.

Zapatero Osorio M. R., Béjar V.J.S., Pavlenko Ya., Rebolo R., Allende Prieto C., Martín E.L., García López R.J., 2002, A&A, 384, 937Z.